Master Thesis, Department of Geosciences

Compaction, rock property evolution and rock physics diagnostics of Askeladd discovery, Norwegian Barents Sea

Mohsen Fardi Golyan

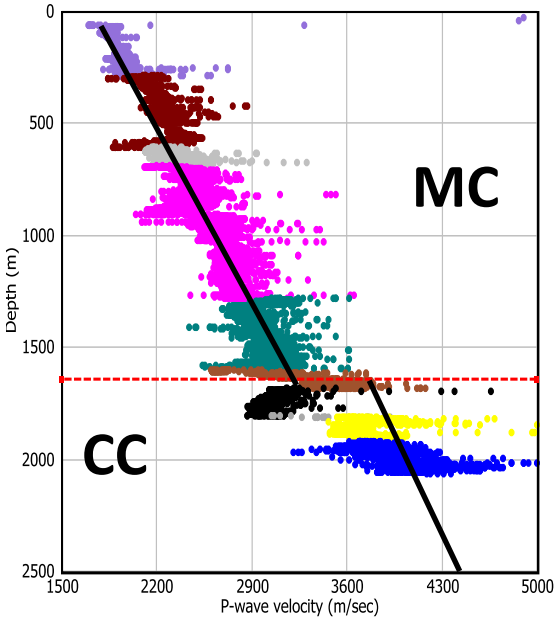

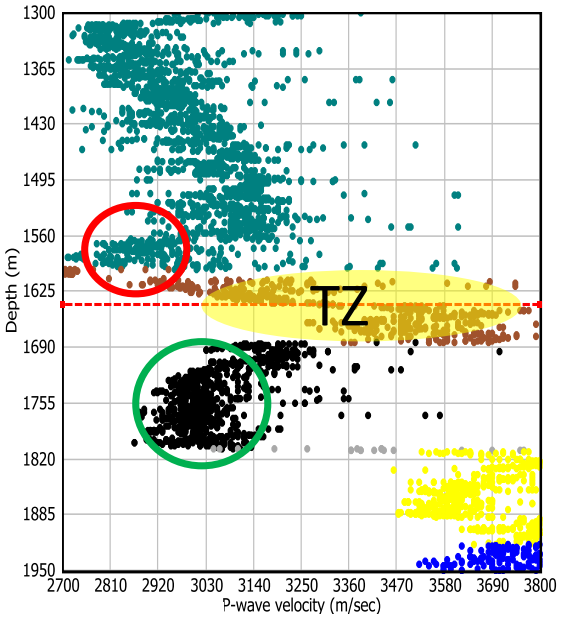

UNIVERSITY OF OSLO

FACULTY OF MATHEMATICS AND NATURAL SCIENCES

Compaction, rock property evolution and rock physics diagnostics of Askeladd discovery, Norwegian Barents Sea

Mohsen Fardi Golyan

Master Thesis in Geosciences

Discipline: Petroleum Geolgoy and Petroleum Geophysics

Department of Geosciences

Faculty of Mathematics and Natural Sciences

University of Oslo

01.06.2012

تقدیم به پدر و مادر نازنینم.

I dedicate this dissertation to my beloved parents.

Acknowledgments

This thesis is an outcome of assistance, support and encouragement of many people without whom this could not possibly be. I would like to take this opportunity to show my respect to all who helped me even with a word.

Primarily, I would like to sincerely present my deepest gratitude to my supervisor Nazmul Haque Mondol for guiding me in the right direction and providing me with comments and also for being patient and supportive throughout the entire period. Special thanks also go out to my friends Toraj, Mohammad, Mohsen, Ahad, Jamil, Danial and Arif for helping me during the last two years.

In addition, I need to mention some people, who helped me throughout this thesis and education, Asdrúbal Bernal, Johan Petter Nystuen, Roy Helge Gabrielsen, Knut Bjørlykke, Jens Jahren, Jenö Nagy, Arnstein Orten, Michael Heeremans, Leiv Jacob Gelius, Oluwakemi Ogebule, Sirikarn Narongsirikul and Dag Arild Karlsen.

I would like to dedicate this dissertation to my beloved parents. Thank you for always loving, supporting and believing in me. Without your support this would have not been achievable.

Mohsen Fardi Golyan

Oslo, June 2012

Abstract

Geologically, Barents Sea consists of platform areas and basins, covered by significant amounts of sedimentary rocks ranging from Paleozoic to Cenozoic age. Several phases of uplift have been occurred, highly influenced the petroleum systems in the region. Askeladd discovery is located in the Hammerfest Basin, South Western part of the Norwegian Barents Sea. In this study, reservoir characteristics of Stø Formation is evaluated according to compaction trends and rock physics diagnostics of five available exploration wells drilled in the area.

Compaction processes change the physical properties of rocks such as velocity, density and porosity. Although investigating the compaction trends (velocity/density/porosity versus depth) in the Askeladd discovery reveals the fact that velocity and density increase with depth and porosity reduce as expected as response to mechanical and chemical compaction. Several other parameters such as overpressure, clay mineralogy and organic rich source rock cause variation in compaction trends compared to general compaction curve in the study area. Transition from mechanical to chemical compaction has taken place in the Knurr Formation and its depth increases slightly toward North and reaches 1770 m (BSF) in well 7120/8-3. In order to correct the burial depth after the basin uplift, exhumation estimation is performed in different wells across the Askeladd discovery by applying different published depth trends. Exhumation estimate increase toward North and reaches its maximum at well 7120/8-3 (900 m burial depth).

Rock physics make a link between geophysical observable to geological parameters and nowadays becomes an important part of reservoir characterization. Various rock physics models have their own benefits and limitations. Fluid and lithology discrimination are carried out for Stø reservoir by applying different rock physics templates (RPTs). By plotting acoustic impedance (AI) versus V_p/V_s ratio, data points concentrate within a narrow zone indicating high AI and V_p/V_s ratio suggest that application of rock physics template in the study area needs significant modification compared to generalized RPTs. Overconsolidation of the reservoir due to quartz cementation results in high values of AI which causes a great deal of ambiguity for lithology and/or fluid discrimination. Therefore, rock physics diagnostic and its application in the Askeladd area is highly dependent on quality of input data as well as model assumptions.

Table of Contents

Acknowledgments IV

Abstract V

Table of Contents VI

Table of Figures IX

Chapter 1 Introduction 1

1.1. General Introduction 2

1.2. Motivation 4

1.3. Research Objectives 5

1.4. Study Area 6

1.5. Chapter Description 8

1.6. Limitation and Future Implications 9

Chapter 2 Geological Background 10

2.1. Geological Setting 11

2.1.1. Greater Barents Sea 11

2.1.2. Hammerfest Basin 14

2.2. Stratigraphy 16

2.2.1. Nordland GP 16

2.2.2. Sotbakken GP 16

2.2.2.1. Torsk Fm 17

2.2.3. Nygrunnen GP 17

2.2.3.1. Kveite Fm 17

2.2.3.2. Kviting Fm 18

2.2.4. Adventdalen GP 18

2.2.4.1. Kolmule Fm 18

2.2.4.2. Kolje Fm 19

2.2.4.3. Knurr Fm 19

2.2.4.4. Hekkingen Fm 19

2.2.4.4.1. Krill Mbr 20

2.2.4.4.2. Alge Mbr 20

2.2.4.5. Fuglen Fm 20
2.2.5. Kapp Toscana GP 20
2.2.5.1. Stø Fm 21
2.2.5.2. Nordmela Fm 21
2.2.5.3. Tubåen Fm 21
2.2.5.4. Fruholmen Fm 22
2.3. Petroleum Systems 24
2.3.1. Source Rocks 26
2.3.2. Reservoir Rocks 27
2.3.3. Caps Rocks 29
2.3.4. Traps 30
Chapter 3 Material and Methods 32
3.1. Data Base 33
3.2. Identify the Transition Zone 34
3.3. Calculation of Shale Volume 34
3.4. Temperature Gradients 35
3.5. Exhumation Estimation 35
3.6. Estimation of V_s 36
3.7. Rock Physics Template (RPTs) 37
Chapter 4 Theoretical Background 39
4.1. Compaction of Sediments 40
4.1.1. Mechanical Compaction 40
4.1.2. Chemical Compaction 43
4.2. Rock Physics Models 44
4.2.1. Bounds 44
4.2.1.1. The Voigt and Reuss Bounds 45
4.2.1.2. Hashin-Shtrikman Bounds 46
4.2.1.3. Modified Hashin–Shtrikman Bounds 48
4.2.2. Velocity-Porosity Models 48
4.2.2.1. Critical Porosity and Nur's Modified Voigt Average 48
4.2.2.2. Wyllie's Time-Average Equation 49

4.2.2.3. Raymer–Hunt–Gardner Relations 50
4.2.2.4. Han's Empirical Relations for Shaley Sandstones 51
4.2.2.5. Castagna's Empirical Relations for Velocities 52
4.2.3. V_p-V_s Relations 53
4.2.4. Cement Models 54
4.2.4.1. The Friable - (Unconsolidated) Sand Model: 54
4.2.4.2. The Contact – Cement model 55
4.2.4.3. The Constant – Cement model 56
4.3. Gassmann's Relations 56
Chapter 5 Compaction and Evolution of Rock Properties 58
5.1. Result 59
5.1.1. Compaction trends 59
5.1.2. Transition zone 70
5.1.3. Exhumation 75
5.2. Discussion 79
Chapter 6 Rock Physics Diagnostics 83
6.1. Result 84
6.1.1. Net to gross ratio 84
6.1.2. V_p-V_s relation 86
6.1.3. Rock physics template (RPTs) of AI versus V_p/V_s 87
6.1.4. Rock physics diagnostic of Stø Formation 89
6.2. Discussion 92
Chapter 7 Summary and Conclusion 95
References 98
References: 99

Table of Figures

Fig. 1.1. Location of the Barents Sea with bathymetry and topography map (modified after Barrère et al., 2008). 3
Fig. 1.2. (a) Location map of Hammerfest Basin (modified after Ostanin et al., 2012) (b) Askeladd gas field discovery and sections (modified from NPD Factpages 2012)..... 7

Fig. 2.1. Tectonic framework of the Barents Sea region (Gabrielsen et al., 1990). 13
Fig. 2.2. Fault-types of the Hammerfest Basin and the Loppa High (modified after Berglund et al., 1986). 15
Fig. 2.3. Generalized lithostratigraphy of the Barents Sea area, with major tectonic events in the area. The potential source rocks and reservoir rocks also indicated in this figure (Ostanin et al., 2012). 23
Fig. 2.4. Petroleum system event s chart (modified after Magon and Dow, 1994) 24
Fig. 2.5. Petroleum systems of the greater Barents Sea (Henriksen et al., 2011). 25
Fig. 2.6. Maturity differences between North Sea and Barents Sea base on reflectance and temperature data (Ohm et al., 2008). 26
Fig. 2.7. Composite logs, (left) and (right) core photo of well 7120/8-2, from Stø Fm (NPD Factpages). 28
Fig. 2.8. Location of the Askeladd Field. Faults B, D, E, F & G are significant for gas accumulation at Askeladd Nord gas filled structure. Dry well 7120/8-3 is located down dip from GWC and its accumulation might be controlled by whatever fault(s) is (are) controlling the accumulation in 7120/8-1 (Bernal, 2009). 30
Fig. 2.9. Significant hydrocarbon plays in the Norwegian Barents Sea. (a) Platform and platform margins. (b) Extensional basin margins and rotated fault blocks (modified after Henriksen et al., 2011). 31

Fig. 3.1. Crossplots of Vp versus Vs in well 7120/8-4 for estimating the shear velocity. 36
Fig. 3.2. RPTs recipe to build a template for the area of interest. 37
Fig. 3.3. A rock physics template (RPT) in the Vp/Vs versus AI cross-plot domain includes rock physics models locally constrained by depth (i.e., pressure), mineralogy, critical porosity, and fluid properties. The template includes porosity trends for different lithology, and increasing gas saturation for sands (assuming uniform saturation). The black arrows show various geologic trends (conceptually): 1) increasing shaliness, 2) increasing cement volume, 3) increasing porosity, 4) decreasing effective pressure, and 5) increasing gas saturation (Ødegaard and Avseth 2004). 38

Fig. 4.1. Different types of stresses dominated in the sedimentary basins (modified after Bjørlykke et al., 2010). 41

Fig. 4.2. (a) Experimental compaction of fine-grained and coarse-grained sand showing that well sorted fine-grained sands are less compressible compared to the coarse-grained sands, (b) The porosity loss as a function of grain size due to more grain crushing (from Chuhan et al., 2007 cited in Bjørlykke & Jahren, 2010). 42
Fig. 4.3. Experimental mechanical compaction of brine-saturated kaolinite aggregates sorted by grain size (after Mondol et al., 2008). The sample containing less than 2 μm sized kaolinite aggregates retained higher porosity compared to all the other mixtures. The maximum porosity reduction is observed in the composite mixture containing all the grain sizes, demonstrating the importance of both grain size and sorting for the rock properties. 42
Fig. 4.4. Schematic illustration of a stylolite which is believed acting as main sources of quartz cementation (Bjørlykke et al., 2010). 43
Fig. 4.5. Bounds for effective elastic bulk modulus of a mixture of two materials (modified after Avseth et al., 2005) 45
Fig. 4.6. Physical interpretation of the Hashin-Shtrikman bounds, lower bound (a) in the left and upper bound, in the right (b) (modified after Gelius & Johansen, 2010). 47
Fig. 4.7. Schematic illustrations of three cement models (modified after Avseth 2005). 55

Fig. 5.1. Crossplots of (a) Vp-depth, (b) density-depth, (c) porosity-depth, and (d) density-Vp, observed from all wells in the Askeladd field, Barents Sea. 61
Fig. 5.2. Log data points observed from well 7120/7-2 outlined in; (a) Vp-depth, (b) density-depth, (c) porosity-depth, (d) velocity-density plots. 63
Fig. 5.3. Data points of well 7120/7-2representing clean sand and shale in (a) Vp-depth, (b) density-depth, (c) porosity-depth, (d) velocity-density plots 64
Fig. 5.4. Log data points observed from well 7120/8-1 outlined in; (a) Vp-depth, (b) density-depth, (c) porosity-depth, (d) velocity-density plots. 65
Fig. 5.5. Log data points observed from well 7120/8-2 outlined in; (a) Vp-depth, (b) density-depth, (c) porosity-depth, (d) velocity-density plots. 66
Fig. 5.6. Log data points observed from well 7120/8-3 outlined in; (a) Vp-depth, (b) density-depth, (c) porosity-depth, (d) velocity-density plots. 67
Fig. 5.7. Data points of well 7120/8-1representing clean sand and shale in (a) Vp-depth, (b) density-depth, (c) porosity-depth, (d) velocity-density plots. 68
Fig. 5.8. Data points of well 7120/8-3representing clean sand and shale in (a) Vp-depth, (b) density-depth, (c) porosity-depth, (d) velocity-density plots. 69
Fig. 5.9. Data points of well 7120/8-3representing clean sand and shale in (a) Vp-depth, (b) density-depth, (c) porosity-depth, (d) velocity-density plots. 70
Fig. 5.10. Right, gamma ray and velocity logs acquired from well 7120/8-2 corresponding to transition zone (highlighted area) and its nearby present depths that is about 1640 m (BSF). Left, velocity-depth plot of the same depths as well log shown at the right side. The bottom plot is color coded with respect to clay content. 72

Fig. 5.11. Right, gamma ray and density logs acquired from well 7120/8-2 corresponding to transition zone and its nearby depths. Left, density-depth plot of the same depths as well log shown at the right side. The bottom plot is color coded with respect to clay content. 73
Fig. 5.12. Right, gamma ray and porosity logs acquired from well 7120/8-2 corresponding to transition zone and its nearby depths. Left, porosity-depth plot of the same depths as well log shown at the right side. The bottom plot is color coded with respect to clay content. 74
Fig. 5.13. Crossplot of velocity versus depth for wells in the Askeladd area to investigate the velocity trend before (a) and after (b) correction of exhumation. The published natural and experimental compaction curves have been included for comparison. 75
Fig. 5.14. Estimation of exhumation observed in wells (a) 7120/7-2, (b) 7120/8-1, (c) 7120/8-2, and (d) 7120/8-3, based on experimental published compaction trend of Mondol 2009. Kaolinite-silt (50:50). 77
Fig. 5.15. Tentative uplift map based on vitrinite reflection and temperature data for Norwegian Barents Sea (a) and local contour map shows exhumation estimated in Askeladd discovery by interpolation of data for each well (b). Dash line represents an approximate boarder between Snøhvit field (up) and Askeladd discovery (down). These field are located in the Hammerfest Basin where the amount of uplift ranging between around 500 m to close 1500 m..... 78

Fig. 6.1. Well correlation of different formation in the Askeladd discovery. A key reservoir unit of prograding coastal sandstones is Stø Formation with Early to Middle Jurassic age. 85
Fig. 6.2. Crossplots of Vp versus Vs for well 7120/8-4. The black trend line represents schematic linear trend among the data point that almost all data fall around this line. 86
Fig. 6.3. Vp-Vs relation plotted from well 7120/8-4 showing the deviation of empirically shear velocity relation from real shear sonic data. 87
Fig. 6.4. Crossplot of AI versus Vp/Vs in well 7120/7-2. Shear velocity calculated from published empirical relation (Castagna et al., 1993) to show the importance of reliability of input data. 88
Fig. 6.5. Crossplot of AI versus Vp/Vs for well 7120/8-4. Data point mainly concentrate close to the water saturated line indicating brine sand. According to NPD Factpages this well is dry. 89
Fig. 6.6. Crossplots of AI versus Vp/Vs for Stø reservoir in well 7120/8-4. Arrows show geologic trends including: (1) increasing gas saturation (2) increasing porosity (3) increasing cementation (4) increasing shaliness. 90
Fig. 6.7. Crossplots of AI versus Vp/Vs for Stø reservoir in well 7120/8-4. Color coded with (a) P-wave velocity, (b) shear velocity, (c) shale volume and, (d) porosity. Arrows also show increasing in different parameters; (a) P-wave velocity, (b) shear velocity, (c) shale volume and, (d) porosity. Arrows also show increasing in different parameters; (a) P-wave velocity, (b) shear velocity, (c) shale volume and, (d) porosity. 91

Chapter 1
Introduction

1.1. General Introduction

The Barents Sea is a large epicontinental sea with the depth varied from less than 100m (Spitsbergenbanken) to 500m (Bjørnøyarenna) and the area of about 1.3 million Km² (Faleide et al., 1984; Worsley, 2008). It is bounded by Novaya Zemalaya on the east, Svalbard and Franz Joseph Land on the north, and Atlantic Ocean on the west and mainland Norway in on the south (Fig. 1.1). Most of the Barents shelf covered by sedimentary deposits; therefore the area is highly concern in terms of petroleum exploration. The U.S. Geological Survey estimates that some 90 billion barrels of oil and one-third of the world's undiscovered natural gas lie hidden in the Arctic region. Norway and Russia, owner of the Barents Sea, have already begun developing the natural resources buried beneath the floor of the Barents Sea.

In the Russian sector, the giant Shtokmanovskoye gas/condensate field was discovered in 1988. The estimated gas and gas condensate reserves of 3.2 tcm (Thousand Cubic Meters) and 30 mm tons (million tons), respectively (Source: the RusEnergy agency information). Two other important gas discoveries in the Russian Barents Sea are Ledovoye and Ludlovskoye that are smaller to the Shtokmanovskoye gas field. Moreover, Pechora Sea, located in the eastern part of the Barents Sea hosting several oil/gas discoveries (Henriksen et al., 2011).

This study focuses on a gas discovery in the Hammerfest Basin, the south-western part of the Norwegian Barents Sea. Norwegian Barents Sea in compare to the North Sea and Norwegian Sea, the hydrocarbon potential is lower due to different geological history. The Barents Sea area has been affected by the extensive uplift which is cause extremely high erosion of the sediments and as a result significant leakage of hydrocarbon occurred through cap rocks (Gabrielsen et al., 1990). The southern part of the Norwegian Barents Sea is studied and exploits more than the Northern part. The first seismic surveys were done in the early of 1970 that was show most of the area is covered by sedimentary rocks. Hydrocarbon exploration drilling started in 1980 and until now 96 exploration wells have been drilled in the Norwegian Barents Sea, with more than half of these located in a relatively small area either in, or in close proximity to the Hammerfest Basin (NPD Factpages).

The Hammerfest Basin has several discoveries including Snøhvit, Askeladd, Alka and Albatross. The Snøhvit development comprises three discoveries-Snøhvit, Albatross and Askeladd has

started production since 2007. Goliat, the first oil field in the area will start production in 2013. There are several reasons slowdown the developments of the exploration and development in this area such as: widespread distribution of hydrocarbon, low price of the natural gas, distance to potential market, difficult logistics, drilling restriction and environmental issues. The two recent discoveries (Skrugard and Havis) in the Norwegian Barents Sea are now triggering an increased interest in this huge, largely unexplored petroleum province. In the future, more consideration should be given to the research and development on this area since both change of universal economic conditions and also develop of the advanced technology resulting reduction the risk of investment.

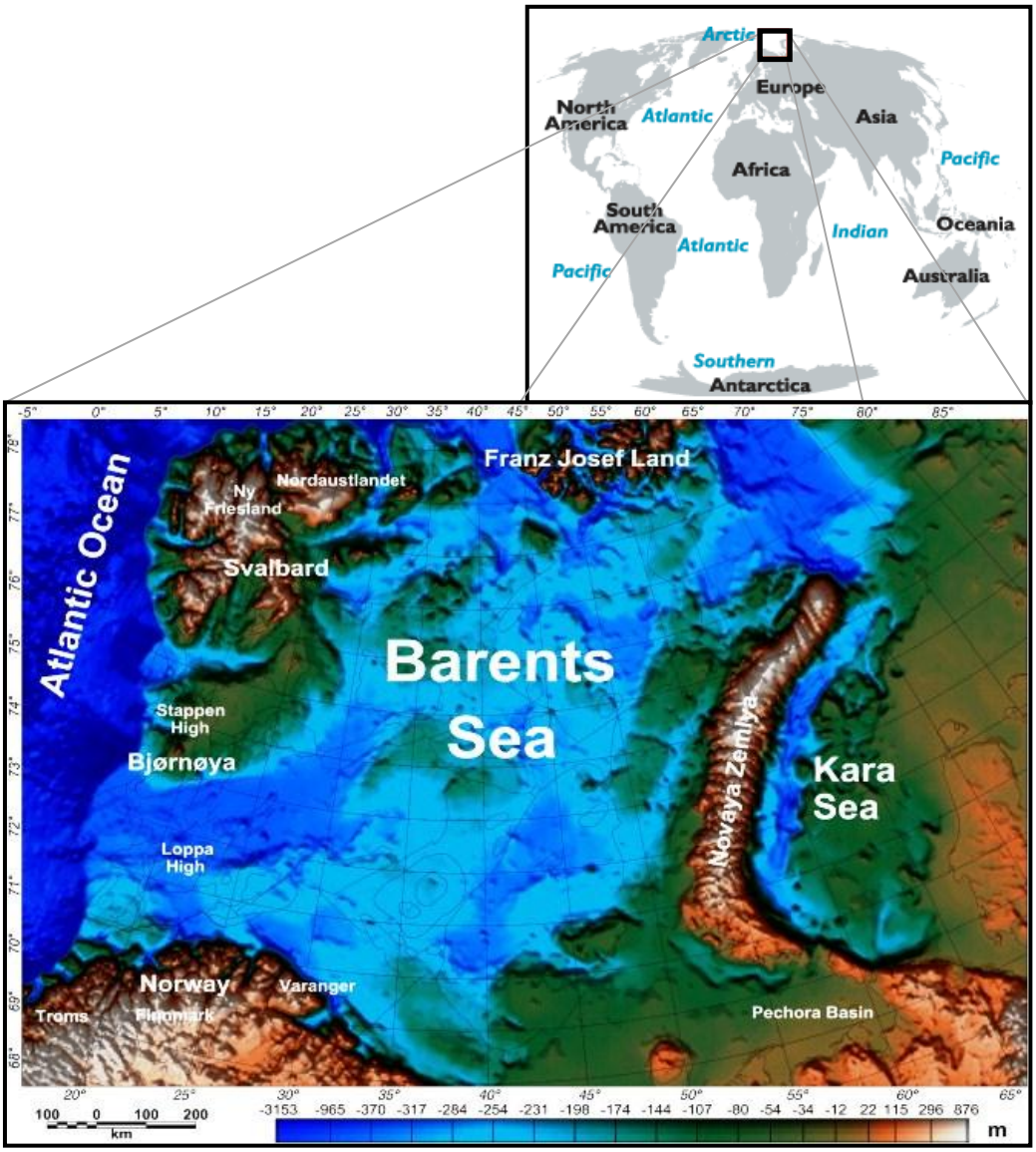

Fig. 1.1. Location of the Barents Sea with bathymetry and topography map (modified after Barrère et al., 2008).

1.2. Motivation

"We will provide geological knowledge about the Barents Sea so that the oil companies can make new discoveries more easily." Faleide (Mr. Barents Sea)

The quest for energy dramatically increases nowadays. However, there is more concern than alternative energy; fossil fuels still stay on high demand. In fact, industrialization of societies is an important factor to order more energy and due to limitation of the resources, the amount of these resources declined consequently. On the other hand, most of the petroleum province to be explored and therefore the ultimate goals are new discoveries in the old area or enhanced the oil recovery. To achieve this goal, oil companies use the new tools to get better data and as a result improved the efficiency of the petroleum fields. In other words, whatever our knowledge than the petroleum systems increasing, the outcome will be more satisfactory.

Reservoir characterization, an integral part of exploration, development and enhance recovery, try to build a model of a reservoir that includes all the characteristics related to its ability in terms of store and produce the hydrocarbon. Therefore it can help to manage the petroleum reservoirs and increase the production. Various sources provide the information need to predict the reservoir properties. General reservoir characterization information such as seismic data and rock physics with integration into the specific reservoir characterization like well data and production history, are the main information should be considered in any reservoir characterization studies (Eidsvik et al., 2004). One of the most significant tools in reservoir characterization is rock physics which link between geophysical data observation to physical properties of rocks to understand the reservoir properties such as porosity, permeability and saturation.

Rock physics diagnostics play a key role as a new geophysical tool because of some benefits bring: a) hydrocarbon detection during exploration; b) identify the shape, size and extent of the hydrocarbon reservoirs; c) reservoir characterization to delineate the heterogeneities of the reservoir and d) reservoir forecasting during production (Avseth, 2000). Extrapolation of data (both geological parameters and seismic observables) away from wells is one of the most powerful applicatioc of rock physics known as "What if" analysis (Avseth et al., 2005).

1.3. Research Objectives

This research is considered a part of the BarRock (Barents Sea Rock Properties) project that focuses on the analysis of rock properties in shales and sandstones in the uplifted Barents Sea area. Moreover, the BarRock project investigates the petroleum system in the Barents Sea by studying porosity, permeability, seal integrity and deformation related to primary and secondary petroleum migration in uplifted cemented sedimentary sequences.

The main objective in the study are to examine the compaction behavior of whole sedimentary sequence and characterization of reservoir rocks in the Askeladd discovery by integrating well logs, seismic, published lab data and rock physics theories. The specific goal can be describe in detail as below:

1. Investigate compaction behavior (both mechanical and chemical compaction) and evolution of rock properties of thick sedimentary successions in the Askeladd area to define the transition zone between mechanical and chemical compaction by comparing well logs and literature data.
2. To investigate diagenetic evolution by comparing time, temperature and depth that corresponds to burial, uplift and reburial history of the Barents Sea sediments.
3. Exhumation estimate based on the changes of three important rock parameters such as P-wave velocity, total porosity and bulk density as a function of depth. Perform rock physics diagnostics of reservoir rocks that includes.
    - Cross-plots of V_p/V_s ratio versus acoustic impedance (AI) for lithology and fluid separation.
    - Finding the relationship between P-wave velocity and shear velocity by using the empirical rock physics relations and comparison of a well in the area where we have V_s data. Calculate porosity, net-to-gross ratio of reservoir rocks and to find their lateral distributions in order to explain their depositional environments.

1.4. Study Area

The Askeladd discovery is located in the south-western portion of the Hammerfest Basin, central part of the block 7120/8 in the Tromsø I area, Norwegian Barents Sea. It is situated 100 Km north from the mainland Norway. The Askeladd structure is filled by relatively dry gas with approximately 5% CO_2 and no H_2S (Westre, 1984). Central part of the block 7120/8 in the Tromsø I area. The gas filled structures in the Askeladd discovery are associated with these downward stepping faults (Fig. 1.2b).

The Hammerfest Basin is composed of huge amount of Upper Paleozoic to Cenozoic sedimentary rocks. It is bounded by Finnmark Platform in the south, Loppa High and Bjarmeland Platform in the north and towards the west the basin connects to the Tromsø Basin through a series of downward stepping faults (Fig. 1.2a).

The Askeladd Field was the first significant find made by Statoil in late 1981 with well 7120/8-1 in the Tromsøflaket. The size of Askeladd gas field was determined by drilling the well 7120/8-2 in 1982. Besides these wells, two other wells drilled in this block, well 7120/8-3 in 1983 and the newest well 7120/8-4 which was drilled in 2007.

The Askeladd gas field can be subdivided into three parts: western, central and northern (Fig. 1. 2b). In the west Askeladd (Askeladd Vest) where the block 7120/7 is located, one well (7120/7-1) drilled in 1982 (not include in this study). The central section (Askeladd central) has one well, 7120/7-2 that was drilled in 1983 and the northern part (Askeladd Nord) has four wells 7120/8-1, 7120/8-2, 7120/8-3 and, 7120/8-4 that the last one drilled in 2007.

According to the completion report, the gas water contact (GWC) in well 7120/8-1 is 2180 m KB in the Jurassic reservoir sandstone. Generally the reservoir sandstones in Askeladd field showed good to excellent reservoir properties. However, as we will discuss later tectonic activity in this area had a significant influence on the reservoir properties and caps rocks integrity.

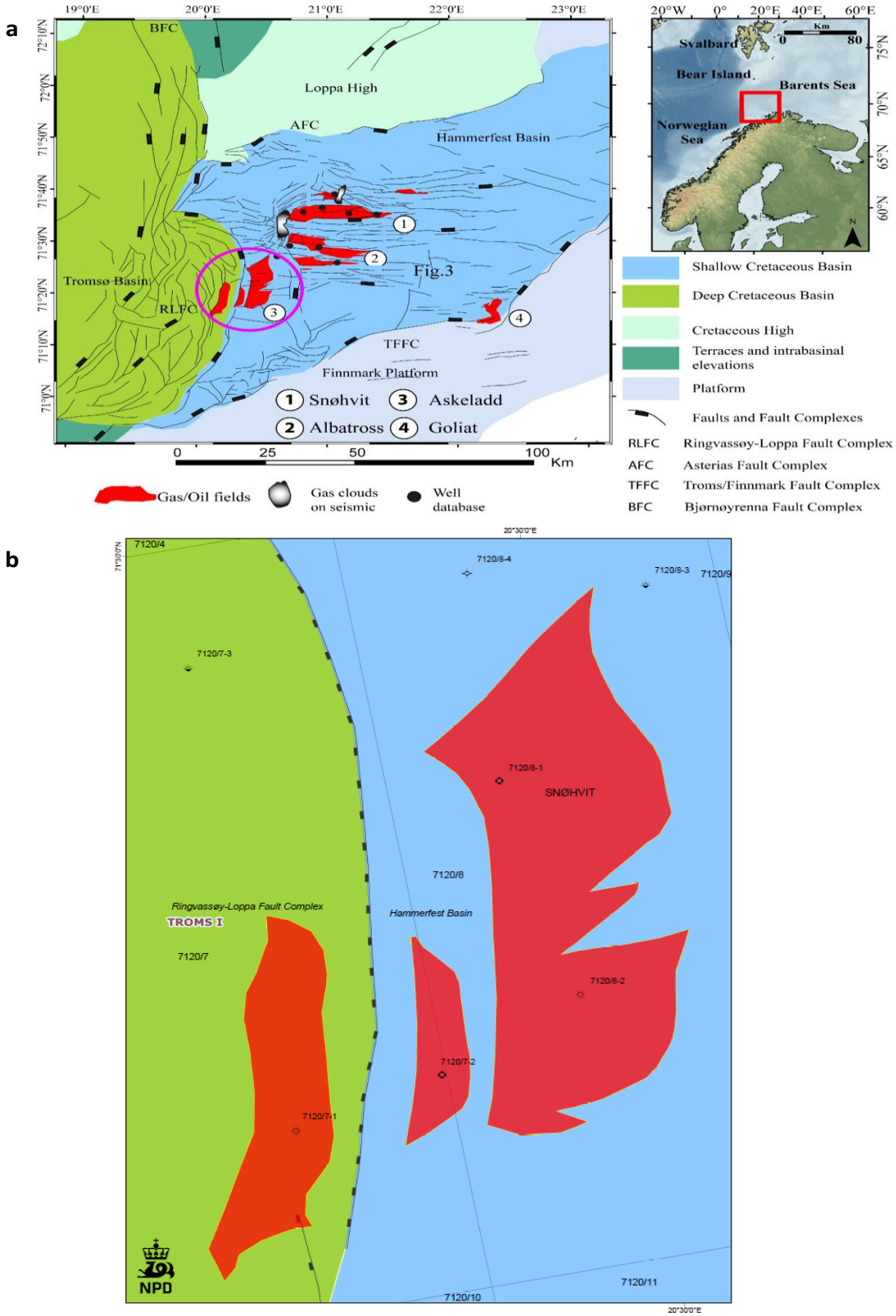

Fig. 1.2. (a) Location map of Hammerfest Basin (modified after Ostanin et al., 2012) (b) Askeladd gas field discovery and sections (modified from NPD Factpages 2012)

1.5. Chapter Description

Chapter 1 is an introduction that is including general overview of the Barents Sea, motivation and objectives of the research, an overview of the study area, limitation and future implication.

Chapter 2 is mainly based on literature reviews and discussing the geological history of the Barents Sea. Geological setting of the Barents Sea and Hammerfest Basin in addition to stratigraphy of groups and formation present in terms of lithology, depositional environment and geologic age. In the second part, petroleum systems dominated in the region is covered in terms of essential elements and processes need to form the petroleum system such as source rocks (generation-migration), reservoir rocks, seals and trap formation.

Chapter 3 describes the materials and methods used in this study. It has divided into database and methodologies used for compaction study and rock physics diagnostics.

Chapter 4 focuses on theories behind the diagenetic processes influence the rock properties, as well as theoretical background of rock physics diagnostics.

Chapter 5 shows results of compaction study and evolution of rock properties as a function of diagenetic process as well as discussion of results. Evaluation of the compaction and estimate the exhumation occurred in the area is the main issues It has subdivided into compaction evaluation studies based on well logs data and exhumation estimation based on comparison of well log data and published compaction curves.

Chapter 6 includes rock physics diagnostics of reservoir rocks particularly the Stø Formation as the main reservoir in the Askeladd discovery.

Chapter 7 is the last part of the thesis will draw conclusions and make a summary of this research.

1.6. Limitation and Future Implications

This thesis is a time limited work while the area of interest seems unlimited. Shear velocity is crucial for rock physics diagnostics and analysis although it is not easy going work to achieve. We had only one well with shear velocity data and for others we used the empirical equations that are not always described the data. The main focus in this thesis is on the reservoir rocks whereas the source rocks, overburden and trap are significant as petroleum systems studies. Moreover, this study has not incorporate core data which are containing valuable information. This is related to time to get permission of sampling, sample preparation and analysis. We also had 3D seismic cube (ST8320) covering study area but we are not using them because of time limitation. To show a more comprehensive reservoir characterization and compaction behavior of sedimentary sequences, one can extend this work even further by combining two other theses which are focusing on two other discoveries (Albatross and Snøhvit) in the Hammerfest Basin and not far from the study area.

Chapter 2
Geological Background

2.1. Geological Setting

2.1.1. Greater Barents Sea

The greater Barents Sea is an intracratonic basin which is subdivided into platforms areas and basins (Dore, 1995).. It is formed by continental collision and subsequently breaks down due to the continental separation. The Caledonian orogeny was the first collision event dates back approximately 400 Ma since the Iapetus Ocean closed. The combination of the Laurentian plate (Greenland, North America) and the Baltic plate (Scandinavian, western Russia) was the result of Caledonian orogeny (Dore, 1995). The Uralian orogeny took place about 240 Ma, in Late Permian-Early Triassic time due to the collision between western Siberia and Laurasian continent. It was the final stage of the merging the continents into a single supercontinent called Pangea in the Permian-Triassic time (Dore, 1995).

Structural framework (Fig. 2.1) of the Barents Sea is almost dominated by the ENW-WSW to NE-SW and NNE-SSW to NNW-SSE trends with local impact of WNW-ESE striking elements (Gabrielsen et al., 1990). There are three main structural elements in the western Barents Sea: Tromsø basin, Bjørnøya basin and Svalbard Platform (Faleide et al., 1993). The western Barents Sea is dominated by a large thickness of sediments ranging from Upper Paleozoic to Cenozoic and composed of three different regions (Faleide et al., 1993):

- The continental margin with three main segments: a) a sheared margin developed along the Senja fracture zone (south); b) a rifted complex with volcanic activity in the southwest of the Bjørnøya basin (central); c) along the Hornsund fault zone, a sheared and rifted margin (north). The COT (continent-ocean transition) occurred over a narrow zone in Early Tertiary continental break up (extensional regime). Post rift sedimentation in the area formed the thick sedimentary wedge succession of Upper Cenozoic.
- The Svalbard Platform was underlined by a relatively flat succession of Upper Paleozoic and Mesozoic deposit.
- A region between Svalbard Platform and Norway mainland that can be dividing into a number of subbasins and high characterized by increasingly noticeable structural relief toward the west.

The post Caledonian tectonic history of the Barents Sea is completely different where the extensional tectonic regime starting to develop in this region. It was started by progressive continental break-up of the Pangea supercontinent. Extensional tectonic movement during the Late Paleozoic-Early Mesozoic undergone the Barents Shelf resulted rift basin system dominated in the area. The major rift phase took place in the western Barents Sea are as below:

- Late Devonian-Carboniferous
- Middle-Jurassic-Early Cretaceous
- Early Tertiary

Extensional tectonic regime as discussed above was the predominant event controlling the structural elements pattern and also basin sedimentation infill during the Late Paleozoic in the western Barents region. The crustal extension taken place in Late Paleozoic followed by the later extension and as a result rifting migrated toward the west, pull-apart basins formed in the southwest, and a belt of strike-slip faults developed in the north. However at the same time, the Svalbard Platform and the eastern part of the basin province have been stable since Late Paleozoic and epirogenic tectonic movement was the only remarkable tectonic activity in this area. The Norwegian Barents Sea (western Barents Sea) has been most active part of the greater Barents Sea during Mesozoic and Cenozoic. Johansen et al., 1993 proposed that the rifting episodes also recorded in Carboniferous, Permian, Triassic and Late Jurassic-Early Cretaceous time resulted to formation of the rift basin in the Barents area. Throughout Triassic period, two important events were subsidence and salt tectonic (Gabrielsen et al., 1990). Rifting activities associated by block faulting continue during the middle Jurassic and increased in the Early Cretaceous. In fact, increasing of rifting activity over the Late Jurassic-Early Cretaceous provided enough accommodation space for thick Cretaceous sedimentary strata. In the northern parts of the Barents Sea, significant volcanic event of the Early Cretaceous affected the area. This volcanism believes to be a part of the Large Igneous Province consists of the Greenland, Svalbard, Franz Josef Land and adjacent shelf area.

The Late Cretaceous time undergone by reverses faulting and folding (basin inversion) associated by extensional fault system along Bjørnøyrenna fault complex (Gabrielsen et al,. 1997). Norwegian Barents Sea experienced the main continental break-up in the middle of

Cenozoic (Oligocene) Era. Geological history of western Barents Sea end up with an extensive uplift event in the Late Cenozoic (Pliocene-Pleistocene) and the subsequent erosion of approximately 3 kilometer of sediments in some region (Nyland et al., 1992).

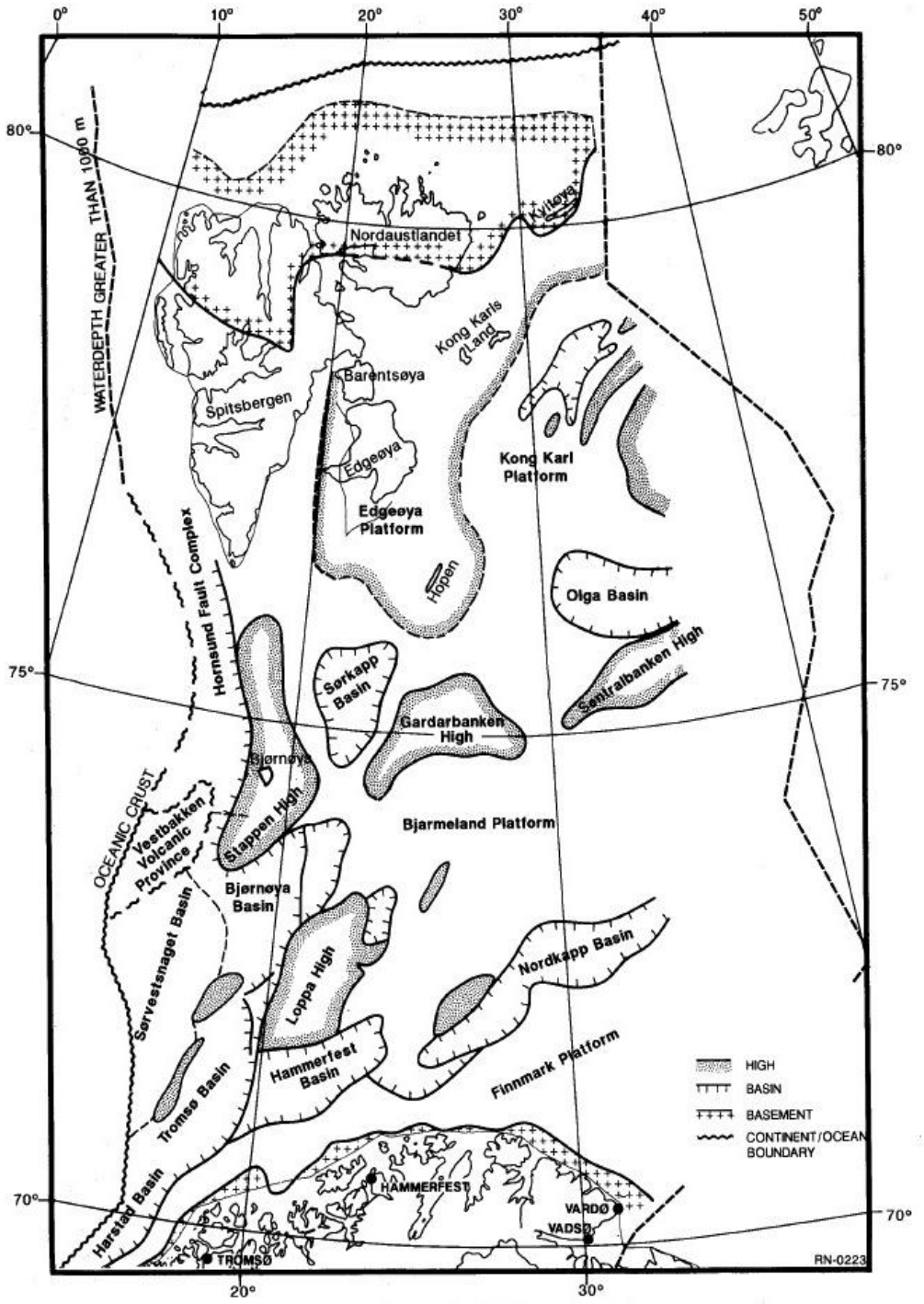

Fig. 2.1. Tectonic framework of the Barents Sea region (Gabrielsen et al., 1990).

2.1.2. Hammerfest Basin

The Hammerfest Basin developed in Mesozoic (Late Jurassic to Early Cretaceous) and bounded by Loppa High and Bjarmeland Platform in the north, Finnmark Platform in the south and the Tromsø Basin in the west. It is a faulting controlled rift basin and composed of western and eastern subbasin which is separated by the extension of the Trolfjord-Komaglev fault (Gabrielsen & Færeseth, 1998). Tectonic history of the basin based on the deformation style revealed that extension has been dominated in the area and strike-slip faulting also led to reactivation of the older faults during Late Jurassic to Early Cretaceous (Gabrielsen et al., 1990). The Hercynian and early Kimmerian tectonic events had not significant affect in this area but the movement seems initially started during the Late Kimmerian orogeny of Late Jurassic time. It was the main tectonic phase associated with tensional regime. Several Large NNW-trending normal fault formed by the Late Kimmerian tectonic phase.

The Hammerfest Basin is a fault blocking basin therefore it is important to classify the fault particularly to understand the petroleum systems dominated in the area. Berglund et al., 1986 defined five different types of fault complexes in the Hammerfest Basin (Fig. 2.2):

- Type 1: one or two major listric faults associated with roll-over anticline and anticline faults represented by the Tromsø-Finnmark Fault Complex (TFFC).
- Type 2: normal fault that were reactivated several times indicates the Ringrussøy-Loppa Fault Complex (RLFC).
- Type 3: two large normal faults dipping south and represented the southern Loppa High Fault Complex (SLHFC)
- Type 4: normal fault with E-W trend that were reactivated in the Early Cretaceous. Although initially strike-slip region led to developing these faults together with updoming along SLHFC at the end Jurassic time.
- Type 5: shallow faults (no penetration the lower Triassic) also dominated in the region and their architecture is similar to the growth faults.

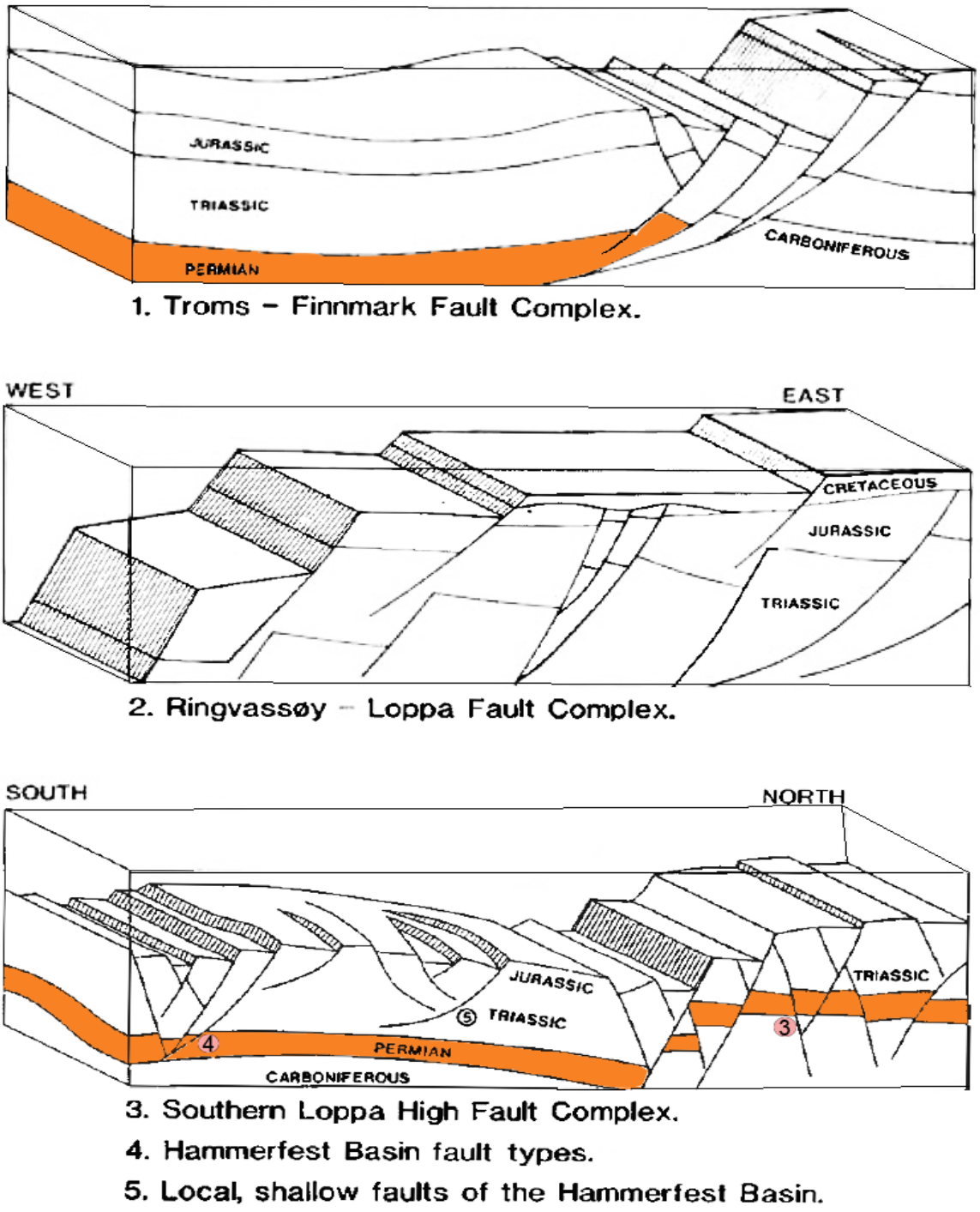

Fig. 2.2. Fault-types of the Hammerfest Basin and the Loppa High (modified after Berglund et al., 1986).

2.2. Stratigraphy

The lithostratigraphic distribution in the area of study shows a great deal of variety from shallow marine sandstones towards deep marine shales (Henriksen et al., 2011). Claystones with interbeded siltstone and dolomite are forming the main lithology domination in quaternary and tertiary whereas cretaceous which is mostly covered by claystones. The Jurassic succession represents both sandstones and shale however the sand bodies mainly date back to Lower and Middle Jurassic. Upper Jurassic succession dominated by deep marine shales with quite high amount of organic matter (Hekkingen Formation). The main reservoir rock believed to refer back Early to Middle Jurassic Stø Formation. Triassic and Permian lithofacies are mostly consisting of marine siliciclastic mudrocks (Henriksen et al., 2011). The oldest rock in Hammerfest Basin related to fluvial to deltaic Carboniferous sediment.

2.2.1. Nordland GP

The Nordland Group is dominated by sandstones and claystones, the sand content increasing upwards. On the upper parts of the group, metamorphic rock, quartzite and granite (cables and boulder) and clays was observed. These kinds of sediments indicate the bathyal to glacial marine environments which are mainly having glacial and post-glacial origin in the Hammerfest Basin. The age is Late Pliocene to Pleistocene/Holocene in the Hammerfest Basin whereas along western shelf margins the age back to the mid-Oligocene. The Nordland Group sequences in the Hammerfest Basin are the youngest sediments based on well data. However only some parts of the sediments was represent in the study area and the thickness is varied from about 250 m in the southern wells to less than 80 m in the study area well (7120/8-4).

2.2.2. Sotbakken GP

The Sotbakken Group is dominated by claystones, minor siltstone, tuff and carbonate. Tectonic activity on the Barents Shelf in the middle Oligocene-Early Pliocene caused the vast erosion in the sediments that were subjected by uplift. Therefore the upper part of the Sotbakken Group is not preserved in the eastern parts of Tromsøflaket. The preserved sequences only observed over the Ringvassøy - Loppa Fault Complex and in the Tromsø Basin where show the late Paleocene to Early/Middle Eocene (Thanetian-Ypresian/Lutetian) age in central and eastern parts of the Hammerfest Basin (Spencer et al., 1984). The thickness is varied from 300 m in the southern

margins of Hammerfest Basin to 1 km in the southwestern parts of the basin but in the study area the maximum thickness was observed about 810 m in the reference well (7120/8-4). Due to transgression occurred in the Barents Sea in the mid-Paleocene, the depositional environment suggested is sublittoral to deep marine shelf that provided a suitable accommodation space for thick claystone layers. The only formation that is recognized within the Sotbakken Group is Torsk Formation with Late Paleocene to Oligocene age.

2.2.2.1. Torsk Fm

The formation mostly is dominated by grey or greenish-grey generally non-calcareous claystones and also small amount of interbeded siltstone or limestone observed throughout the section, and in the lower part tuffaceous horizons dominated. The sediments succession age is Late Paleocene to Oligocene where deposited on the open to deep marine shelf environment. The thickness is approximately 345 m in the type well whereas in the study area shows increasing up to 810 m in the northern parts (7120/8-4).

2.2.3. Nygrunnen GP

The Nygrunnen Group is dominated by greenish grey to grey claystones with thin limestone on the Tromsø Basin and western parts of the Hammerfest Basin and become more calcareous or sandy condensed sequences in the southern and eastern parts of the Barents Sea and. The age will be varied from late Cenomanian to Maastrichtian (Late Cretaceous).As we can see from sediments types, the depositional environment suggested for this group show a diversity from open marine, deep shelf environments in the west passed into shallower shelf regimes (uplifted at times) in the east. The Thickness approximately 250 m in the type area in the Hammerfest Basin and decrease eastward to less than 50 m, but in the study area is about 94 m (well 7120/8-1). Two formations can be defined within this group, the Kviting and Kveite Formations.

2.2.3.1. Kveite Fm

The Kveite Formation lithology is consists of the greenish-grey to grey shales and claystones associated with thin interbeds of limestone and siltstone. The age suggested for the Kveite Formation is late Cenomanian to early Maastrichtian (Late Cretaceous). In terms of depositional environments, the Kveite Formation indicates the deep open shelf with normal circulation. The maximum thickness in the reference well is about 1200 m whereas in the study area decrease to

115 m (7120/7-2). This formation laterally thinning eastwards and change to the sand and carbonates of the Kviting Formation.

2.2.3.2. Kviting Fm

Lithology represents in the Kviting Formation is calcareous sandstones with interbeded sandy and glauconitic mudstones of the Late Cretaceous age (Campanian). The depositional environment determined in this formation is deep to shallow shelf environments with normal circulation. The lateral extension of the Kviting Formation is restricted to central and eastern parts of the Hammerfest Basin and the thickness is about 17 m in the type well and increases in the study area to 133 m (7120/8-3).

2.2.4. Adventdalen GP

The thickness of this group is about 1000-1750 m in Barents Sea but in study area is about 1000 based on well data. Sediments dominated including shales, siltstones and sandstones with Late Jurassic to Early Cretaceous age. During the late Cretaceous uplift this group was eroded. The Adventdalen Group dominated by mudstones, deltaic and shelf sandstones and also carbonate condensate layers therefore depositional environment will be varied from marine to deltaic progradation sediments. The Fuglen, Hekkingen, Klippfisk, Knurr, Koljeand Kolmule Formations are defined within the group on the Barents Sea. However, in the study area Klippfisk was not observed. The main source rock in the Barents Sea, Hekkingen Formation is consists of marine black shale with about 20% TOC and Upper Jurassic age.

2.2.4.1. Kolmule Fm

The Kolmule Formation is dominated by Dark grey to green claystone and shale, thin siltstone interbeds and limestone and dolomite stringers. Moreover, traces of glauconite and pyrite observed in this formation. The age of this formation is Aptian to mid-Cenomanian (Early to Late Cretaceous) where the sediments deposited in the open marine environment. The thickness will be varied from 945 m in the type well to about 574 m in the study area reference well (7120/7-2) and the lateral extension into Tromsø Basin shows thicker deposits in compare to a slight increase toward the Hammerfest Basin.

2.2.4.2. Kolje Fm

The Kolje Formation is dominated by Dark brown to dark grey shale and claystone with limestone and dolomite interbeds. However, in the upper part of the formation, thin interbeds of light grey-brown siltstone and sandstone also observed. The age suggested for this formation is early Barremian to late Barremian/early Aptian (Early Cretaceous). The depositional environment suggested for this formation is distal open marine environment with high amount of water circulation. The Kolje Formation is thicker westward in compare to the central part of the Hammerfest Basin and shows different thickness from about 437 m in the type well to 321 m in the study area reference well (7120/7-2).

2.2.4.3. Knurr Fm

The lithology of the Knurr Formation comprises the dark grey to greyish brown claystone with thin limestone and dolomite interbeds. In the lower parts of this formation thin sandstones are also seen, but there is no lateral extension of the sandstones toward the Hammerfest Basin. Based on microfossils the age of the Knurr Formation is suggested Ryazanian/Valanginian to early Barremian (Early Cretaceous). Distal open marine environment is the depositional environment suggested for this formation. The thickness of is 56 m in the type well whereas in the study area decrease to about 30 m in the reference well (7120/7-2).

2.2.4.4. Hekkingen Fm

The Hekkingen Formation is a main source rock in the Hammerfest Basin and consists of brownish-grey to very dark grey shale and claystone with thin interbeds of limestone, dolomite, siltstone and sandstone. The gamma ray values show increasing in the lower parts of Hekkingen Formation (20% TOC). Production of organic matters need an anoxic environment with little water circulation and one of the environments can provide this condition is deep marine waters. Based on palynomorphs, the age was suggested for the Hekkingen Formation is late Oxfordian/early Kimmeridgian to Ryazanian (Late Jurassic). The thickness is varied from about 360 m in the type well to about 85 m in the study area wells. The thinning toward the north occurred along the axis of the Hammerfest Basin and indicates that the development of the semi-graben structures along the basin margins while doming was active along the basin axis. The

Hekkingen Formation can subdivide into two members; the lower Alge member and the upper Krill Member.

2.2.4.4.1. Krill Mbr

Krill Member is the Upper part of Hekkingen Formation and dominated by brownish-grey to very dark grey shale and mudstone with thin interbeded limestone, dolomites, sandstones and siltstones. The thickness of the Krill Member in the study area based on the reference well is about 50 m but the maximum thickness is about 300 m in the other areas. The age is about Kimmeridgian -Volgian and the unit was deposited in the open marine shelf environments.

2.2.4.4.2. Alge Mbr

This member forms the lower parts of Hekkingen Formation and dominated by black paper shales with high content of organic matter. The thickness is about 29 m in the reference well in the study area and the maximum thickness reach 50 m in other areas. Based on palynology and macrofossils, the age of the Alge member is about Late Oxfordian-Kimmeridgian. Depositional environment of the Alge member is marine shelf environment (Dalland et al., 1988).

2.2.4.5. Fuglen Fm

The Fuglen Formation is dominated by pyritic dark brown mudstones with interbeded white to brownish grey thin limestone. The age of this formation is about Late Callovian to Oxfordian (Upper Jurassic). The thickness in the study area is about 10 m but in the different areas reach to 50 m. during the highstand associated with tectonic movement the Fuglen Formation deposited in the marine environments. It is believed that, Fuglen Formation is one on the cap rocks of hydrocarbon in the Snøhvit field in addition to the Hekkingen Formation.

2.2.5. Kapp Toscana GP

The Kapp Toscana Group is composed of shales, sandstones and siltstones of Late Triassic to Middle Jurassic (Ladinian to Bathonian). Five formations can be defined within this group that is mostly dominated by sandstones and shales hence shallow marine to deltaic (fluviodeltaic) deposits may be represented the depositional environment for this group. The thickness will be

varying up to 475 m in Svalbard to about 373 m in the reference well (7120/7-2) on the study area and 2000 m in the Barents Sea shelf region

2.2.5.1. Stø Fm

The Stø Formation is the main reservoir rock of Early to Middle Jurassic (late Pliensbachian to Bajocian) age in the Hammerfest Basin. The main lithology dominated in this reservoir is sandstone with good to excellent reservoir properties (well sorted and mature sand). It is also contain thin layer of siltstone and shales. Therefore the depositional environment which fit this lithology is prograding coastal regimes. Regional transgression although occurred in the late Toarcian and late Aalenian and shales and siltstones intervals deposited.

The Stø Formation defined by three depositional sequences: the base defined by transgressive episodes and it is only present in the western parts of the Hammerfest Basin. Maximum transgression in the area occurred in the middle sequence (Toarcian/Aalenian). The last sequence (Bajocian) is highly variable because it is belonging to the syn-depositional uplift. In southwestern wells thickness rich maximum while thinning generally eastwards. In the study area the thickness of Stø Formation is about 100 m.

2.2.5.2. Nordmela Fm

The Nordmela Formation is dominated mainly by sandstones, interbeded siltstones, shales and claystones with minor coals. The age of this formation is Early Jurassic (Sinemurian to the late Pliensbachian). The suggested depositional environment for this area is tidal flat to flood plain environments but especial sandstones present within the formation represented the estuarine and tidal channels which dissected this low-lying area. The early Kimmerian subsidence over the site of the Ringvassøy-Loppa Fault Complex led to increasing thickness westward. The thickness in the type well is 62 m while in the study area it is reached approximately 150 m.

2.2.5.3. Tubåen Fm

The Tubåen Formation is consist of the stacked series of high energy marginal marine sandstones just identify tidal inlet dominated barrier complex and/or estuarine and also marine shale which represent the more distal depositional environment. Shale volume will be increases towards the northwest while coals were found near southeastern basinal margins while die out to the

northwest. The formation age refer back to the Late Triassic to Early Jurassic (late Rhaetian-early Hettangian). The highest thickness is observed in the Askeladd field within two blocks (7120/7 and 7120/8) and reach 147 m in well 7120/8-4 in the Askeladd Beta discovery.

2.2.5.4. Fruholmen Fm

The Fruholmen Formation dominated by grey to dark grey shales which is gradually changing into the interbeded sandstones, shales and coals. The age of the Fruholmen Formation is Late Triassic-Early Jurassic (Norian-Hettangian). Depositional environments will be varied from open marine into coastal and fluvial sequences. In fact, the central parts of the basin covered by flood plain deposited whereas the northern part represents the fluvial deltaic progradation environment.

The thickness of the Fruholmen Formation is about 221 m in the type well whereas in the study area show decrease to about 140 m. Three members can be defining in this formation, the Akkar (Squid) Reke (Prawn) and Krabbe (Crab) members (Dalland et al., 1998).

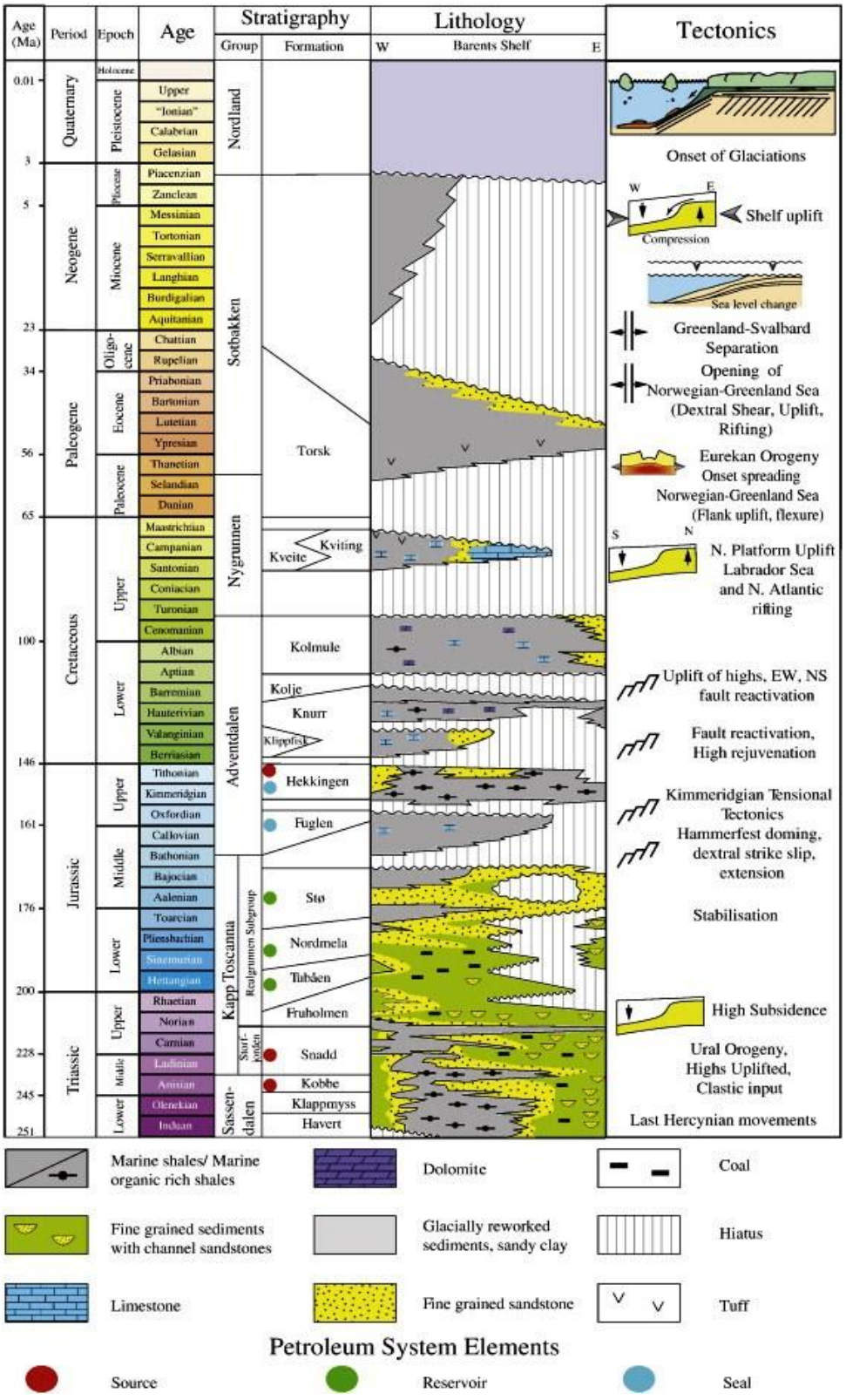

Fig. 2.3. Generalized lithostratigraphy of the Barents Sea area, with major tectonic events in the area. The potential source rocks and reservoir rocks also indicated in this figure (Ostanin et al., 2012).

2.3. Petroleum Systems

The petroleum system is an old concept needs to develop all times. Magon and Dow (1994) discussed this idea in more detail and we are following their definition and ideas entire this section. "A petroleum system encompasses a pod of active source rock and all related oil and gas and includes all essential elements and processes needed for oil and gas accumulation to exist." There are two crucial concepts to be concern, first the essential elements which are source rock, reservoir rock, seal rock and overburden rocks. Then the processes include the generation, migration, accumulation and entrapment of hydrocarbon in the sedimentary basins. According to the petroleum system event charts, all events must be place in proper time and space (Fig. 2.4). Critical moment try to highlight the point that, the generation and migration of the hydrocarbon must be place after formation of the hydrocarbon traps, otherwise redistribution may be occurred.

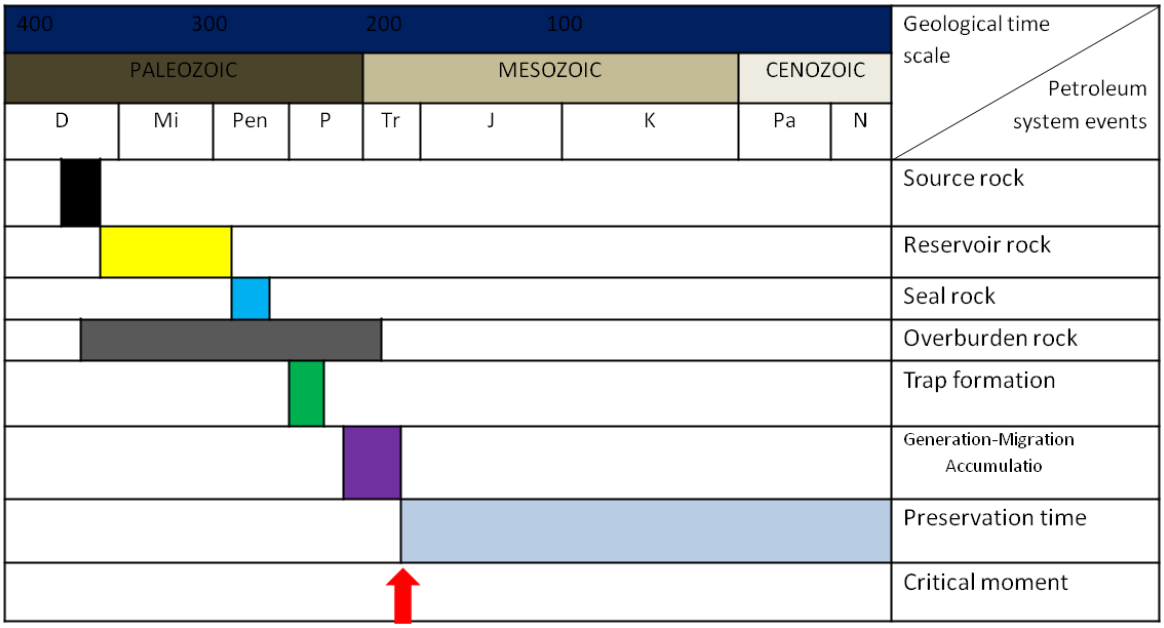

Fig. 2.4. Petroleum system event s chart (modified after Magon and Dow, 1994)

Three main petroleum systems defined in the Barents Sea including: Paleozoic, Triassic and, Late Jurassic as demonstrated in Figure 2.5. As we can see from the figure, distribution of the Mesozoic petroleum system in the Norwegian Barents Sea is higher in compare to Russian Barents Sea whereas Paleozoic petroleum systems mainly refer to the Russian part of the Barents Sea (Henriksen et al., 2011).

The greater Barents Sea is an overfilled petroleum system but nevertheless several uplift events during the evolution of this basin, resulted the depletion of hydrocarbon. The uplift consequences extensive erosion of overburden sediments and leakage of hydrocarbon will be expected but it is not the only risk associated by uplifment in the Barents Sea region. Redistribution of the remaining oil and gas is another problem because hydrocarbon distributes over a large area hence exploration plan shifted to the traps with amount of leakage (partly leakage) in the area of interest. It means hydrocarbon will be migrated to the traps which are under other circumstances would not be filled. Hydrocarbon continues to generate while the temperature remain at the proper level. Uplift and erosion reduce the temperature in the Barents region therefore hydrocarbon generation may be end up in some area. Goliath and Nucula oil discoveries prove that, the Barents Sea is not only gas prone petroleum filed lead to more oil discoveries in the Barents Shelf (Ohm et al., 2008).

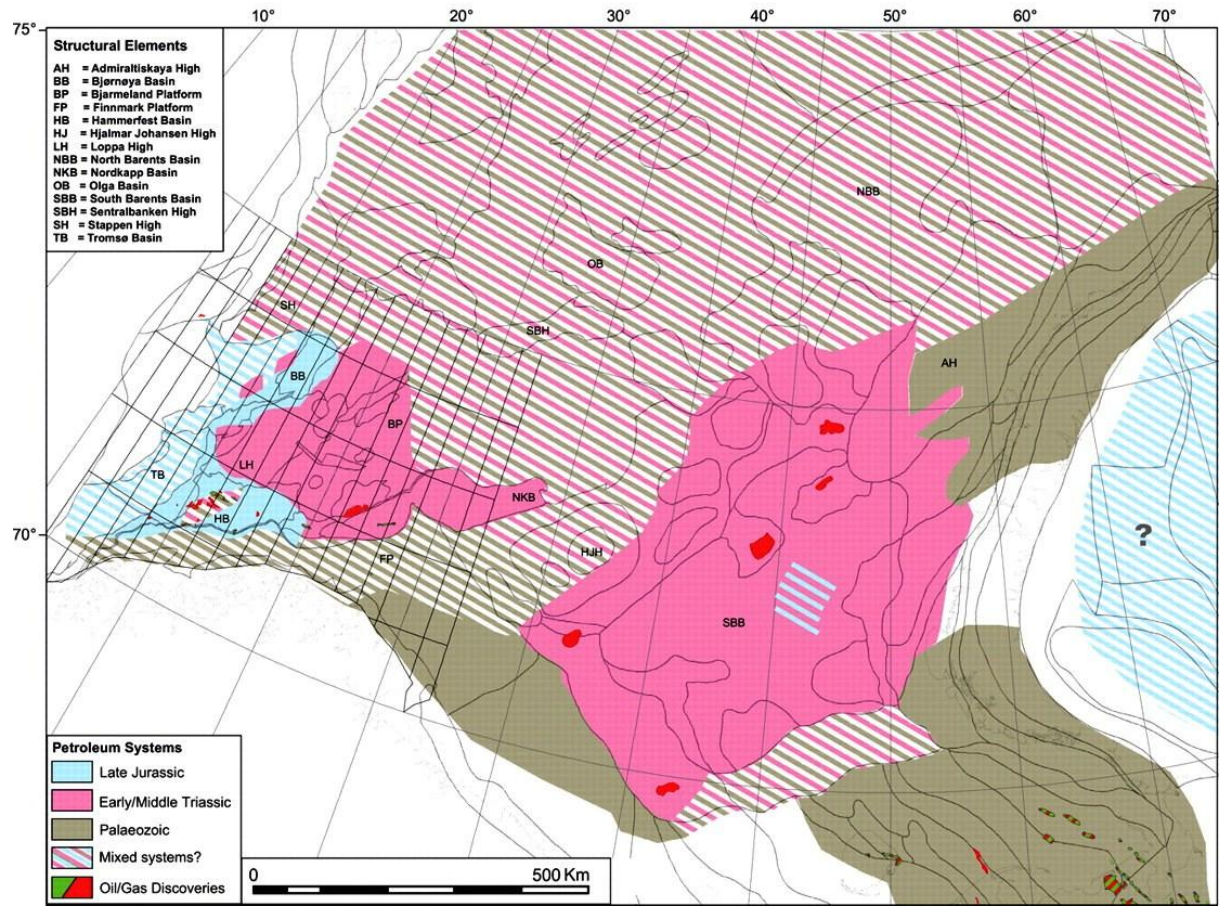

Fig. 2.5. Petroleum systems of the greater Barents Sea (Henriksen et al., 2011).

2.3.1. Source Rocks

Ohm et al., (2008) considering the Norwegian Barents Sea as an overfilled petroleum system with multisourced petroleum source rocks ranging from Carboniferous to the Cretaceous. Based on analysis of the samples gathered from the Norwegian Barents Sea, the Upper Jurassic Hekkingen Formation shale is the most favorable source rock (high TOC) entire the region. Although different source rocks (Fuglen, Nordmela, Tubåen, Snadd, Kobbe and Permian source rocks) dominated in the area have potential to generate hydrocarbon (multisourced basin).

The vitrinite reflectance is a good indicator for petroleum source rocks maturation. The Figure 2.6 illustrated the Ro versus depth for 67 exploration wells in the western Barents Sea. The maturation trend demonstrates that, Barents Sea source rocks are more mature than North Sea. It is due to the higher temperature gradient dominated in the Barents Sea.

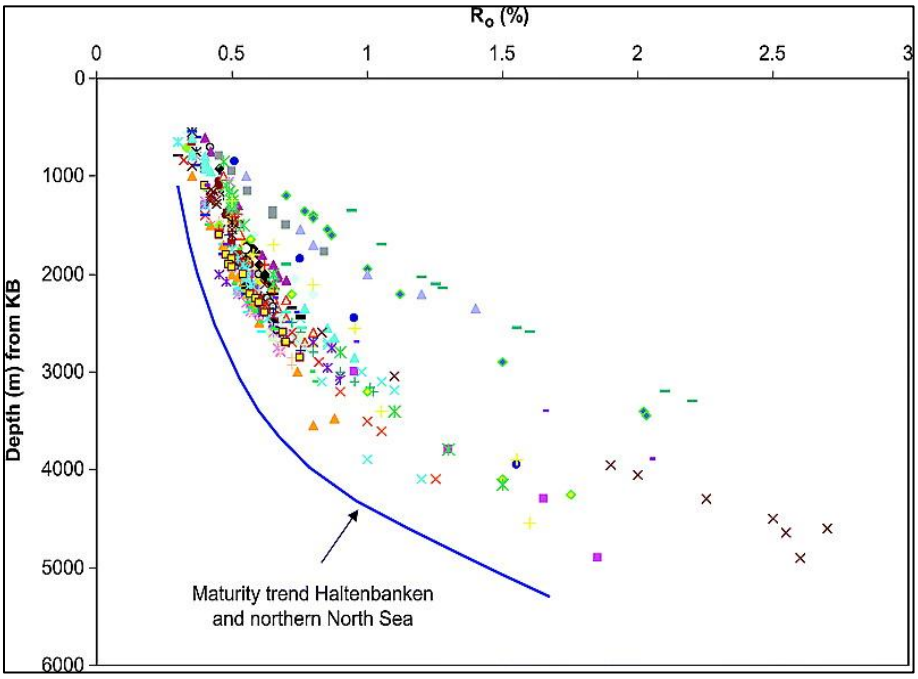

Fig. 2.6. Maturity differences between North Sea and Barents Sea base on reflectance and temperature data (Ohm et al., 2008).

As discussed, depositional environment suggested for Hekkingen Formation is deep marine waters with low water circulation and influx of terrigenous sediments. It is also support by the more detail geochemical analysis where showing anoxic condition and low cataclastic input indicating the distal part of the basin. The Kerogen types of the Hekkingen shale is mainly type

II & III and the maturity of source rock in compare to the North Sea is higher due to higher temperature gradient in the Barents region (Ohm et al., 2008). Despite the rich potential source rocks in amount and maturity it is still important to concern the uplift and erosion consequences for assess the source rock maturation and migration entire the basin. Temperature has a significant role in order to generation of hydrocarbon and will be decrease during the time of uplifment and as a result hydrocarbon generation may be stop in the area experienced most uplift event. In summary, the Barents Sea is a high potential area in terms of petroleum generation due to presence the rich source rocks. It is also essential to know uplift occurred in this basin had a significant effect on migration and maturation of hydrocarbon.

The potential source rocks and reservoir rocks in the Barents region demonstrated in Figure 2.3. The most important petroleum source rocks in both the Norwegian and Russian Barents Sea date back to Jurassic age. The Late Jurassic Hekkingen shale is Norwegian Barents Sea is equivalent with Bazhenov Formation in the Russia Barents Sea. The Paleozoic source rock however only developed as major source rock in the Russian side of the Barents Shelf and it is oil prone source rock (Domanik facies) (Dore`, 1995).

According to the source rock analysis in two wells in the Askeladd field, the best potential source rock is Upper Jurassic shales. Another candidate source is Hauterivian (Early Cretaceous) to Triassic shales. The amount of total organic carbon (TOC) increase downward and the kerogen type is mixed of type II and III. The migration of gas into the reservoir maybe started in Late Cretaceous time (Westre, 1984).

2.3.2. Reservoir Rocks

Reservoir rock is a porous and permeable subsurface rock that contains fluid (petroleum here). Sandstones and carbonates are the main two groups of reservoir rocks. In the area of study the most important reservoir rock is dominated in the Stø Formation with Lower-Middle Jurassic age. It is believed that, about 85% of the Norwegian Barents Sea resources lie within this formation and almost all of these resources are natural gas except the thin oil column in the Snøhvit Field (Westre, 1984). It is composed of well sorted mature sandstones facies of Early Jurassic to Middle Jurassic age represented a prograding coastal sedimentary environment. The Stø Formation shows good to excellent reservoir properties and porosity varied from 15% to

30% (well 7120/8-1). In the Askeladd gas field the thickness of the Stø Formation in different wells varied from 85 m (well 7120/8-3) to 109 m (well 7120/8-2). Figure 2.7 illustrated the composite logs of well 7120/8_2 for Stø Formation in the Askeladd field. As we can see, reduction of gamma ray values in the reservoir (Stø Formation) in compare to upper layers (Fuglen Fm) indicated that, lithology variation from shale to sandstone. Moreover negative separations of neutron porosity log than bulk density differentiate the sand bodies whereas the positive separation mostly related to the shale. The cores also good to indicating lithology.

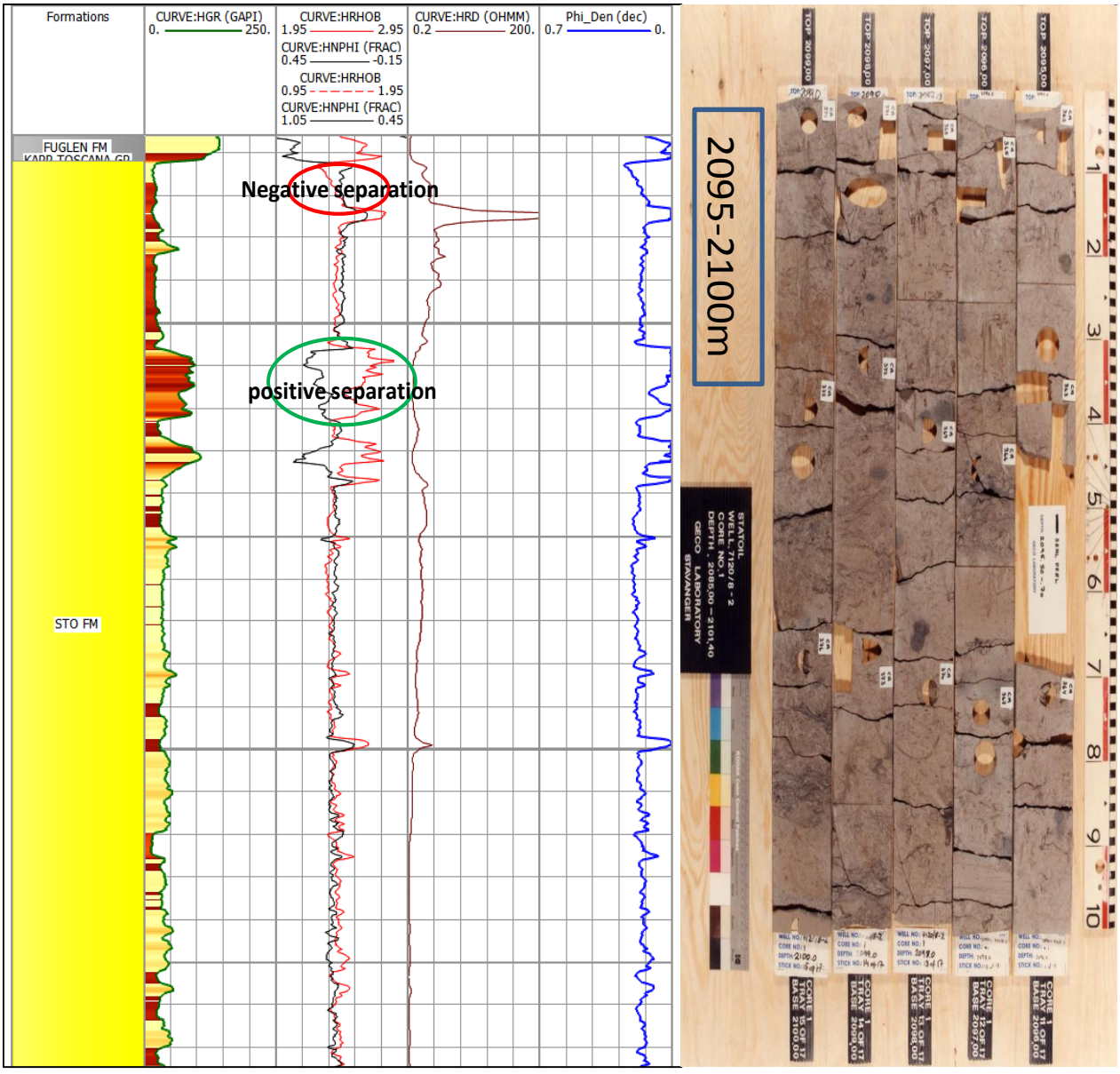

Fig. 2.7. Composite logs, (left) and (right) core photo of well 7120/8-2, from Stø Fm (NPD Factpages).

2.3.3. Caps Rocks

Cap rock (seal rock) is an impermeable rock covered the reservoir and prevents oil and gases deplete from the reservoir hence preserve the hydrocarbon accumulated in the reservoir. Cap rocks fracturing will be happen during both burial and uplift time. In other word, cap rock quality is highly influenced by the tectonic evolution of the basins and tectonic events like uplifment reduce the seal integrity. In the area of study, Fuglen and Hekkingen shales are two main potential cap rocks units. These formations dominated in whole area by thickness variation ranging from 4 m to 14 m and 24 m to 96 m in Fuglen and Hekkingen respectively. The Fuglen Formation is dominated by pyritic dark brown mudstones with interbeded white to brownish grey thin limstones of Upper Jurassic age.

The Hekkingen Formation is a main source rock in the Hammerfest Basin but it can acts also as a cap rock. The main lithology distributed entire the Hekkingen Formation is shale with Late Jurassic age. Thin interbeds of limestone, dolomite, siltstone and sandstone also observed. Deep marine environment is a suggested depositional environment for the Hekkingen Formation. Lithology distribution of cap rocks in the Hammerfest Basin represents a good quality but due to the uplift, fractures developed in cap rocks and reduce the ability of cap to accumulate the hydrocarbon (seal integrity).

Makurat et al., (1992) examine the Cenozoic uplift effect on the seal integrity in the Barents Sea (Hekkingen Fm) by combining the map of total erosion with fracture modeling studies. They conclude that, during the Late Plio-Pleistocene erosion phase (1600-1700 m), fracturing may be occurred within the caps duo to the generation of deviatoric stresses (σ_{ij}) and leakage will be decrease through the area experienced less uplift (less than 1600-1700 m).

Bernal (2009) studied the Askeladd Beta structure to find out the factors controlling the economical hydrocarbon accumulations in the Askeladd Field. The Askeladd Beta structure is located approximately 5 km to the north-west of the Askeladd Nord discovery well (Fig. 2.8). The question here is, why in spite of presence of all petroleum system elements and process, the Askeladd Beta well is dry? He noted that, accumulation of hydrocarbon in this area is followed a balance relation between amount of leaking due to the fault activity and traps charging during or

after the leakage. Vertical leakage along the main fault boundaries seems the main factor for presence an incomplete petroleum system in Askeladd Beta structure.

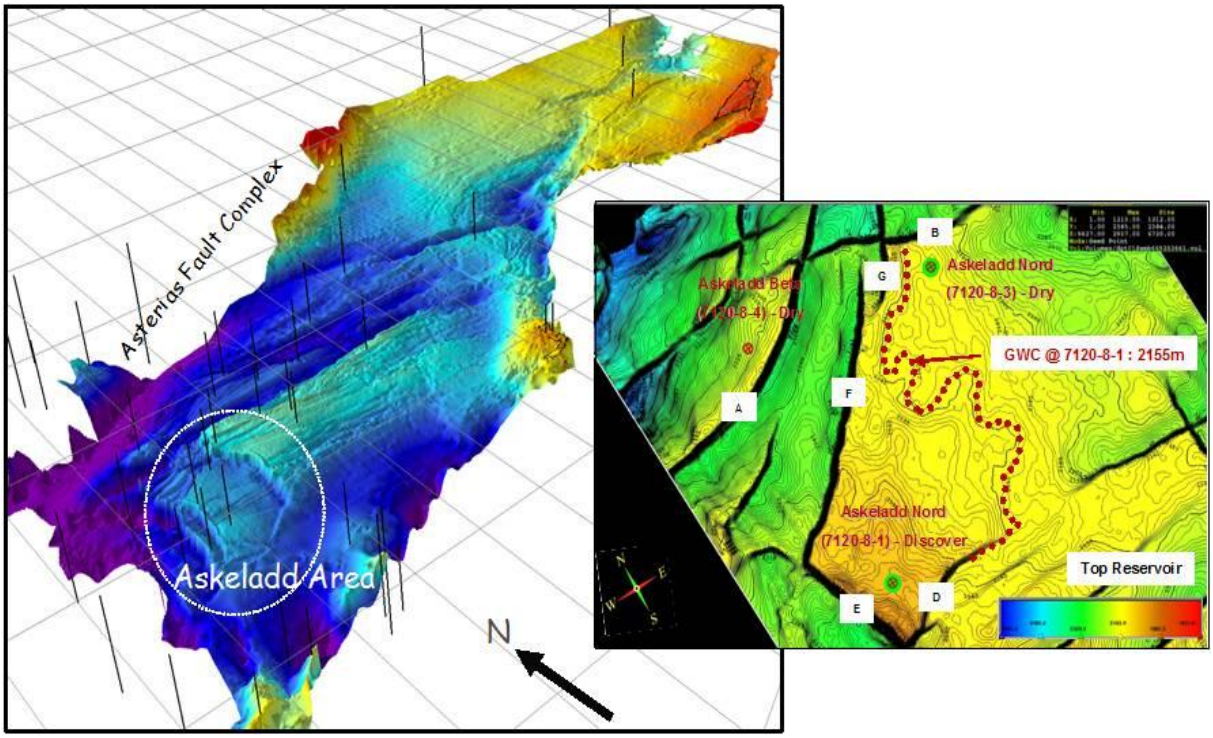

Fig. 2.8. Location of the Askeladd Field. Faults B, D, E, F & G are significant for gas accumulation at Askeladd Nord gas filled structure. Dry well 7120/8-3 is located down dip from GWC and its accumulation might be controlled by whatever fault(s) is (are) controlling the accumulation in 7120/8-1 (Bernal, 2009).

Therefore, once this structure was filled with hydrocarbon and later on due to fault activity, leakage taken place along the fault boundaries. It is necessary to know, fault seal analysis is not enough to explain what exactly cause successful accumulation in one well whereas another well that is close to it not?

2.3.4. Traps

Trap is one of the essential elements for accumulation of the hydrocarbon. It is believed that, trapping of hydrocarbons in the Jurassic sandstone reservoirs of Hammerfest Basin occurred during Paleocene-Eocene (Berglund et al., 1986). Different types of traps including faulted domes, tilted fault blocks and roll-over anticlines (Fig 2.9a) exist in the Barents Sea. The Hammerfest Basin (Fig 2.9b) indicated extensional trap type (tilted fault blocks trap). In the Askeladd field trap types are tilted fault block associated with a rift episode in late Jurassic to early cretaceous time (Bernal, 2009). As discussed, several phases uplift and erosion, causing

tilting of traps and reservoir exhumation (Doré and Jensen, 1996). The effect of tilting is remobilization of hydrocarbon throughout the area (Ohm et al., 2008).

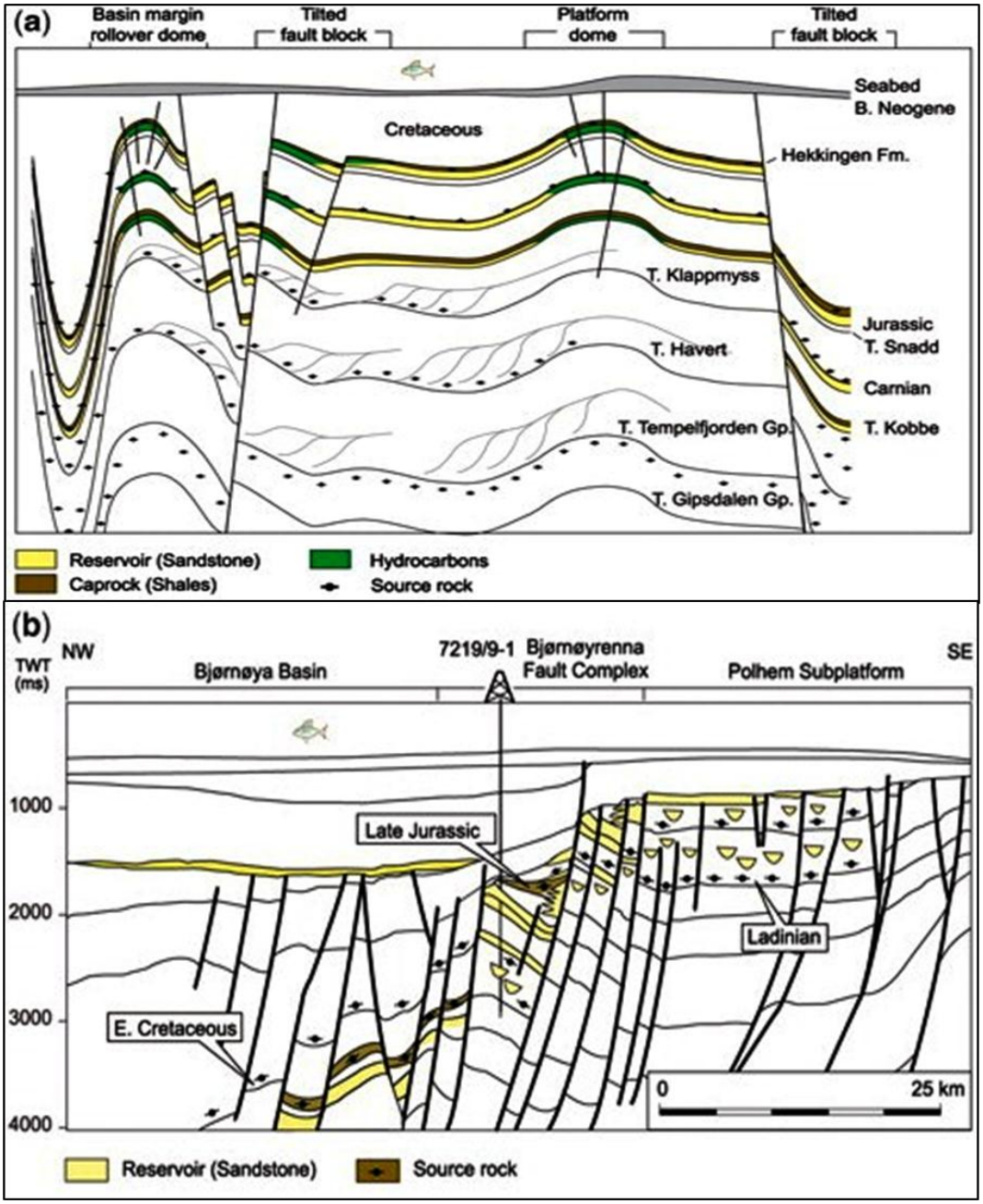

Fig. 2.9. Significant hydrocarbon plays in the Norwegian Barents Sea. (a) Platform and platform margins. (b) Extensional basin margins and rotated fault blocks (modified after Henriksen et al., 2011).

Chapter 3

Material and Methods

3.1. Data Base

This study focuses exclusively compaction and rock physics study of five wells available in and around the Askeladd discovery. Cores and seismic are not used due to time constrain. Table 3.1 shows the detail information of five wells included in this study.

Table.3.1. General information of studied wells (modified after NPD Factpages, 2012)

Wellbore name	7120/7-2	7120/8-1	7120/8-2	7120/8-3	7120/8-4
Discover year	1983	1981	1982	1983	2007
Main area	Barents Sea	Barents Sea	Barents Sea	Barents Sea	Barents Sea
Basin	Hammerfest Basin	Hammerfest Basin	Hammerfest Basin	Hammerfest Basin	Hammerfest Basin
Field	Snøhvit	Snøhvit	Snøhvit	Snøhvit	Snøhvit
Discovery	Askeladd Central	Askeladd	Askeladd	Askeladd	Askeladd Beta
Block	7120/7	7120/8	7120/8	7120/8	7120/8
Type	Exploration	Exploration	Exploration	Exploration	Exploration
Purpose	Wild cast	Wild cast	Appraisal	Appraisal	Wild cast
Content	Gas	Gas/condensate	Gas	Shows	Dry
Reservoir	Stø Fm	Stø Formation	Stø Formation	Stø Formation	Dry
HC accumulation (m)	2149-2228	2092-2180	2081-2161	2192-2286	Dry
GWC	2228	2180	2161	shows	Dry
Core Data	2166-2244	2112-2270	2085-2218.5	2198-2234	--------
TD (m RKB)	2523	2610	2590	2335	2697
BHT (°C)	97	95	91	58	--------

The petrophysical and rock physical analyses were carried out by popular software, Interactive Petrophysics (IP); mostly used for petrophysical analysis as well as rock physics diagnostics and analysis. For quality control of well logs and generate different crossplots, the Microsoft Excel was also used.

3.2. Identify the Transition Zone

For determination of the transition zone from mechanical to chemical compaction we used published experimental (Mondol et al., 2007 and Mondol, 2009) and natural compaction trends (Storvoll et al., 2005; Japsen, 1999 and Marcussen et al., 2010). To identify the transition zone of mechanical and chemical compaction, a combination of different crossplots (e.g. porosity-depth, velocity-depth and density-depth) has been analyzed. The total porosity of different sedimentary packages is calculated from the density log. The acoustic velocity (mainly V_p) is calculated from the sonic log. We also used Gamma Ray Log as a lithology indicator, Deep Resistivity Log as a fluid indicator and Neutron Log to derived porosity in reservoir zones.

3.3. Calculation of Shale Volume

Gamma Ray Log has been used for shale volume calculations. The first step is to calculate gamma ray index (I_{GR}) using the following equation:

$$I_{GR} = \frac{GR_{log} - GR_{min}}{GR_{max} - GR_{min}} \qquad (3.1)$$

Where, I_{GR} is the gamma ray index, GR_{log} is the gamma ray reading of formation, GR_{min} is the minimum gamma ray (clean sand or carbonate) and GR_{max} is the maximum gamma ray (shale) (Asquith and Krygowski, 2004). The first order estimation of shale volume is the linear relation of I_{GR} whereas different nonlinear equations also used. For example Larionov (1969) presented the following equations for young and older rocks and we use both in this study.

$$V_{sh} = 0.083(2^{3.7 \times I_{GR}} - 1), \text{ Tertiary (younger) rocks} \qquad (3.2)$$

$$V_{sh} = 0.33(2^{2 \times I_{GR}} - 1), \text{ older rocks} \qquad (3.3)$$

The equation 3.2 is used to derive porosity for mechanically compacted zone whereas the equation 3.3 is used for chemical compacted zone.

3.4. Temperature Gradients

Chemical compaction is highly depend on the temperature variation because the mineral transformation is depends on it. The temperature used in this study, calculated from bottom hole temperature (BHT). The following equation is used to calculate temperature gradient in 4 well locations:

$$m = \frac{y-c}{x} \qquad (3.4)$$

Where m is the geothermal gradient, y is the bottom hole temperature (BHT) c is the mean annual surface temperature and x is the total depth. The annual surface temperature used in this study is 5^0C (Norwegian Meteorological Institute). The BHT is missing in the well 7120/8-4. The calculated geothermal gradients of four wells are given bellow (Table 3.2):

Table.3.2. Geothermal gradients of different wells in Askeladd discovery.

Well Name	Total Depth RKB(m)	Bottom Hole Temperature (BHT)	Geothermal Gradients (^{0}C/km)
7120/7-2	2523	97	≈ 36
7120/8-1	2610	95	≈ 34
7120/8-2	2590	91	≈ 37
7120/8-3	2335	58	≈ 23

3.5. Exhumation Estimation

The amount of uplift/erosion (exhumation) occurred in the study area is essential for understanding the rock properties and burial history of the Hammerfest basin. A rough estimation of exhumation is carried out in this study by comparing log compaction trends and experimental compaction curve of kaolinite-silt (50:50) (Mondol, 2009). We defined pure shale unit to set cut-off $V_{sh} \geq 0.75$. Simplistic approaches are employed to estimate exhumation:

1. The transition zone from mechanical to chemical compaction at present day burial depth is deciphered using rock physics crossplots.

2. Volumetric shale fraction (V_{sh}) corresponding to mechanical compaction at present day burial depth is calculated and then cross-plotted as function of depth with experimentally compacted trends for kaolinite – silt (50:50) mixture (Mondol, 2009).
3. The difference along the depth (Y-axis) gives a rough estimate of the magnitude of exhumation in the area.

3.6. Estimation of V_s

Shear velocity is an important parameter for rock physics analysis. We have V_s only in a well 7120/8-4. We derive a local V_p-V_s relation to use well 7120/8-4 (Fig. 3.1). The equation resulted from the cross plot is:

$$V_s = 0.804153V_p - 915.77 \qquad (3.5)$$

We applied this equation to estimate V_s for other four wells. Besides this, we also used empirical relation such as Castagna et al. (1985), Castagna et al. (1993) and Han (1986) to calculate V_s where it is missing (see section 4.2.1.6).

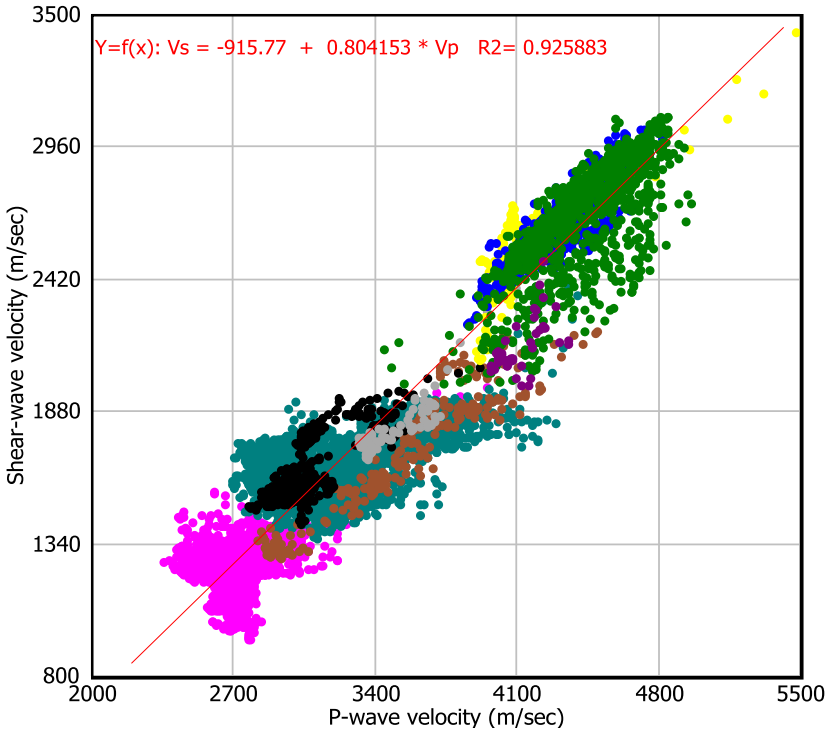

Fig. 3.1. Crossplots of Vp versus Vs in well 7120/8-4 for estimating the shear velocity.

3.7. Rock Physics Template (RPTs)

Ødegaard and Avseth (2004) described how to construct a rock physics template. According to Ødegaard and Avseth (2004), RPT is a toolbox that helps to discriminate lithology and pore fluids of well log data. It also helps to interpret seismic inversion results. The most common rock physics template is a crossplots of acoustic impedance (AI) and V_p/V_s ratio (Fig. 3.3). Local geology and well data providing the rock physics model which is the initial step to create the template (Ødegaard and Avseth, 2004). The procedure of making the template for our area can be simplified as follow:

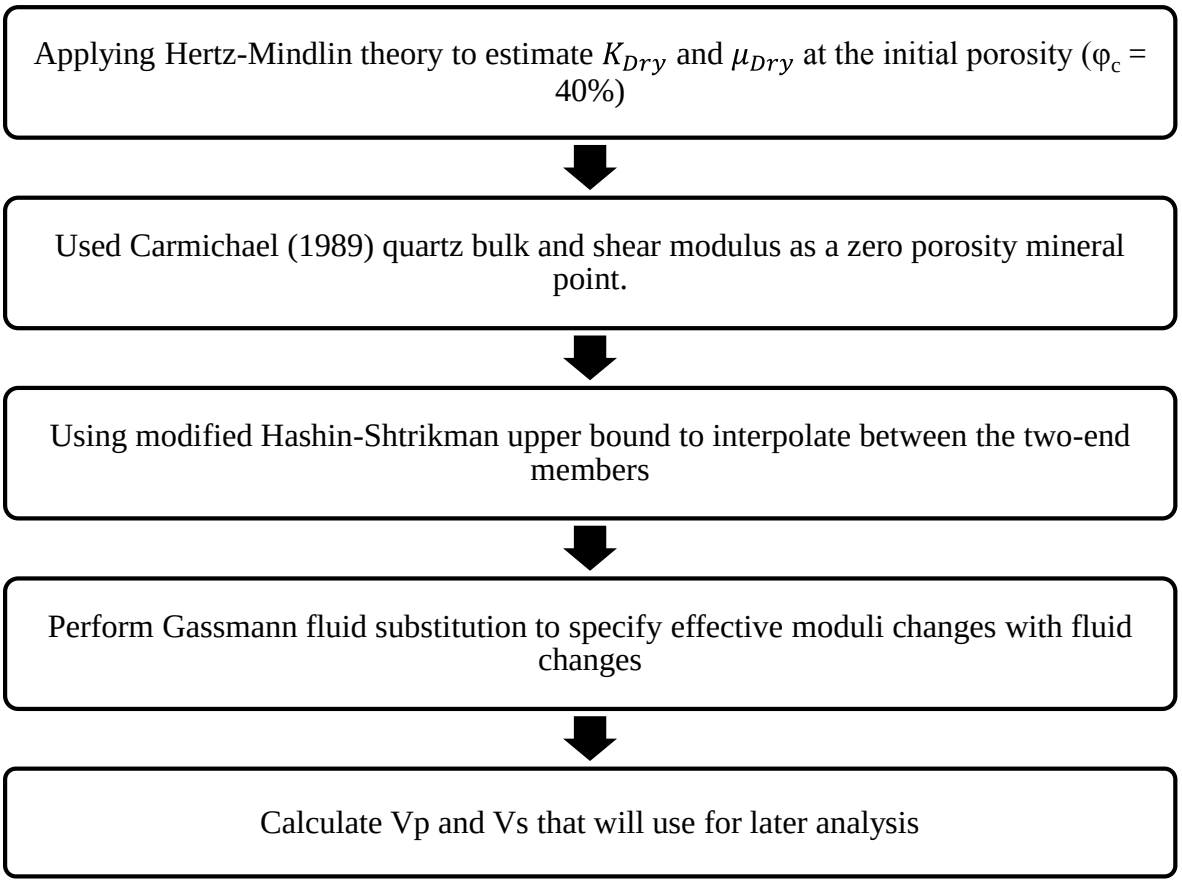

Fig. 3.2. RPTs recipe to build a template for the area of interest.

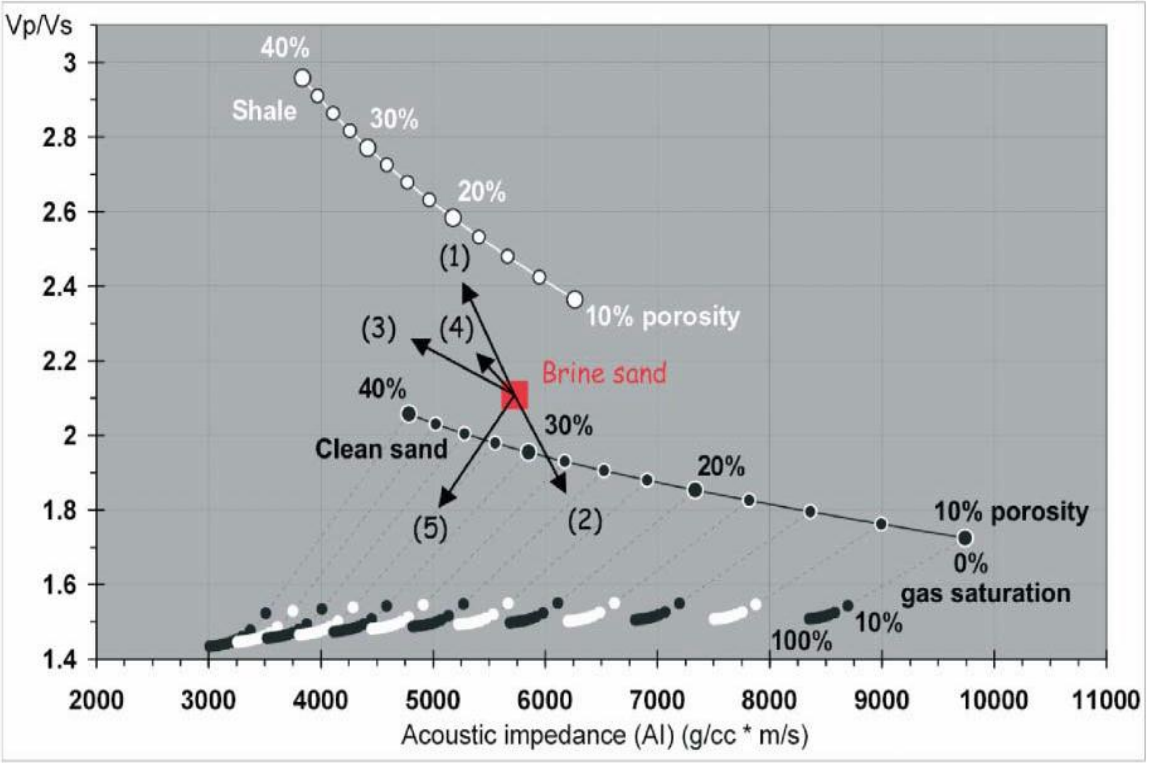

Fig. 3.3. A rock physics template (RPT) in the Vp/Vs versus AI cross-plot domain includes rock physics models locally constrained by depth (i.e., pressure), mineralogy, critical porosity, and fluid properties. The template includes porosity trends for different lithology, and increasing gas saturation for sands (assuming uniform saturation). The black arrows show various geologic trends (conceptually): 1) increasing shaliness, 2) increasing cement volume, 3) increasing porosity, 4) decreasing effective pressure, and 5) increasing gas saturation (Ødegaard and Avseth 2004).

Chapter 4

Theoretical Background

4.1. Compaction of Sediments

Sedimentary rocks are the main reservoir for oil and gas. Rock properties change continuously due to the diagenetic processes occurred after the deposition of sediments and continuous burial or uplift. These diagenetic processes have a great influence on the rock properties such as velocity, porosity and permeability. It is therefore essential to understand the processes in order to accurately predict rock properties. Diagenesis covered any physical, chemical or biological change experienced by sediment after deposition and prior to metamorphism (Bjørlykke & Jahren, 2010). Diagenetic processes are very complex and mainly depended on primary composition of sediments, subsurface pressure and temperature and pore water properties (Bjørlykke, 1988). Physical properties of rocks like velocity and elasticity also affected by digenetic processes. For instance, seismic velocity will be changes quite significantly by the onset of quartz cementation in sandstones and mudstones (Peltonen et al., 2008; Thyberg et al., 2010). Two main diagenetic processes; mechanical and chemical compaction may damage the reservoir quality. Near surface diagenesis is also common where shallow sediments usually cemented by carbonate and may prevent mechanical compaction.

4.1.1. Mechanical Compaction

Terzaghi (1943) introduce the theories for consolidation of clays. Although in the deeper depth, stress is not the only factor control the compaction but temperature plays a key role on evolution of rock properties (Bjørlykke et al., 2010).Stress (σ) simply defined as force per unit area. Total vertical stress or lithostatic stress computed as follow:

$$\sigma_v = \rho_b \, g H \qquad (4.1)$$

Where ρ_b is equal to the average bulk density of overburden sediments, g represents the gravitational force and H is thickness of the overburden sediments. The effective stress or average intergranular stress implies the fact that, overburden weight (lithostatic stress) is not the only factor control the stress distribution in the sedimentary basins but the pore pressure must be considered. The effective total stress computed as follow:

$$\sigma_v^{'} = \sigma_v - U \qquad (4.2)$$

Where $\sigma_v^{'}$ is effective stress; σ_v is the overburden total stress; and U is pore (fluid) pressure. Effective stress increases during burial will be a determining factor in mechanical compaction and control by overburden pressure and pore pressure. While the sediments undergone the effective stress, the stress of grain-to-grain contact will be increasing as a function of overburden pressure and time. Horizontal effective stress can be calculated by total horizontal stress minus pore pressure. It is not equal to the effective vertical stress. There are some field methods to calculate the horizontal stress. Figure 4.1 illustrates the schematic diagram showing the increase in vertical total stress (lithostatic) and hydrostatic pressure as a function of depth. At point (P_1) that hydrostatic pressure is dominated, the effective stress is $\sigma_v^{'} = H_g(\rho_b - \rho_w)$ whereas the effective stress at (P_2) is $\sigma_v^{'} = H_g(\rho_b - \rho_2)$.

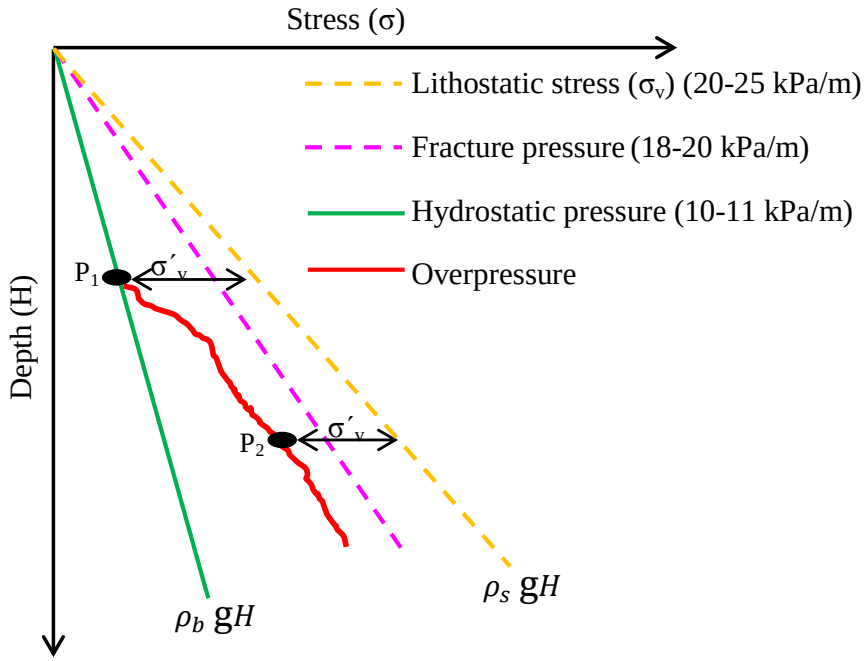

Fig. 4.1. Different types of stresses dominated in the sedimentary basins (modified after Bjørlykke et al., 2010).

Mechanical compaction is important at the shallow depth down to 2 – 4 Km where temperature is less than 60-70^{0}C. Overpressure defined as abnormal subsurface pressure and changes the effective vertical stresses when it is higher than the hydrostatic pressure (pore pressure). In overpressure regime effective stress reduces and therefore, decreases the rate of mechanical compaction. In deeply buried sandstones porosity may preserved due to coatings.

Mechanical compaction mechanism involves: reorientation and fracture of grains due to increase ineffective stress as a result, the porosity decrease and rock become more compressible (Mondol et al., 2007). Mechanical compaction as a function of the vertical

effective stresses begins immediately after deposition. Initial composition of sediments (mineral composition), grain size and rate of fluid exile during compaction are also control the mechanical compaction (Waples and Couples, 1998, Bjørlykke et al., 2004). For example well sorted coarse-grained sand is more compressible than fine-grained sand (Fig. 4.2). It is may be happen due to more grain crushing in coarse grain sediment (increase interagranular stresses). Mechanical compaction of mudstones and shales is more complicated and depended on grain strength, grain size, specific surface area and also surface charges (Bjørlykke et al., 2010). Although they revealed the similar trend when compacted mechanically and the coarse-grained shales undergone more compaction compared to the fine-grained shale (Fig. 4.3) (Storvoll et al., 2005; Mondol et al., 2007; Marcussen et al., 2010, Thyberg et al., 2010).

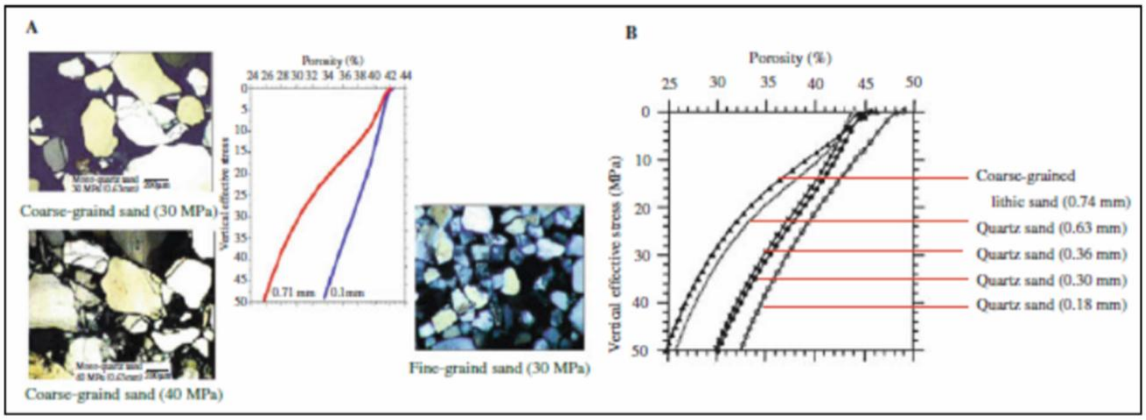

Fig. 4.2. (a) Experimental compaction of fine-grained and coarse-grained sand showing that well sorted fine-grained sands are less compressible compared to the coarse-grained sands, (b) The porosity loss as a function of grain size due to more grain crushing (from Chuhan et al., 2007 cited in Bjørlykke & Jahren, 2010).

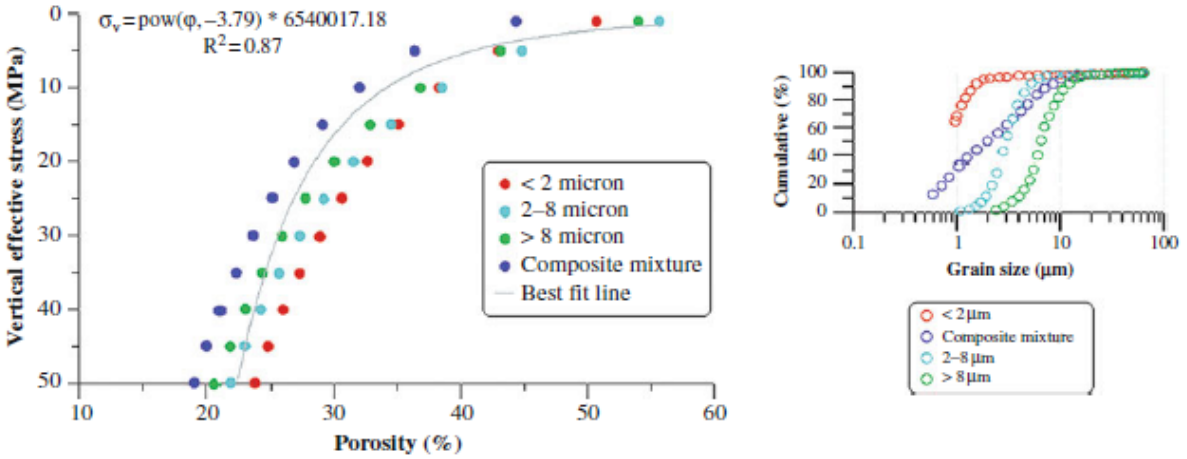

Fig. 4.3. Experimental mechanical compaction of brine-saturated kaolinite aggregates sorted by grain size (after Mondol et al., 2008). The sample containing less than 2 µm sized kaolinite aggregates retained higher porosity compared to all the other mixtures. The maximum porosity reduction is observed in the composite mixture containing all the grain sizes, demonstrating the importance of both grain size and sorting for the rock properties.

4.1.2. Chemical Compaction

Chemical compaction is including mineral dissolution, precipitation and cementation. This process usually occurs at deeper parts of the sedimentary basins, normally started from 2 to 2.5 km (depends on geothermal gradient). Temperature is the key factor control onset of chemical compaction. Temperature higher than 70-80^{0}C, usually determining the Transition zone between mechanical and chemical compaction in sandstones and can be defined by onset of quartz cementation. The transition from mechanical to chemical compaction in mudstones and sandstones are different. In sandstones the transition starts from 70-80^{0}C whereas in shales it does not simply occur at a specific depth or temperature, but it is rather a function of the stability of the primary minerals and burial history (Bjørlykke, 1998, Peltonen et al., 2008). Chemical compaction has two phases: First, dissolution of thermodynamically less stable minerals and precipitation of more thermodynamically stable. In mudstones, the transformation of smectite and precipitation of illite is an important reaction that also releases silica:

$$\text{Smectite} + \text{K-feldspar} = \text{Illite} + \text{Quartz}$$

It is corresponded to the temperature between 70 to 100^0 C and 2 to 2.5 km burial depth. One of the important sources for quartz cement in the shallow depth (45^0 C) is dissolution of amorphous silica (opal A). In the deeper part the source for quartz cementation come from pressure solution of detrital quartz. The mechanism suggested silica dissolved first at grain contact or along stylolite due to pressure and then transported by diffusion on the grain contact (Fig. 4.4) (Bjørlykke et al., 2010).

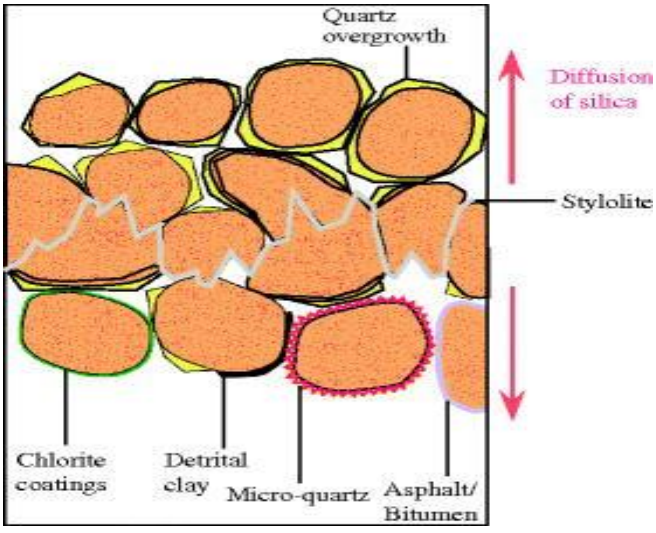

Fig. 4.4. Schematic illustration of a stylolite which is believed acting as main sources of quartz cementation (Bjørlykke et al., 2010).

Another reaction which is very important during the chemical compaction (120-130^{0}C) is transformation of kaolinite in the presence of K-Feldspar to illite (Storvoll and Brevik, 2008; Bjørlykke & Jahren, 2010). Alteration of kaolinite to the illite at the greater depth may reduce permeability and damage the reservoir quality.

K-Feldspar + Kaolinite = Illite + Quartz

Precipitation of cement increases the rock stiffness and prevents further mechanical compaction. Only 2% to 4 % quartz cement stops the mechanical compaction processes. On the other hand it damaged reservoir quality because it filled porosity usually more in the unconsolidated rocks compared to cemented rocks. Cementation of quartz depends on the grain surface area for quartz precipitation and the time-temperature integral. For instance high temperature gradient and slow rate of subsidence resulted further quartz cementation (Bjørlykke et al., 2010).

Shales and mudstones diagenetic processes are more complex due to wide range of physical and chemical properties in these types of rocks. Mineral composition and grain size distribution are the main factors control their behavior during burial. Porosity remains relatively high (20% - 40%) while sediments buried to 1-2 km where mechanical compaction is a major diagenetic process. Grain coating such as micro quartz, detrital clay, asphalt (bitumen) and chlorite can preserve the reservoir quality at deeply buried reservoir (Bjørlykke & Jahren, 2010). Hence, it should be considered as important factor for reservoir studies.

4.2. Rock Physics Models

4.2.1. Bounds

By using the bounds (upper and lower bounds), we can achieve useful and elegant framework for velocity-porosity relations. Therefore numerous "effective-medium" models have been published in order to describe theoretically the effective elastic moduli of rocks and sediments (Avseth et al., 2005). Models generally should be capable to clarifying three important points (Avseth et al., 2005): 1) Determine the volume fraction of the various constituents; 2) Specify elastic moduli of the various phases; and 3) Describe the geometric details of rock and sediments (only approximations incorporate into the models not real data).

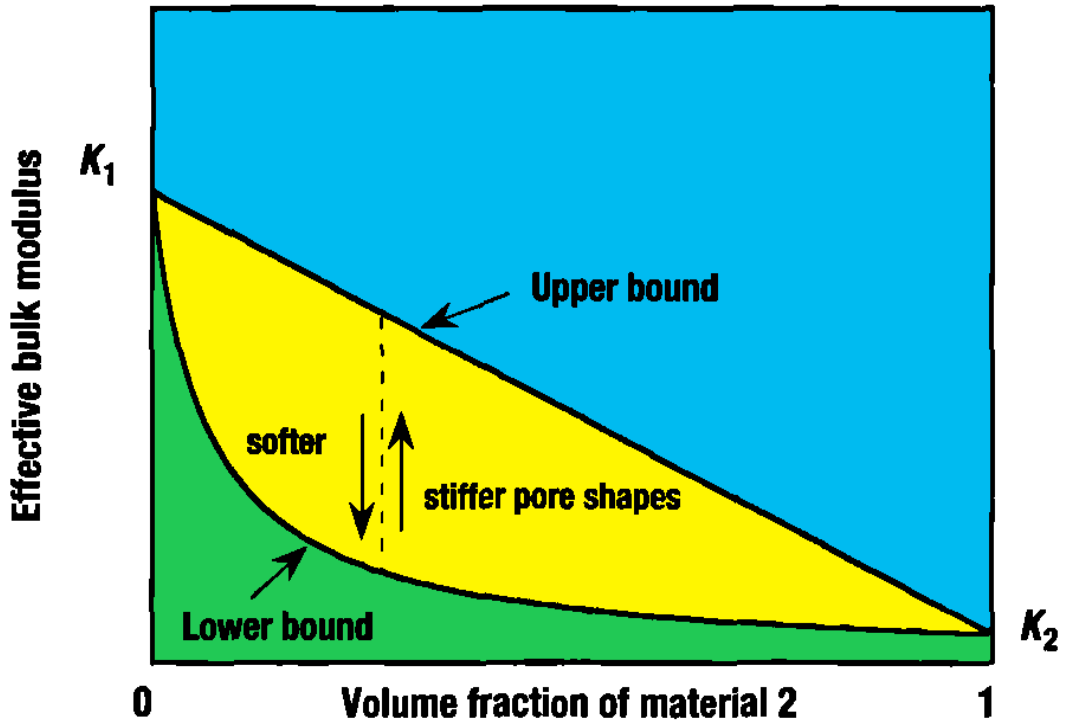

Fig. 4.5. Bounds for effective elastic bulk modulus of a mixture of two materials (modified after Avseth et al., 2005)

Figure 4.5 illustrates the concept of bounds (upper and lower) and as seen the effective modulus of the mixture (minerals or a mineral plus fluid) will fall between the bounds base on the volume fraction of constituents. However by defining the geometric details it is also possible to get precise value of effective moduli of constituents. The terms "stiff pore shapes" and "soft pore shapes" revealed the geometric variations, ranging from higher to lower value respectively.

4.2.1.1. The Voigt and Reuss Bounds

The Voigt and Reuss bounds was introduced by Voigt (1910) and Reuss (1929) that are specify the upper and lower effective elastic modulus of a mixture of grains and pores (Avseth et al., 2005). The Voigt upper bound can be written as equation below (4.3) where f_i represents the volume fraction of the ithconstituent and M_i is the elastic modulus of the ith constituent.

$$M_v = \sum_{i=1}^{N} f_i M_i \qquad (4.3)$$

The Reuss lower bound of the effective elastic modulus or M_R that is also called isostress average can be written as equation below:

$$\frac{1}{M_R} = \sum_{i=1}^{N} \frac{f_i}{M_i} \qquad (4.4)$$

In these two equations the M represent any modulus: K (bulk modulus), μ (shear modulus), E

(Young's modulus) etc. However, K and μ are the main elastic modulus and other parameters will be computing from these.

Application

- Compute the estimated range of average mineral modulus for different minerals.
- Compute the bounds for dissimilar constituents (mineral and pore fluid).

Assumptions and limitations

- Each constituent (solid or fluid) follow the isotropic, linear, and elastic condition

4.2.1.2. Hashin-Shtrikman Bounds

It is known as a best bound for isotropic linear elastic composite that has capability to giving the narrowest possible range without defining anything about the geometries of the constituents (Hashin and Shtrikman, 1963). For only two constituents, the bounds can be written as:

$$K^{HS\pm} = K_1 + \frac{f_2}{(K_2 - K_1)^{-1} + f_1\left(K_1 + \frac{4}{3}\mu_1\right)^{-1}} \quad (4.5)$$

$$\mu^{HS\pm} = \mu_1 + \frac{f_2}{(\mu_2 - \mu_1)^{-1} + 2f1\,(k1 + 2\mu_1)/\left[5\mu_1\left(K_1 + \frac{4}{3}\mu_1\right)\right]^{-1}} \quad (4.6)$$

Where K_1 and K_2 are the bulk moduli of individual phases; μ_1 and μ_2 are the shear moduli of individual phases; and $f1$ and f_2 are the volume fractions of individual phases. The upper and lower bounds distinguish by interchanging which material is termed 1 and which is termed 2. The term 1 specify the upper bound (HS^+) when it is includes stiffer material and when softer material represents term 1 is become the lower bound (HS^-) (Mavko et al., 2009). Physically, the Hashin-Shtrikman bounds illustrated in Figure 4.6 where the lower bound defined when the stiffer material formed cores and softer material forming shelf (Fig. 4.6a) and upper bound represented by stiffer material as a shelf and softer one as core (Fig. 4.6b).

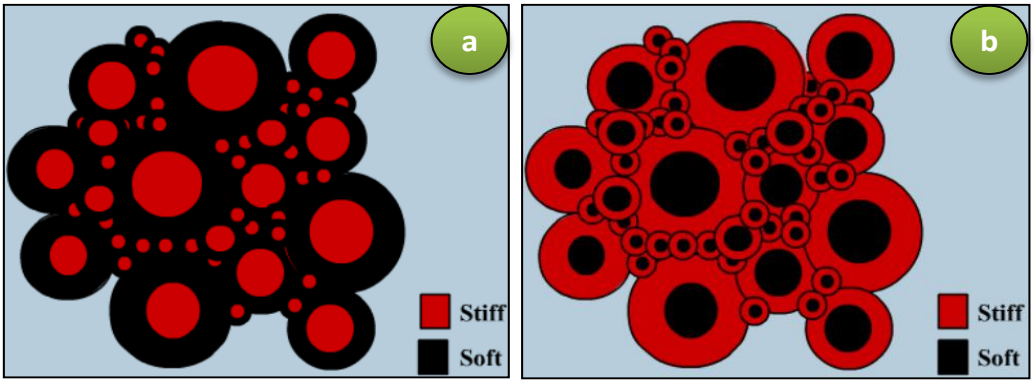

Fig. 4.6. Physical interpretation of the Hashin-Shtrikman bounds, lower bound (a) in the left and upper bound, in the right (b) (modified after Gelius & Johansen, 2010).

The more general forms of Hashin-Shtrikman equations modified after Walpole (1966) and written as below:

$$K^{HS\pm} = K_1 + \frac{f_2}{(K_2 - K_1)^{-1} + f_1\left(K_1 + \frac{4}{3}\mu_m\right)^{-1}} \qquad (4.7)$$

$$\mu^{HS\pm} = \mu_1 + \frac{f_2}{(\mu_2 - \mu_1)^{-1} + f1\left[5\mu_1 + \frac{\mu_m}{6}\left(\frac{9K_m + 8\mu_m}{K_m + 2\mu_m}\right)\right]^{-1}} \qquad (4.8)$$

Terms 1 and 2 again related to the properties of the two components. Here upper bound defined when K_m & μ_m represents the maximum bulk and shear moduli of the individual constituents, and when they are minimum, lower bound can be defined. Different constituents control the amount of separation between the upper and lower bounds. For example, common minerals show within a factor of 2 of moduli of each other. It is revealed the quite similar solids mixed with each other's whereas quite different constituents (solids and fluids) separation will be clearer and as a result we lose some of the predictive value. In the case one when we face up with the same mineralogy, most of the effective-medium models (e.g., Biot, Gassmann, Kuster-Toksoz, etc.) assume a homogeneous mineral modulus therefore, it will be useful to define the "average mineral" with an equal to either one of the bounds or to their average $(M^{HS+} + M^{HS-})/2$ (Mavko et al., 2009).

Application

- Compute the estimated range of average mineral modulus for different minerals.
- Compute the bounds for dissimilar constituents (mineral and pore fluid).

Assumptions and Limitations

- Each constituent (solid or fluid) follow the isotropic, linear, and elastic condition
- The rock follows linear and elastic behavior.

4.2.1.3. Modified Hashin–Shtrikman Bounds

The modified Hashin-Shtrikman bounds are similar to the equations of Hashin-Shtrikman-Walpole and the only difference is the constituent end members are selected differently. For instance, a mineral mixed with a fluid–solid suspension or stiffly packed sediment mixed with a fluid-solid suspension (Mavko et al., 2009).

$$K^{HS\pm} = K_1 + \frac{f_2}{(K_2 - K_1)^{-1} + f_1\left(K_1 + \frac{4}{3}\mu_m\right)^{-1}} \quad (4.9)$$

$$\mu^{HS\pm} = \mu_1 + \frac{f_2}{(\mu_2 - \mu_1)^{-1} + f1\left[5\mu_1 + \frac{\mu_m}{6}\left(\frac{9K_m + 8\mu_m}{K_m + 2\mu_m}\right)\right]^{-1}} \quad (4.10)$$

The modified upper Hashin–Shtrikman curve is a useful trend to explain the diagenetic trend in the clean sandstones and observationally sandstone moduli are lie on or below it most of the time. In other words it can illustrate how the elastic moduli of clean sandstones change from deposition to compaction and cementation (Mavko et al., 2009).

Uses

- Useful for determine the depth-trend lines for sand and chalk sediments.

Assumptions and Limitations

- Isotropic linear elasticity model; and
- Contain at least some heuristic elements (they can't match with any data)

4.2.2. Velocity-Porosity Models

4.2.2.1. Critical Porosity and Nur's Modified Voigt Average

There are several attempts, particularly Nur et al., (1991-1995) to defenses this idea that, P-wave velocity and S-wave velocity of rocks imply two limits, first the mineral grains in the limit of low porosity and the next one the high porosity limit that values for a mineral-pore-fluid suspension point (Mavko et al., 2009). Prove of this idea needs introduced a critical porosity ϕ_c that was based on the observation for most porous materials. Two distinct domains can be defining base on the separation of the mechanical and acoustic behavior of the porous materials by critical porosity (φc). First, the suspension domain where, $\varphi > \varphi c$ the effective modulus can be calculated using the Reuss (isostress) average

$$K_R^{-1} = (1 - \varphi)K_0^{-1} + \varphi K_{f1}^{-1},\ \mu_R = 0 \quad (4.11)$$

Where K_0 and K_{f1} are bulk moduli of the mineral and fluid, respectively. The effective shear modulus of the suspension is zero because the shear modulus of fluid is zero. In the load-bearing domain, $\varphi < \varphi c$, a sharp decrease observed in the moduli of minerals ranging from zero porosity to the suspension values at the critical porosity. Interpretation of the mineral-to-critical-porosity trend in terms of geometry revealed the point that the grains contact is no longer exist and also rock must lose its stiffness if we apply the large enough porosity. Geological point of view, the weak suspension state at critical porosity refer to the condition that sediments undergone the initial depositional prior the onset of compaction and diagenesis. Two factors controlled the critical porosity(φc), the grain sorting and the angularity at deposition. Porosity will be decreasing during the time that sediments undergone compaction, meanwhile elastic stiffness increased (Mavko et al., 2009).

Uses

- Examine the velocity and porosity relation.

Assumptions and Limitations

- The critical porosity result is empirical; and
- Other corrections such as clay content must apply to get a proper result.

4.2.2.2. Wyllie's Time-Average Equation

Wyllie et al. (1956, 1958, and 1963) experimental data imply the relatively sameness relation between velocity and porosity in sedimentary rocks under the certain conditions: quite uniform mineralogy; high effective pressure dominated; and fluid-saturated rocks (Mavko et al., 2009). Wyllie et al expression or time-average equation can be written as follow:

$$\frac{1}{Vp} = \frac{\varphi}{Vp-f1} + \frac{1-\varphi}{Vp\_0} \qquad (4.12)$$

Where, V_p is P-wave velocity; $V_p - 0$ (Table 4.1) & $V_p - f_1$ are P-wave velocity of the saturated rocks and pore fluid. This equation simply interpreting as the addition of transit time in the mineral and transit time in the pore fluid resulted the total transit time.

Table.4.1. Typical mineral P-wave velocities (modified after Mavko et al., 2009)

Lithology	$\boldsymbol{Vp\_0}$
Sandstones	5480 – 5950
Limestones	6400 – 7000
Dolomites	7000 – 7925

Uses

- Estimation of the expected seismic velocities base on the mineralogy and pore fluid
- Estimation of the porosity, specify the rock type and pore-fluid content

Assumptions and Limitations

- The rock must be isotropic;
- The rock must be fluid saturated;
- The high enough effective pressure (terminal velocity) must be present in the rock;
- Not apply in the unconsolidated uncemented rocks;
- It is works best with primary porosity;
- The assumption is a single homogeneous mineralogy; and
- Best result comes from the intermediate porosities.

4.2.2.3. Raymer–Hunt–Gardner Relations

Raymer et al. (1980) improved the Wyllie's empirical relations as follows:

$$V = (1-\varphi)^2 V_0 + \varphi V_{f1} \qquad \varphi < 37\% \qquad (4.13)$$

$$\frac{1}{\rho V^2} = \frac{\varphi}{\rho_{f1} V_{f1}^2} + \frac{1-\varphi}{\rho_0 V_0^2} \qquad \varphi < 47\% \qquad (4.14)$$

Where V is rock velocity; $V_{f1}$and V_0 are velocity in the pore fluid and minerals respectively; ρ is rock density; and ρ_{f1} & $\rho_0$are pore fluid and minerals density respectively. Note that the second relation is the same as the isostress or Reuss average of the P-wave moduli. A third expression for intermediate porosities is derived as a simple interpolation of these two:

$$\frac{1}{V^2} = \frac{0.47-\varphi}{0.10}\frac{1}{V_{37}} + \frac{\varphi-0.37}{0.10}\frac{1}{V_{47}} \qquad (4.15)$$

The V_{37} computed from the low-porosity formula at $\varphi < 37\%$, and V_{47} measured from the high-porosity formula at $\varphi < 47\%$ (Mavko et al., 2009).

Uses

- Estimation of the expected seismic velocities base on the mineralogy and pore fluid;
- Estimation of the porosity, specify the rock type and pore-fluid content

Assumptions and Limitations

- The rock must be isotropic;

- The rock must be fluid saturated;
- The high enough effective pressure (terminal velocity) must be present in the rock;
- Not apply in the unconsolidated uncemented rocks; and
- Minerals must have the same velocities.

4.2.2.4. Han's Empirical Relations for Shaley Sandstones

Han (1986) introduced the empirical relation based on laboratory works (80 well-consolidated Gulf Coast sandstones with $3\% \leq \varphi \leq 30\%$ and $0\% \leq C \leq 55\%$). He attempted to find out the relation between ultrasonic velocities to porosity and clay content.

According to his measurement, very high accuracy associated by the clean sandstone velocities-porosity relation while by adding the clay, correlation becomes relatively poor (Mavko et al., 2009). However it is possible to get very accurate correlation if we also considering clay volume in the regression (regressions are shown in table 4.2).

Moreover, Eberhart-Phillips (1989) have been modified the Han's empirical relations by combining another factor, effective pressure P_e (kilobars) to his measurements and found two equations as follow:

$$V_p = 5.77 - 6.94\varphi - 1.73\sqrt{C} + 0.446(P_e - 1.0e^{-16.7P_e}) \qquad (4.16)$$

$$V_s = 3.70 - 4.94\varphi - 1.57\sqrt{C} + 0.361(P_e - 1.0e^{-16.7P_e}) \qquad (4.17)$$

Table 4.2. Han's empirical relations between ultrasonic V_P and V_S (km/s) with porosity and clay volume fractions (modified after Mavko et al., 2009).

Clean sandstones (determined from ten samples)		
Water-saturated		
40 MPa	V_p = 6.08 – 8.06 φ	V_s = 4.06 – 6.28 φ
Shaley sandstones (determined from 70 samples)		
Water-saturated		
40 MPa	V_p = 5.59 – 6.93 φ – 2.18C	V_s = 3.52 – 4.91 φ – 1.89C
30 MPa	V_p = 5.55 – 6.96 φ – 2.18C	V_s = 3.47 – 4.84 φ – 1.87C
20 MPa	V_p = 5.49 – 6.94 φ – 2.17C	V_s = 3.39 – 4.73 φ – 1.81C
10 MPa	V_p = 5.39 – 7.08 φ – 2.13C	V_s = 3.29 – 4.73 φ – 1.74C
5 MPa	V_p = 5.26 – 7.08 φ – 2.02C	V_s = 3.16 – 4.77 φ – 1.64C
Dry		
40 MPa	V_p = 5.41 – 6.35 φ – 2.87C	V_s = 3.57 – 4.57 φ – 1.83C

Uses

- It can be useful to find out the empirical relation of porosity, velocity and clay content.

Assumptions and Limitations

- Empirical relation always including some restriction and they seems locally valid. Although, one can extend these relation more generally for other area to many consolidated sandstones.
- There is a slight change of linear regression coefficients with confining pressure as it is more and less stable above 10 MPa while below this, variation is more considerable, and then correlation coefficients decrease.
- Comparison of empirical coefficients of different equations is not meaningful. For example, we know Wyllie's equations are only heuristic and values for the velocities of water and clay derived from this cannot interpret in Han's equations. It means, theoretical justification is not possible and they can't match with any data.
- Extrapolation of data is not possible away from the range of experiments.

4.2.2.5. Castagna's Empirical Relations for Velocities

Castagna et al., (1985) employed the log data to determining the velocities-porosity and clay content relation, under water-saturated conditions. Their work for mudstones implies the relation between V_p and V_s (in km/s) as below:

$$V_p = 1.36 + 1.16V_s \qquad (4.18)$$

When they considering porosity (φ) and clay volume (C) (shaley sands of the Frio Formation):

$$V_p = 5.81 - 9.42\varphi - 2.21C \qquad (4.19)$$

$$V_s = 3.89 - 7.07\varphi - 2.04C \qquad (4.20)$$

Uses

- Used to relate velocity, porosity, and clay content empirically in shaley sandstones.

Assumptions and limitations

- As other empirical relations, they apply only to the set of rocks studied; and
- Comparison of empirical coefficients with other equations is wrong (section 4.2.2.4).

4.2.3. V_p-V_s Relations

The V_p - V_s relations are very important for indication of lithology from seismic or sonic log data and also using as a direct seismic detector of pore fluids (AVO analysis) (Mavko et al., 2009). There is a great deal of published V_p - V_s relations although most of them taking place in two steps: first, making the empirical relations among parameters such as V_p, V_s, and φ for one reference pore fluid (water-saturated or dry); then use Gassmann's fluid substitution theory (Mavko et al., 2009). We only discuss more popular relations for sandstones and shales.

Castagna et al. (1993) for water-saturated sandstones and shales:

$$V_s = 0.804V_p - 0.856 \quad (km/s) \qquad (4.21)$$

Castagna et al. (1985) or "mudrock line":

$$V_s = 0.862V_p - 1.172 \quad (km/s) \qquad (4.22)$$

Han (1986) that it is based on laboratory ultrasonic data:

$$V_s = 0.794V_p - 0.787 \quad (km/s) \qquad (4.23)$$

Castagna et al. (1993) suggest that if the lithology is well known, one can fine tune these relations to slightly lower V_s/V_p for high shale content and higher V_s/V_p in cleaner sands. When the lithology is not well constrained, the Han and the Castagna et al. lines give a reasonable average. Han (1986) and Castagna et al. (1985) relations shows best overall fit to the sandstones while mudrock line leads to the lower V_s since it is includes the most shaley samples. Castagna et al. (1993) discussed the lithology impact on V_s/V_p values when it is well known. The higher amount of shale cause slightly lower V_s/V_p whereas high V_s/V_p imply the clean sandstones. The average line of the Han and Castagna can apply for unsure lithology constrains (Mavko et al., 2009). It will be good to considering the effect of different porosity and also clay content on the empirical relation. Hence very short summary can be shows that as follow (next page):

Clay effects, Han (1986):

$$V_s = 0.842V_p - 1.099, \quad clay > 25\% \tag{4.24}$$

$$V_s = 0.754V_p - 0.657, \quad clay < 25\% \tag{4.25}$$

Porosity effects, Han (1986):

$$V_s = 0.756V_p - 0.662, \quad \varphi > 15\% \tag{4.26}$$

$$V_s = 0.853V_p - 1.137, \quad \varphi < 15\% \tag{4.27}$$

Higher amount of clay ($clay > 25\%$) shows better fit with mudrock line. Low porosity line is almost fit with the mudrock line whereas high porosity is similar to the clean sandstone (see section 7.9 Mavko et al., 2009 for more detail).

4.2.4. Cement Models

4.2.4.1. The Friable - (Unconsolidated) Sand Model:

Two theoretical models introduced by Dvorkin and Nur (1996) for high-porosity sands, friable-(unconsolidated) sand and contact-cement model (Fig. 4.7). The velocity-porosity behavior versus sorting associated with specific effective pressure is the base of friable model. It is in fact valid for well sorted, high-porosity (around 40%) and interpolation by using the lower bound employ for intermediate porosities (poorly sorted) (Mavko et al., 2009). Elastic moduli computed by Hertz-Mindlin theory (Mindlin, 1949) as follow:

$$K_{HM} = \left[\frac{n^2(1-\varphi_c)^2\,\mu^2}{18\pi^2(1-\nu)^2}\,P\right]^{1/3} \tag{4.28}$$

$$\mu_{HM} = \frac{5-4\nu}{5(2-\nu)}\left[\frac{3n^2(1-\varphi_c)^2}{2\pi^2(1-\nu)^2}\,P\right]^{1/3} \tag{4.29}$$

Where K_{HM} and μ_{HM} specify bulk and shear modulus respectively at critical porosity φ_c; effective pressure defined by P; and terms μ and ν also shear modulus and poisson's ratio and n coordination number that is calculated as follow:

$$n = 20 - 34\varphi + 14\varphi^2 \tag{4.30}$$

The Poisson's ratio:

$$\nu = \frac{3K-2\mu}{2(3K+\mu)} \qquad (4.31)$$

Effective pressure versus depth is obtained with the following formula:

$$P = \mathrm{g}\int_0^Z (\rho_b - \rho_{fi})dZ \qquad (4.32)$$

Where g implies the gravity constant, ρ_b, ρ_{fi} and Z are bulk density, fluid density and depth respectively. For other end point in this model, section 2.2 from Avseth et al. (2005) is suggested.

4.2.4.2. The Contact – Cement model

The cement volume will be change during the burial of sediments as a function of digenetic processes. The velocity-porosity will be change by onset of cementation and this model try to determine the relation between velocity-porosity and cement volume at the high porosity fraction (Fig 4.7).For practical purposes, we assume this porosity to be equal or close to the well-sorted end member of the friable-sand model. Elastic moduli computed as follow:

$$K_{dry} = n(1-\varphi_c)M_c S_n/6 \qquad (4.33)$$

$$\mu_{dry} = (3K_{dry})/5 + 3n(1-\varphi_c)\mu_c S_\tau/20 \qquad (4.34)$$

Where φ_c is critical porosity; $M_c = K_c + 4\mu_c/3$ when $\mu_c$and $K_c$are shear and bulk modulus of cement respectively and; the coordination number, n implies the average number of contacts per grain and S_τ and S_n are saturated cements (see section 2.2 Avseth et al., 2005).

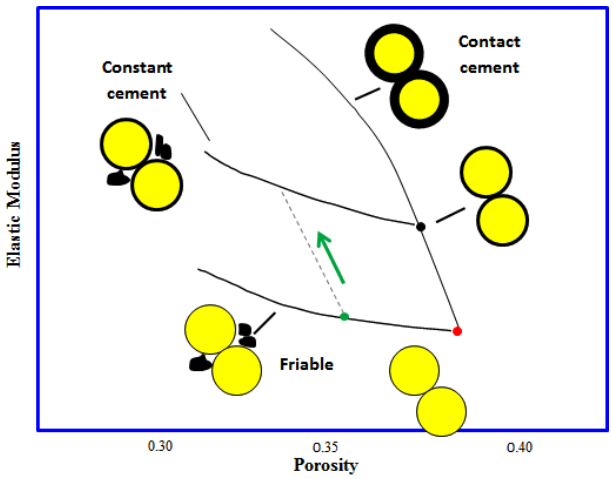

Fig. 4.7. Schematic illustrations of three cement models (modified after Avseth 2005).

4.2.4.3. The Constant – Cement model

This model introduced by Avseth (2000) and tries to explain the relation between velocity-porosity and sorting at a specific cement volume (specific depth). Therefore sometimes it is called `constant-depth model` because normally corresponding to a specific depth. As discussed, the contact-cement model (Fig. 4.7) employ for high-porosity member and calculating the velocity-porosity for well-sorted sandstone whereas the constant-cement volume described the lower bound between this well-sorted end member and zero porosity by interpolation between these two bound. The equation can be written as follow:

$$K_{dry} = \left[\frac{\varphi/\varphi_b}{K_b+(\frac{4}{3})\mu_b} + \frac{1-\varphi/\varphi_b}{K+(\frac{4}{3})\mu_b}\right]^{-1} - \frac{4}{3}\mu_b \qquad (4.35)$$

$$\mu_{dry} = \left[\frac{\varphi/\varphi_b}{\mu_b+Z} + \frac{1-\varphi/\varphi_b}{\mu+Z}\right]^{-1} - Z \quad where, Z = \frac{\mu_b}{6}\left(\frac{9K_b+8\mu_b}{K_b+2\mu_b}\right) \qquad (4.36)$$

The φ_b represent the initial-cement porosity as shown in Figure 4.7 and subscript b in the equations above mentioned this point. Other parameters are similar to the previous models.

4.3. Gassmann's Relations

Gassmann's relations (1951) try to predict the rock modulus changes while pore fluids change. The changes in bulk density and rock compressibility resulted from pore fluids; hence for substitution problem these effects must be considered (Avseth et al., 2005).

Gassmann's equations written as follow:

$$\frac{K_{Sat}}{K_s-K_{Sat}} = \frac{K_{Dry}}{K_s-K_{Dry}} + \frac{K_f}{\varphi\,(K_s-K_f)} \qquad (4.37)$$

$$G_{Sat} = G_{Dry} \qquad (4.38)$$

Where, K_{Sat} & K_{Dry} are bulk modulus of rock with fluid and dry rock respectively; K_f is bulk modulus of pore fluid; K_s is bulk modulus of mineral phase; and φ is porosity. In equation (4.38), G_{Sat} and G_{Dry} are shear modulus of rock with fluid and shear modulus of dry rock respectively.

The bulk modulus of rock saturated and dry rock can be written as follow:

$$K_{Sat} = K_s\,\frac{\varphi K_{Dry} - (1+\varphi)K_f K_{Dry}/K_s + K_f}{(1-\varphi)K_f + \varphi K_s - K_f K_{Dry}/K_s} \qquad (4.39)$$

$$K_{Dry} = K_s \frac{1-(1-\varphi)K_{Sat}/K_s-\varphi K_{Sat}/K_f}{1+\varphi-\varphi K_s/K_f-K_{Sat}/K_s} \quad (4.40)$$

These dry and saturated moduli are related to the velocities (V_p&V_s) as follow:

$$V_p = \sqrt{(K_{Sat} + \frac{4}{3}G_{Dry})/\rho_{Sat}} \quad (4.41)$$

$$V_s = \sqrt{G_{Dry}/\rho_{Sat}} \quad (4.42)$$

$$\rho_{Sat} = \rho_{Dry} + \varphi\rho_{Fluid} > \rho_{Dry} \quad (4.43)$$

Where, V_p & V_s are P-wave velocity and shear velocity respectively and ρ_{Sat} implies the density of saturated rock.

Caution and Limitation:

There are several pitfalls in order to using the Gassmann's relations and here we only mentioned those without explanation (see section 1.3.3, Avseth 2005).

- A gas-saturated rock is not a "dry rock";
- Only valid for low frequencies;
- Only valid for isotropic rocks;
- Homogeneous mineralogy assumption; and
- Only describe the change in moduli of one saturation (100%) to another (not mixed saturation)

Chapter 5

Compaction and Evolution of Rock Properties

Diagenetic processes will change the physical properties of rocks such as velocity and density (Marcussen et al., 2010). Mechanical compaction mainly occurs in shallow depths and is controlled by effective stress, whereas chemical compaction dominates the deeper parts of basins where temperature plays a key role in dissolution, precipitation and cementation of rocks (Bjørlykke et al., 2010). Therefore, it is essential to consider these processes when characterizing a potential reservoir (Marcussen et al., 2010). This study thus shows the variation of velocity, density and porosity with depth as a function of diagenetic processes (mechanical and chemical compaction).

In addition, the transition between mechanical compaction and the onset of quartz cementation (chemical compaction) is analyzed by studying the well logs and comparing the results with laboratory data. Finally, the amount of exhumation is estimated in the area of study in order to properly evaluate the rock properties in the Barents Sea region.

5.1. Result

5.1.1. Compaction trends

The velocity, density and, porosity-depth trends for 4 wells in the Askeladd discovery demonstrate variations due to differences in compaction processes undergone within the sediments. Figure 5.1 shows an approximately linear trend for velocity in all wells from about 50 m (BSF) depth (top of Nordland group) down to about 1750 m burial depth (base of Kolje formation). This possibly corresponds to a zone of mechanical compaction where velocity increases gradually from about 1800 m/s to around 3500 m/s; hence the velocity/depth gradient is around 67 m/s per 100 m burial depth. Another trend is distinguished from about 1750 m down to around 2400 m where velocity rises dramatically from about 3000 m/s to nearly 4500 m/s within a rather thin section of sediments (i.e. top of Knurr Formation to bottom of Fruholmen Formation). The velocity/depth gradient is thus approximately 200 m/s per 100 m burial depth. This sharp increase in velocity can be attributed to chemical diagenesis processes.

A dramatic velocity increase is observed from 1750 m down to 2000 m where the velocity has risen from about 3500 m/s to around 4000 m/s within a thin of sediments. This high velocity zone which is highlighted by a yellow rectangle in Figure 5.1(a) demonstrates a velocity-depth gradient of 250 m/s per 100 m increase in burial depth. The rapid velocity increase in these depths can be attributed to an onset of chemical diagenetic reactions. In other words,

this zone can be described as a transition zone from mechanical compaction to chemical compaction. After this very sharp change in velocity, a decline in velocity is observed and the velocity-depth gradient shows a value less than 80 m/s per 100 m travel in depth. The average velocity reaches more than 4300 m/s at a depth of 2400 m.

The bulk density versus depth relation demonstrates less variation than the velocity-depth trend thereby making it not so simple to distinguish the zone of transition from mechanical to chemical compaction. An exponential trend can be identified for the whole interval from about 50 m to about 2500 m depth (Fig. 5.1 b). The porosity log is calculated from the density log, and the porosity-depth trend appropriately follows the density/depth trend in an opposing downward reduction with depth (Fig. 5.1 c). Like density, the trend follows an exponential function. At shallower depths, porosity decreases dramatically (50% to 18%), whereas quite small changes in porosity is observed at greater depths (18% to 12%).

Velocity-density plot clearly differentiates between the two compaction processes. The data points are segragated into two distinct clusters when velocity is plotted against density (Fig. 5.1 d). The more extensive blue cluster/ellipse is indicative of mechanical compaction where velocity increases gradually as density increases with a gentle gradient while, the green cluster/ellipse shows greater Vp values and steep gradient which can be attributed to rock stiffness and quartz cementation.

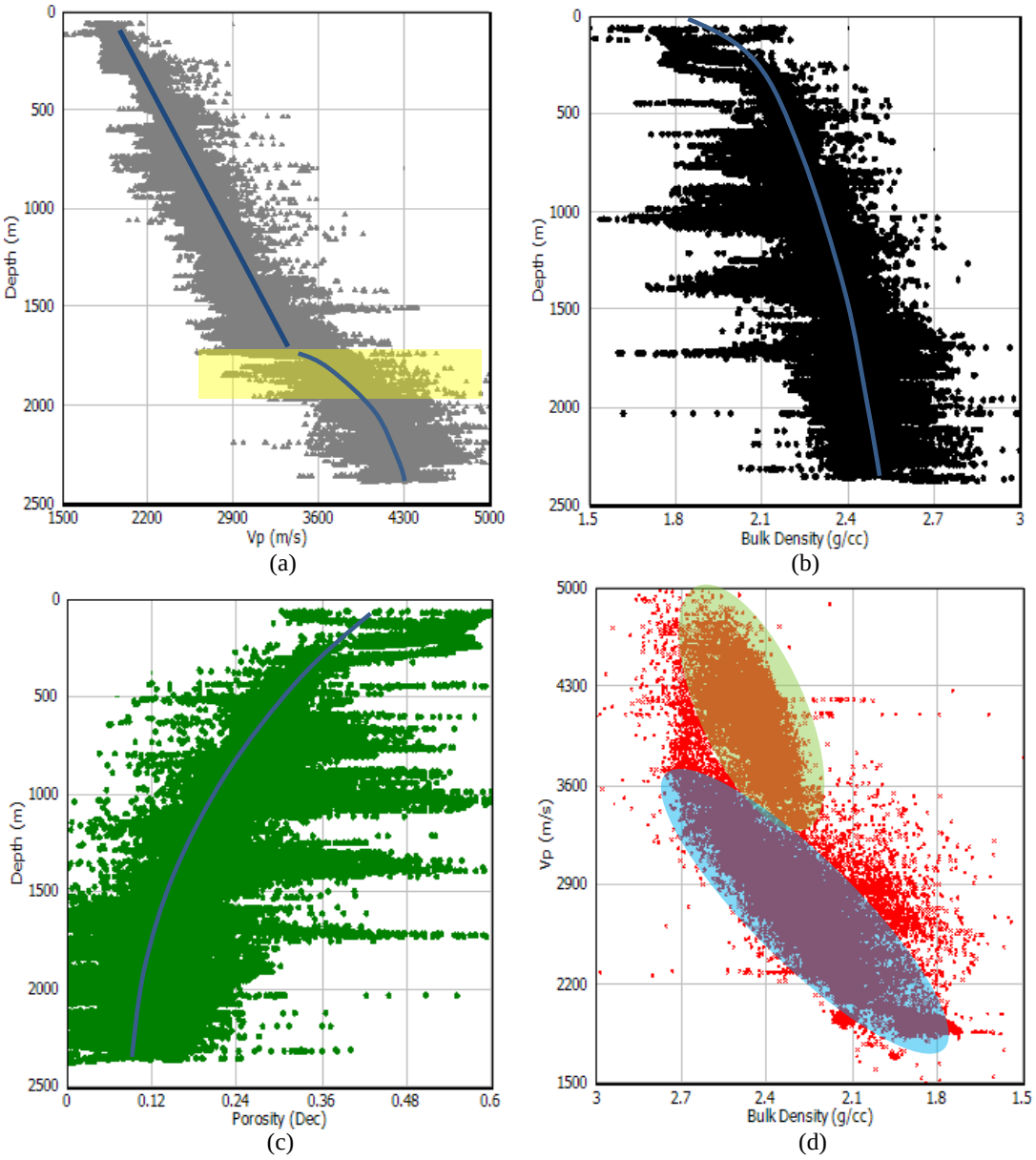

Fig. 5.1. Crossplots of (a) Vp-depth, (b) density-depth, (c) porosity-depth, and (d) density-Vp, observed from all wells in the Askeladd field, Barents Sea.

Depth trends are also generated for every well (Figs. 5.2, 5.3, 5.4, 5.5 and, 5.6) to investigate both the compaction processes and their limits in every well. These provide a general view about sediment compaction as it occurred in the study area. Well 7120/7-2 is chosen as a reference well to investigate the compaction trends because it has more reliable data set and more depth coverage in logging interval among the other studied wells for the Askeladd field. Apart from well 7120/8-4 where the data are incomplete, similar comparable plots are made for the rest of the wells in the area (wells 7120/8-1, 7120/8-2 and, 7120/8-3). The velocity-depth trend for well 7120/7-2 can be divided into two different linear trends. From the top of glacial marine sandstones of Nordland Group down to bottom of deep marine shales of Kolje

Formation, the velocity increases slightly (about 2000 to 3100 m/s). Notwithstanding, substantial changes is observed within the distal open marine claystones of Knurr Formation, velocity increasing from 3000 m/s to 4200 m/s that probably implies on the onset of quartz cementation. It has been continued towards the marine and fluvial sequences of Fruholmen Formation (Fig. 5.2). An exceptional case here is the Hekkingen Formation which shows an abnormal behavior and a velocity drop downward to 2900 m/s. Organic-rich Hekkingen Formation which is outlined by black dots in Figure 5.2a indicates lower velocity than adjacent layers, while showing higher density.

The density- and porosity-depth trends in general conform to trends for all wells; however, the Hekkingen Formation shows abnormal behavior particularly in the lower part where density decreases and porosity increases with depth. The density-velocity cross-plot is applied to determine the transition zone between mechanical and chemical compaction. In well 7120/7-2, two sets of data points are labeled based on density-velocity relation (Fig. 5.2d). As can be seen, bulk density values reveal a narrow range, while the velocity values show dramatic increase. Therefore in spite of more and less similar values for density, velocity shows much difference between sediments undergone different compaction. If sediment bearing the chemical compaction therefore, velocity increase suddenly by onset of cementation (Bjørlykke et al., 2010)

The upper part of shallow buried Torsk Formation sediments show much lower density than the interpolated (or expected) trend of the whole sediments within the well. The same outliers on the density-depth plot also correspond to points which show deviation from the general linear trend on the velocity-depth plot. These points, enclosed in green ellipses in Figure 5.2a and 5.2b, have lower velocities and densities than their adjacent sediments. These evidences may imply an overpressure which reduces both velocity and density.

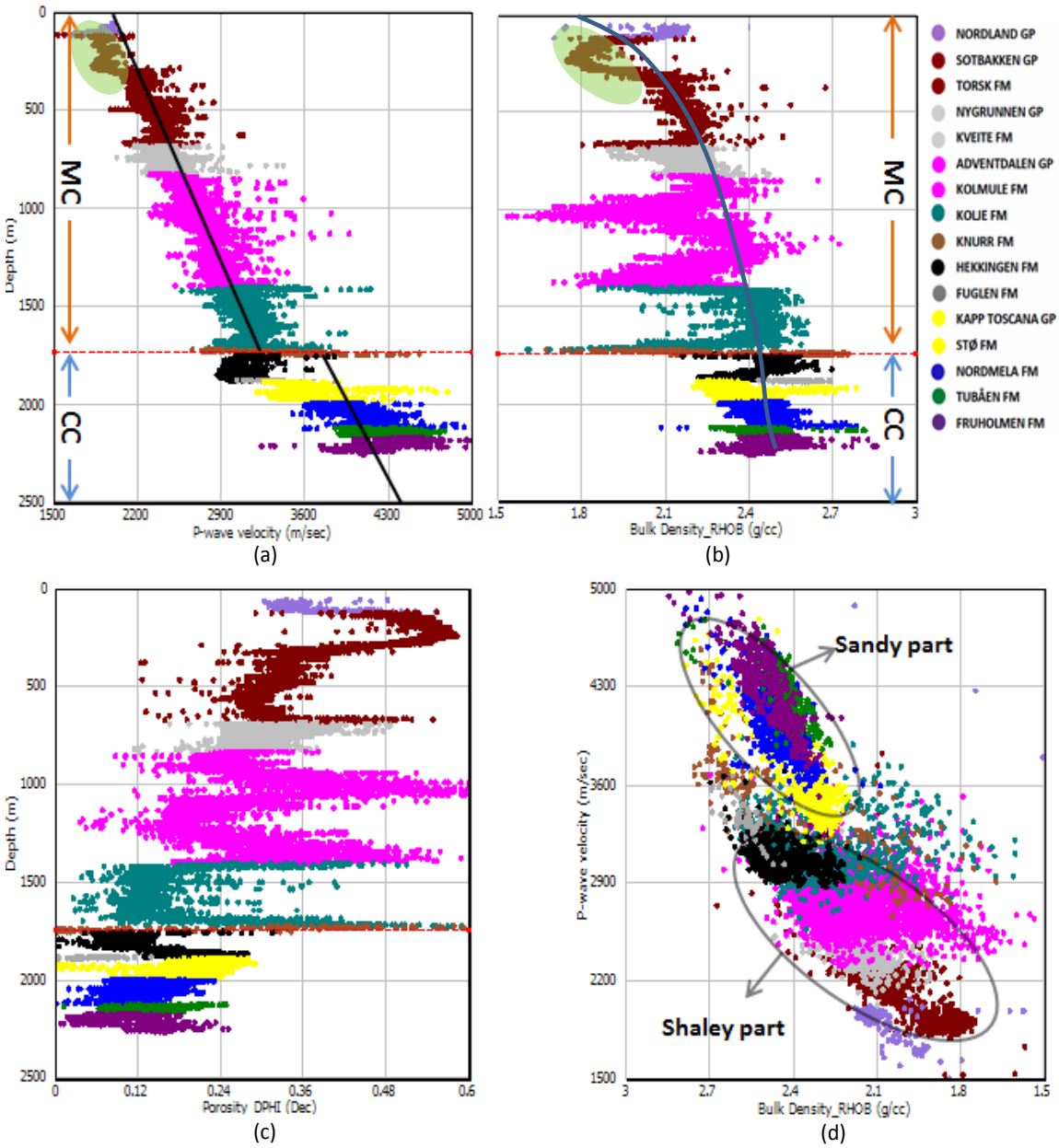

Fig. 5.2. Log data points observed from well 7120/7-2 outlined in; (a) Vp-depth, (b) density-depth, (c) porosity-depth, (d) velocity-density plots.

The lithology distribution in sedimentary basins can be controlled by volume of shale; hence the same plots have been made with volume of shale as a color code in order to study the compaction trends in the area of interest. Volume of shale is calculated from gamma ray log readings. In these plots, only the points related to clean sand and shale are plotted and the data points between these two extremes have been eliminated. Clean sand and shale are defined as V_{sh}<25% and V_{sh}>75% respectively. Similar trends are observed as previously described when lithology is discriminated by volume of shale (Fig. 5.3). These plots show stronger separation between the two compaction domains.

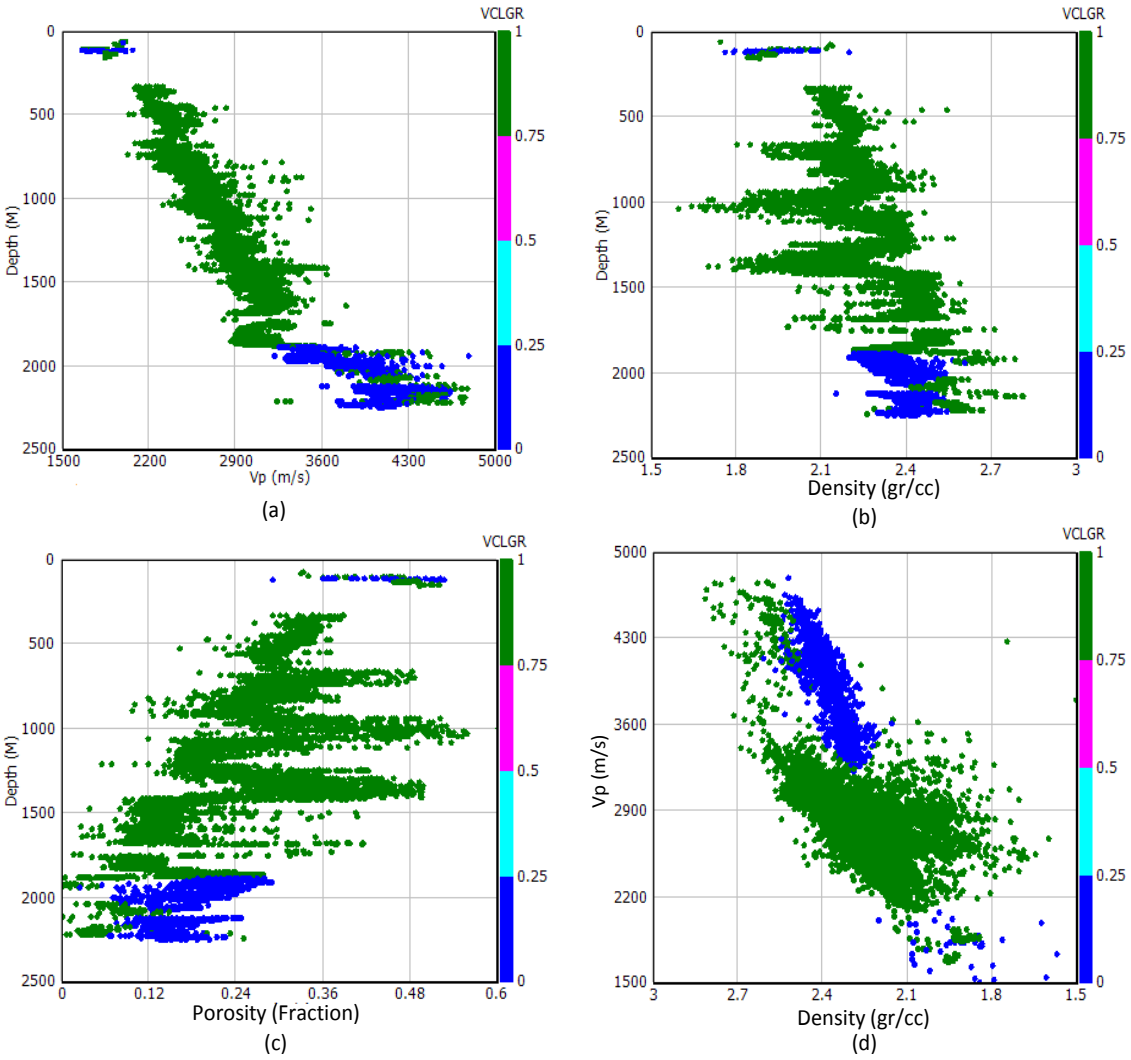

Fig. 5.3. Data points of well 7120/7-2representing clean sand and shale in (a) Vp-depth, (b) density-depth, (c) porosity-depth, (d) velocity-density plots

The other wells in this area (wells 7120/8-1, 7120/8-2 and 7120/8-3) express the same results as achieved before for well 7120/7-2 (Figs. 5.4, 5.5, 5.6, 5.7, 5.8 and, 5.9). The velocity-depth trends display two different zones with distinctive gradients. Knurr Formation can be distinguished for these wells as the border isolating the two compaction zones. The great increase in velocity values above and below of the Knurr Formation provides a good characteristic for discriminating the zones. Hekkingen Formation keeps its anomalous behavior in the V_p-depth trend for the other wells.

Density and porosity trends for these wells display similarly increasing and decreasing trends with depths as seen in well 7120/7-2. Although a sharp distinction in density/porosity values cannot be detected in depth trends, the two zones are segregated reliably in Vp-density cross-plots (Figs. 5.4d, 5.5d and, 5.6d). Lithology plots for these wells are also generated after discriminating sand and shale data points.

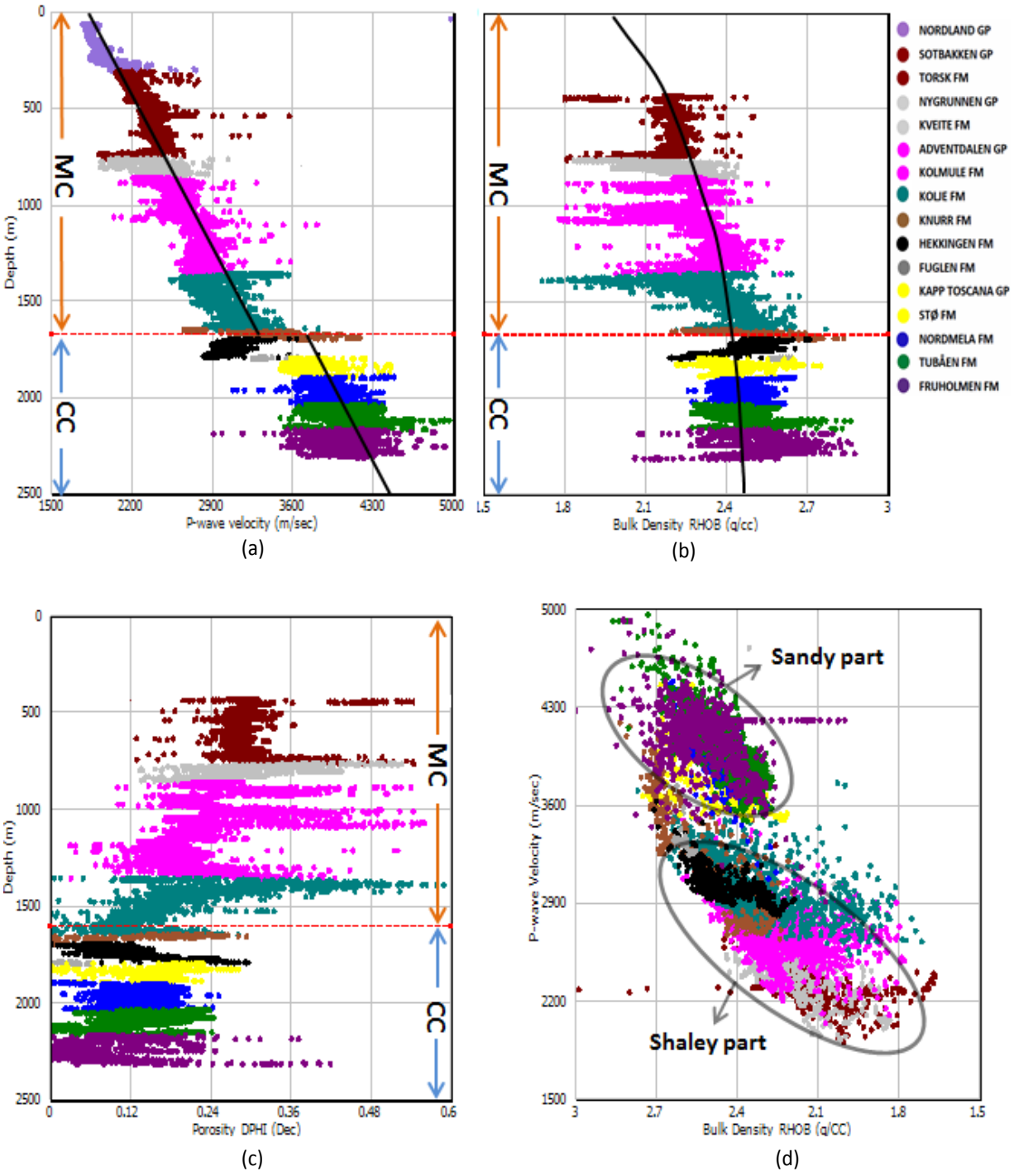

Fig. 5.4. Log data points observed from well 7120/8-1 outlined in; (a) Vp-depth, (b) density-depth, (c) porosity-depth, (d) velocity-density plots.

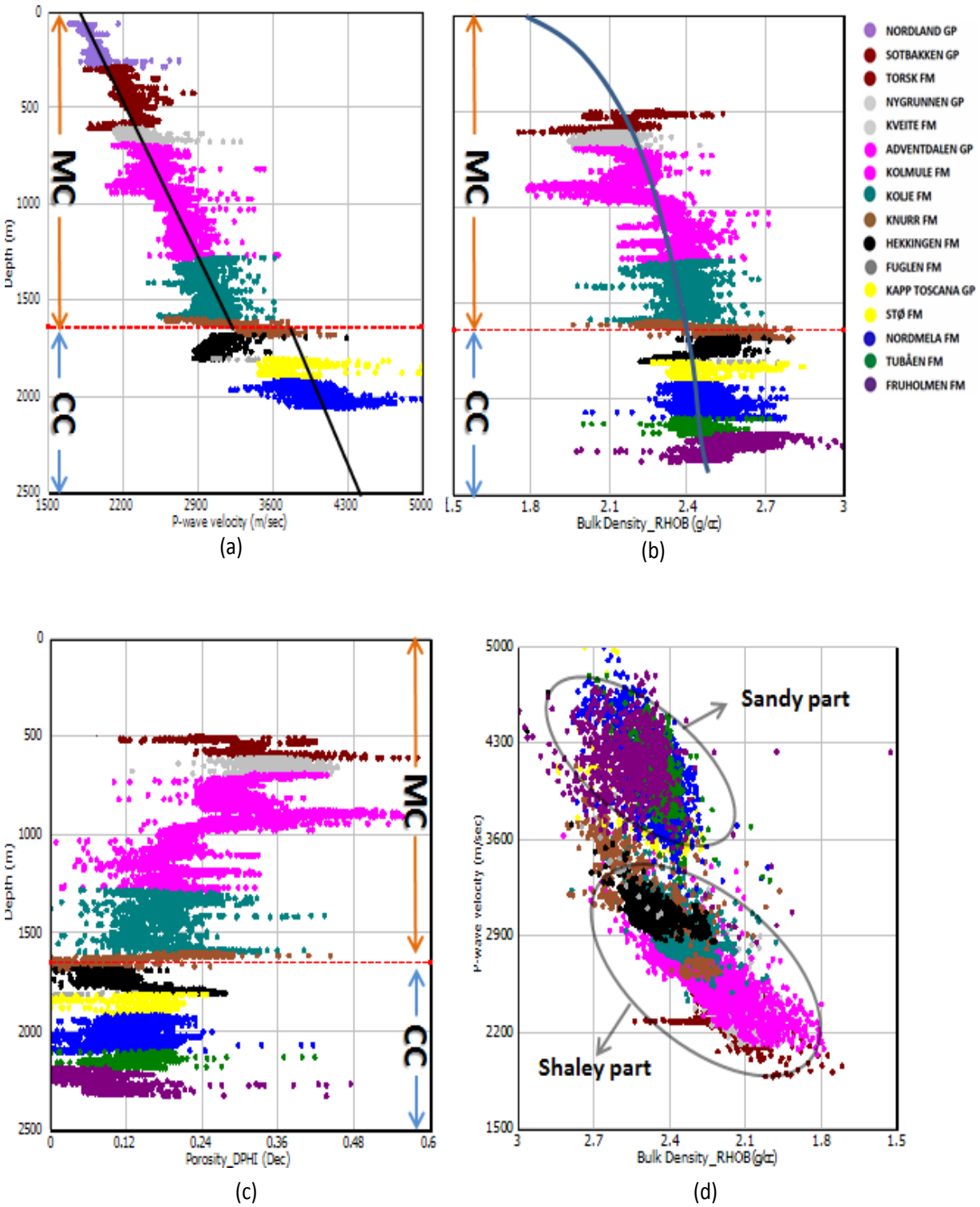

Fig. 5.5. Log data points observed from well 7120/8-2 outlined in; (a) Vp-depth, (b) density-depth, (c) porosity-depth, (d) velocity-density plots.

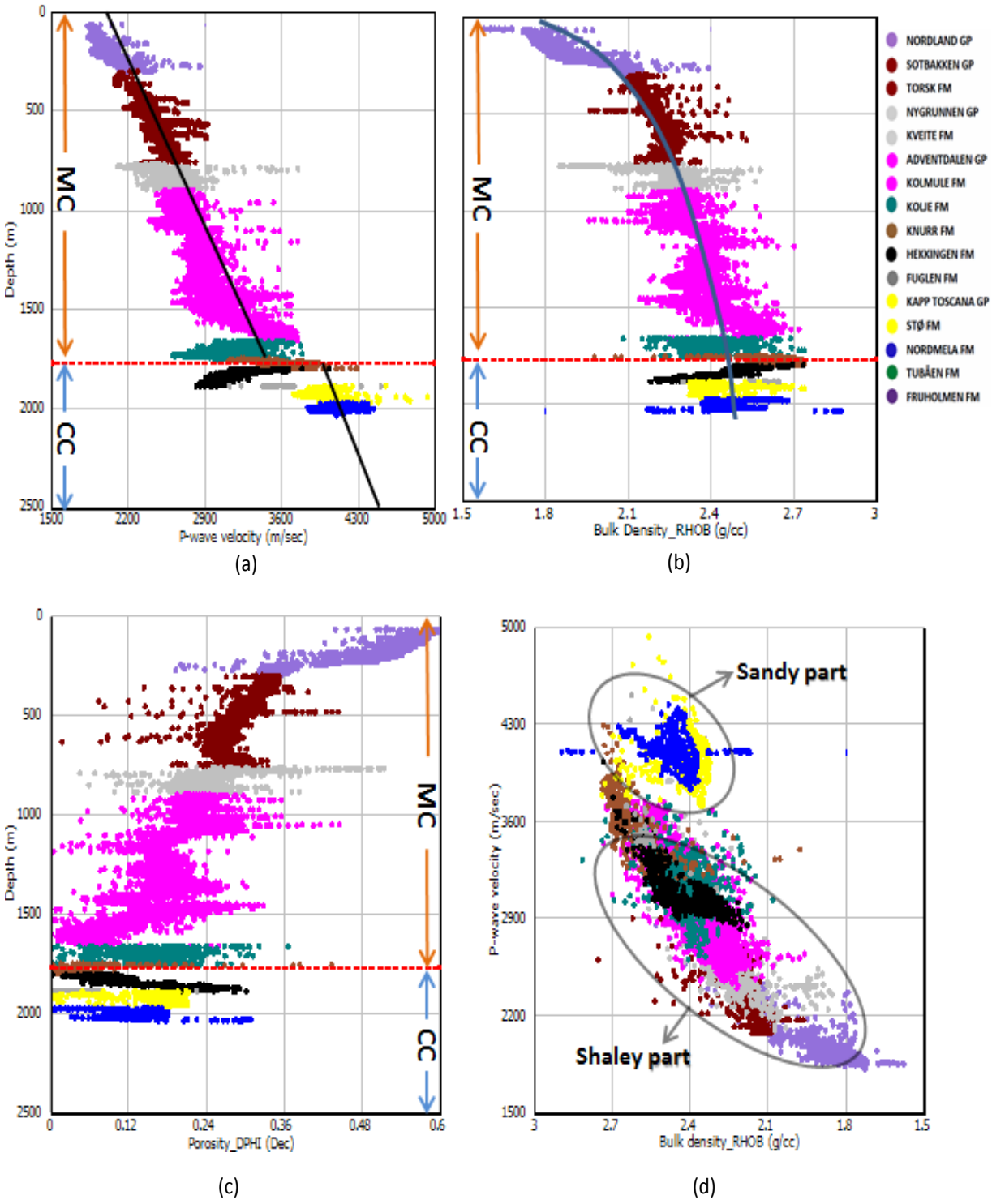

Fig. 5.6. Log data points observed from well 7120/8-3 outlined in; (a) Vp-depth, (b) density-depth, (c) porosity-depth, (d) velocity-density plots.

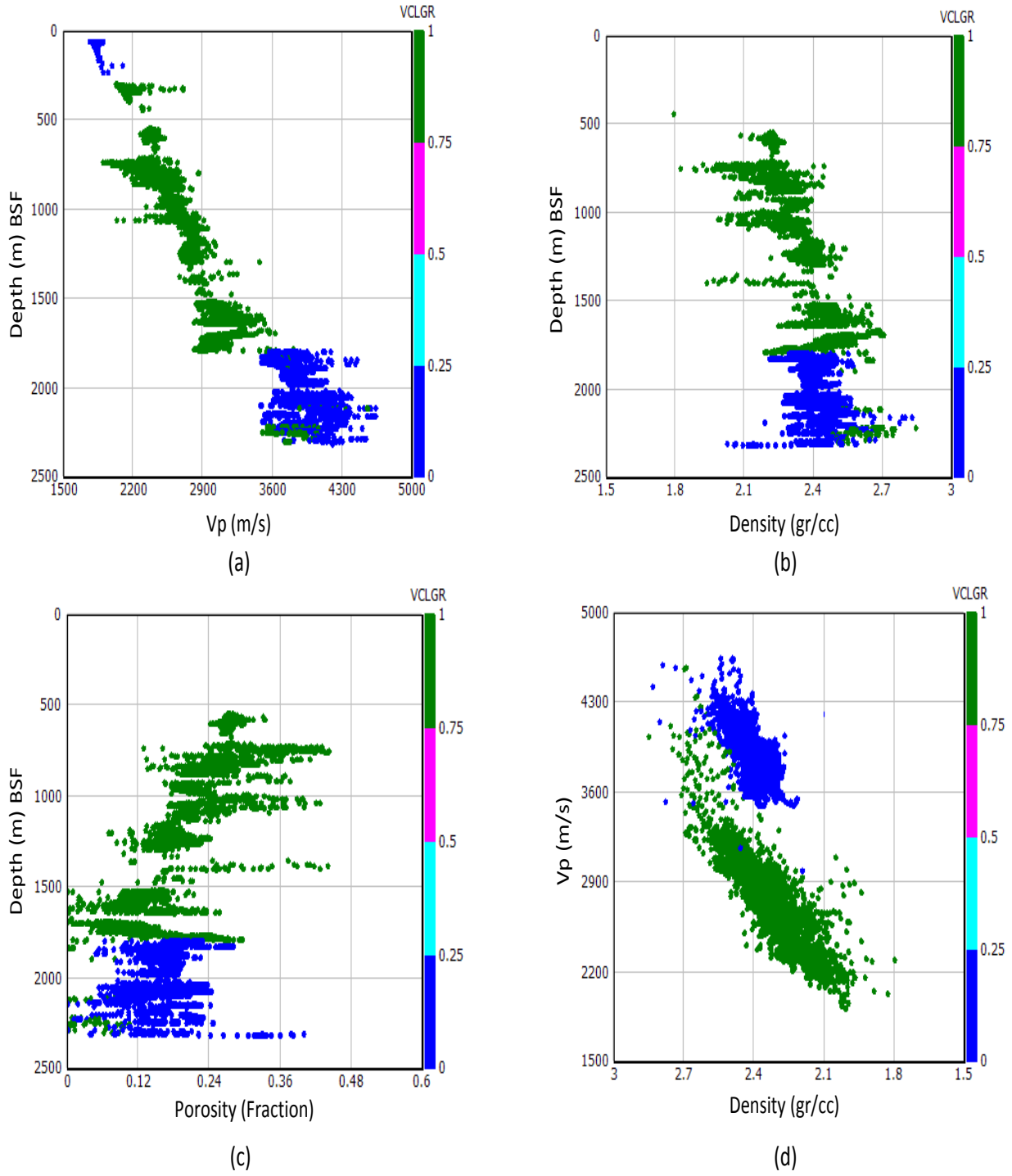

Fig. 5.7. Data points of well 7120/8-1representing clean sand and shale in (a) Vp-depth, (b) density-depth, (c) porosity-depth, (d) velocity-density plots.

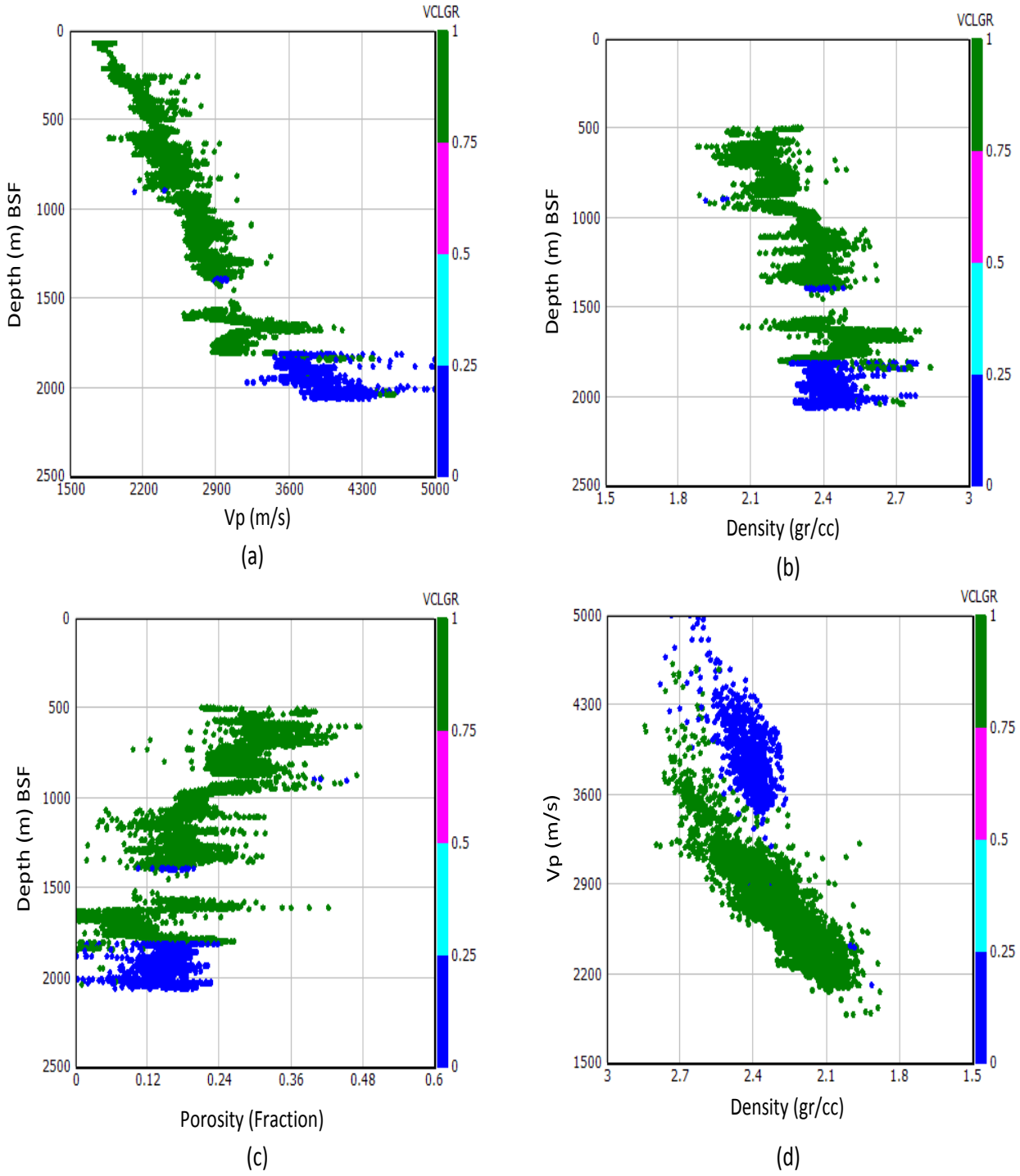

Fig. 5.8. Data points of well 7120/8-3representing clean sand and shale in (a) Vp-depth, (b) density-depth, (c) porosity-depth, (d) velocity-density plots.

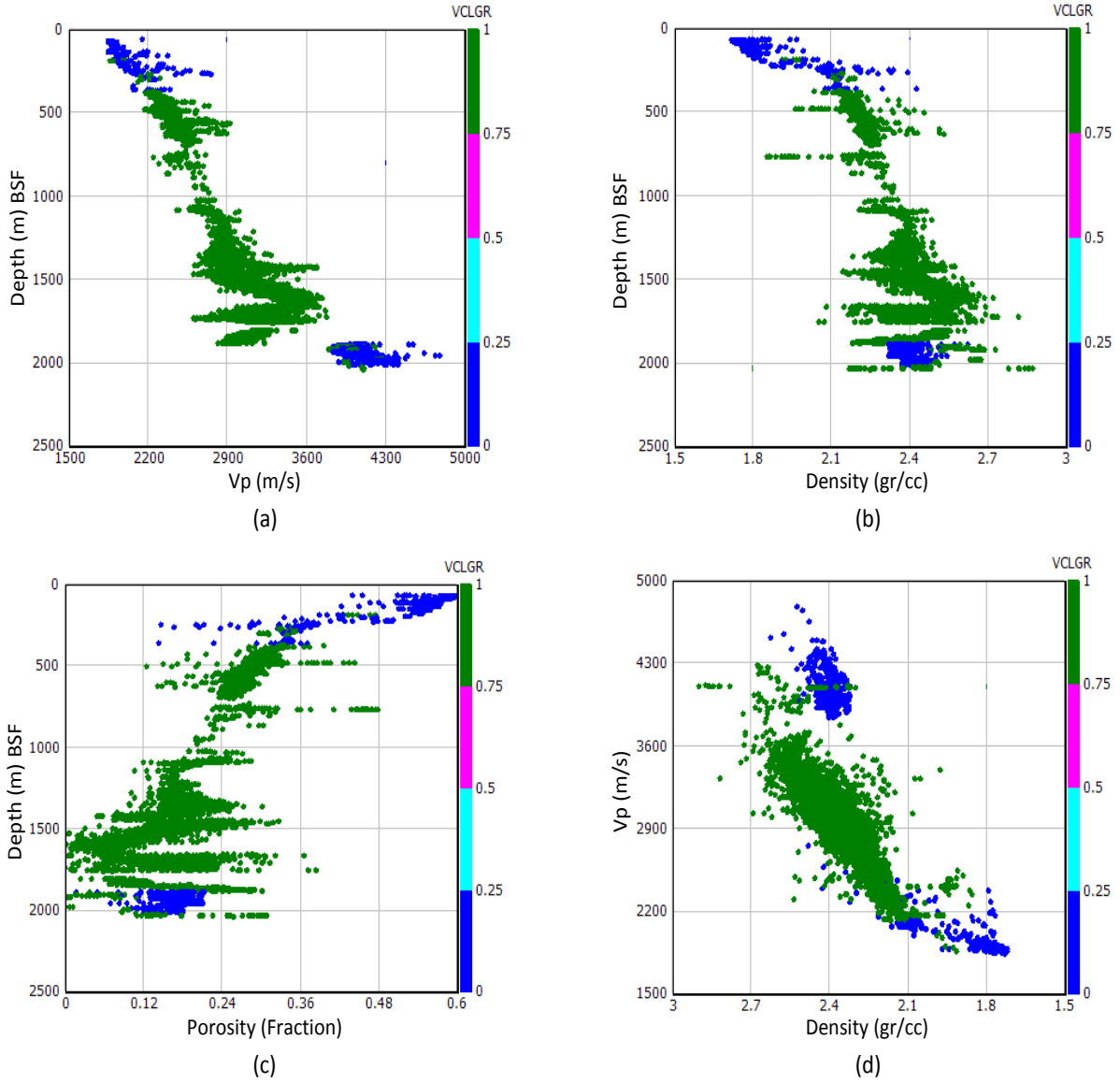

Fig. 5.9. Data points of well 7120/8-3representing clean sand and shale in (a) Vp-depth, (b) density-depth, (c) porosity-depth, (d) velocity-density plots.

5.1.2. Transition zone

According to the well log analysis particularly sonic velocity logs, the transition zone from mechanical to chemical compaction occurs within the Knurr Formation. This is determined by plotting three petrophysical logs with depth ($V_{p,}$ RHOB and DPHI) and also by crossplot of density and velocity (Fig. 5.5). Well 7120/8-2 is selected as a reference well detailed study because of good lateral extension of Knurr formation and also for availability of more complete data base. At the present bottom sea floor depth (BSF), the transition zone for well 7120/8-2 is found at 1640 m burial depth corresponding to the temperature of 61^0C; however after correction for exhumation the transition depth shifts toward nearly 2000 m burial depth and temperature of 74^0C (Table 5.1).

Table.5.1. Transition zone before and after exhumation correction and also corresponding temperature base on geothermal gradient derived from BHT data (see section 3.4).

Well Name	Depth (BSF) (m)	BHT (^{0}C)	TZ (BSF) (m)	Temperature (^{0}C)	TZ (exhumation correction)	Temperature (exhumation correction)
7120/7_2	2260	97	≈ 1741	≈ 63	≈ 2541	≈ 92
7120/8_1	2315	95	≈ 1670	≈ 57	≈ 2465	≈ 84
7120/8-2	2320	91	≈ 1640	≈ 61	≈ 1970	≈ 74
7120/8_3	2033	58	≈ 1770	≈ 40	≈ 2670	≈ 60

Besides the velocity-depth plot, the density-velocity cross-plot also reveals the Knurr Formation as a good candidate for transition zone. In spite of quite similar bulk density ranges for the two different zones above and below the transition depth, significant increase is observed in velocity values starting close to 3000 m/s and reaching up to 4000 m/s throughout the Knurr Formation. This is due to the beginning of quartz cementation (Fig. 5.5d). In addition, this transition zone at the present depth has been recognized in other wells except well 7120/8-4 (Figs. 5.2, 5.4, 5.5 and, 5.6).

Here, the Knurr Formation has been more focused and the changes of three different petrophysical logs including P-wave velocity calculated from sonic log (DT), bulk density (RHOB) and, porosity log calculated from bulk density log (DPHI) have been investigated (Figs 5.10, 5.11 and, 5.12). The trend of P-wave velocity shows fluctuation with depth depicting slight overall increase towards the end of the Kolje Formation, but afterwards, throughout the Knurr Formation, a remarkable increase of velocity can be observed from around 3000 m/s to about 4000 m/s indicating the beginning of chemical compaction. The lithology dominated in the Knurr Formation is mainly deep marine shales with high gamma ray values and a thickness of about 86 m (see gamma ray log in Figs 5.10, 5.11 and, 5.12).

The porosity and density logs reveal little variation between upper and lower boundaries covering the Knurr Formation (Fig. 5.11) and therefore are not appropriate indicators of transition zone, whereas velocity log changes significantly only by 2%-4% cement precipitation (Marcussen et al., 2010; Storvoll et al., 2005). Density displays increase within the Knurr Formation ranging between approximately 2.15 g/cc and about 2.67 g/cc and porosity decrease from about 25% down to around 3% at the lowest part of the formation. As well as compaction trend results for other wells, the Hekkingen Formation as a source rock

demonstrates unusual results where velocity decreases down to about 2900 m/s. This may be result from the relatively soft kerogen content dominated in this formation (Storvoll et al., 2005).

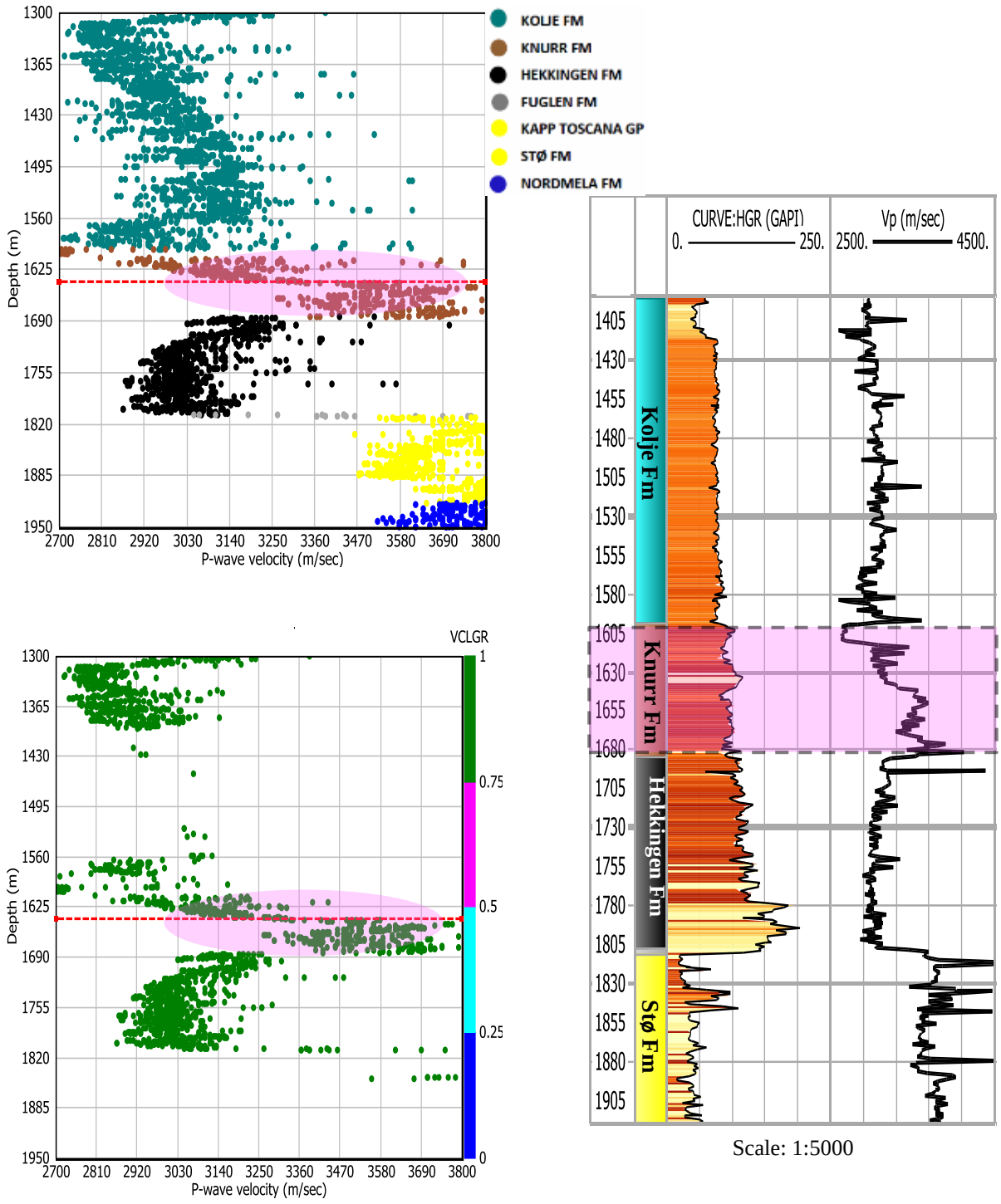

Fig. 5.10. Right, gamma ray and velocity logs acquired from well 7120/8-2 corresponding to transition zone (highlighted area) and its nearby present depths that is about 1640 m (BSF). Left, velocity-depth plot of the same depths as well log shown at the right side. The bottom plot is color coded with respect to clay content.

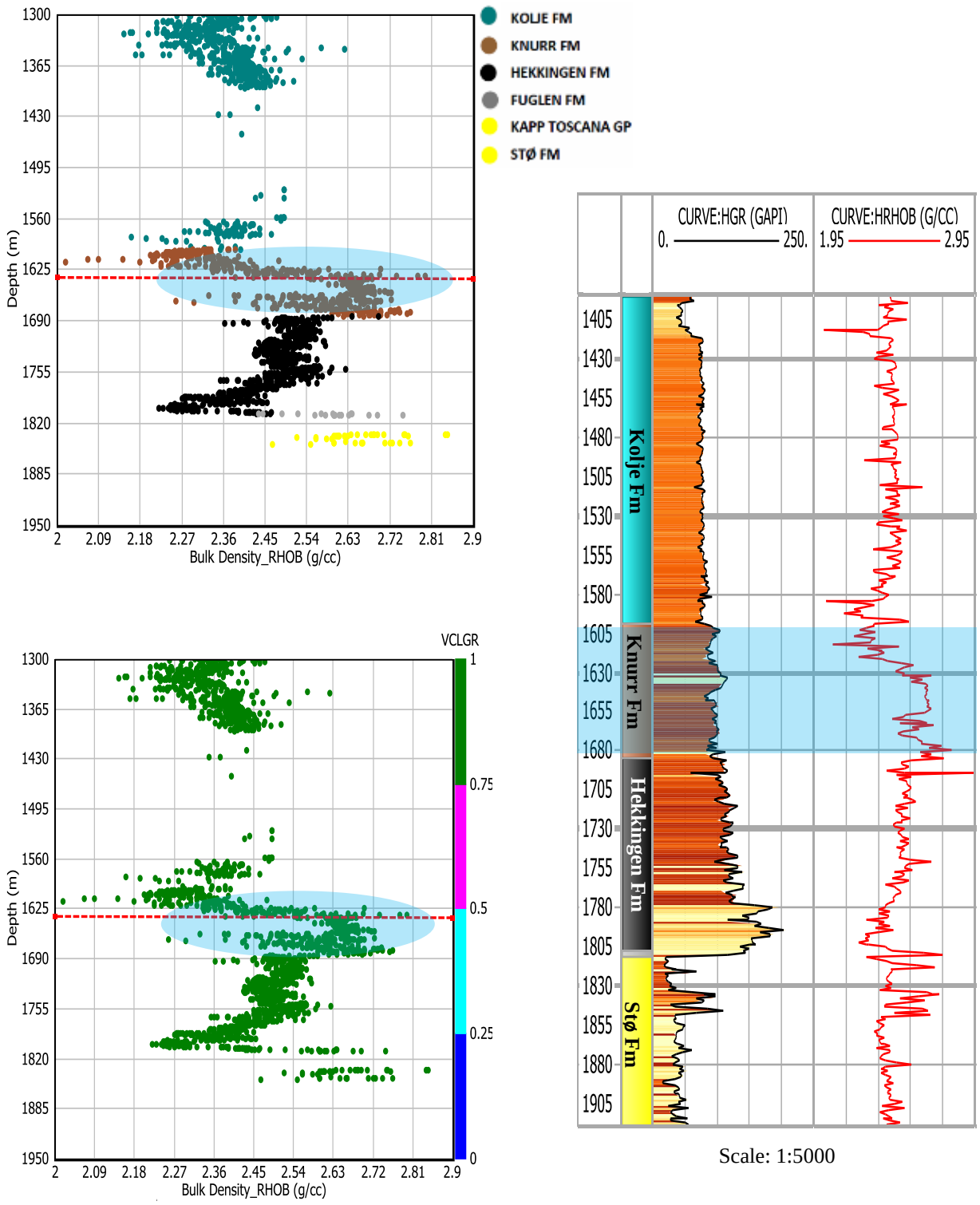

Fig. 5.11. Right, gamma ray and density logs acquired from well 7120/8-2 corresponding to transition zone and its nearby depths. Left, density-depth plot of the same depths as well log shown at the right side. The bottom plot is color coded with respect to clay content.

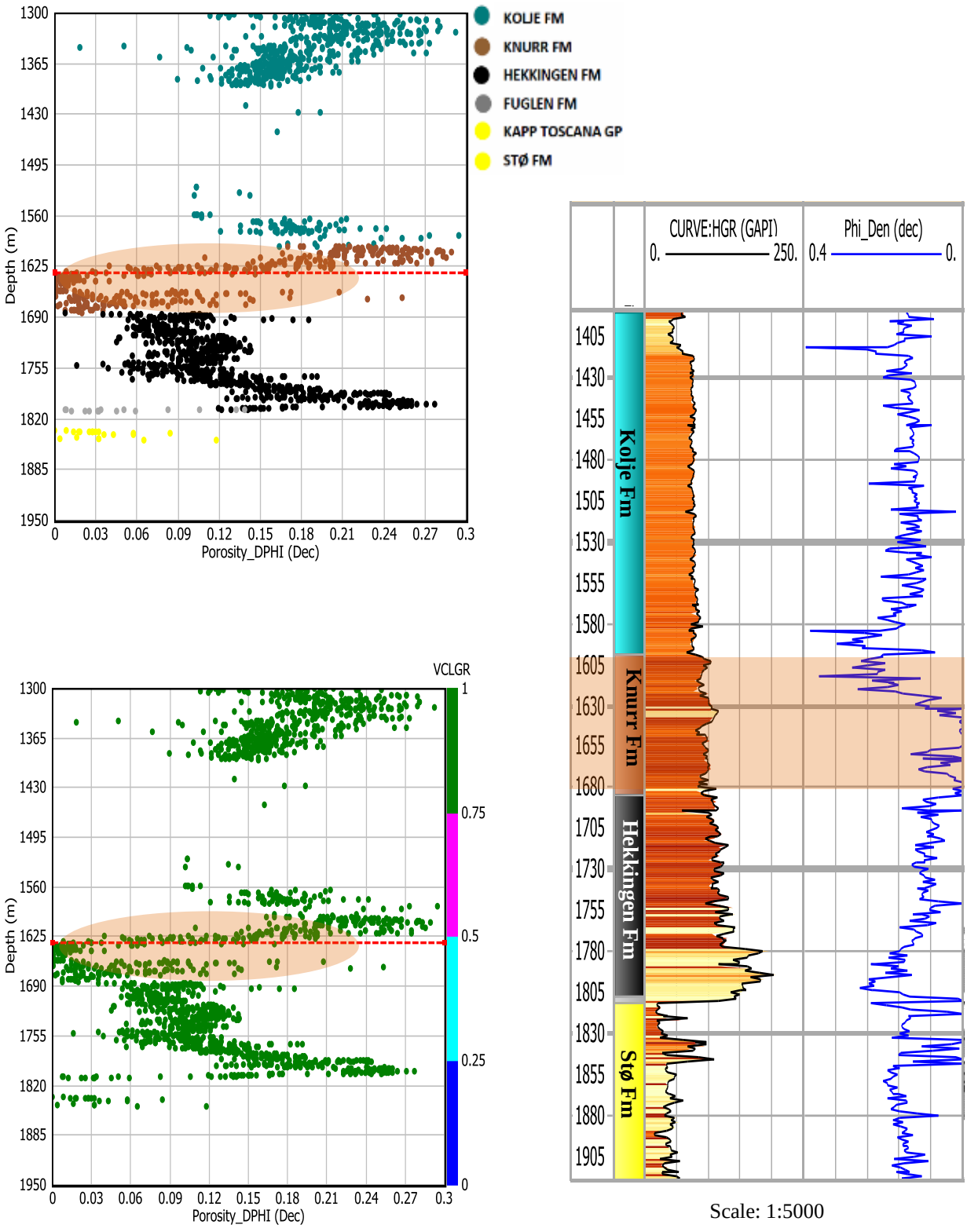

Fig. 5.12. Right, gamma ray and porosity logs acquired from well 7120/8-2 corresponding to transition zone and its nearby depths. Left, porosity-depth plot of the same depths as well log shown at the right side. The bottom plot is color coded with respect to clay content.

5.1.3. Exhumation

Figure 5.13 displays the velocity-depth plot accompanied with curves derived from experimental compaction of variable samples conducted by different authors. An obvious deviation between data points and experimental curves can be followed from surface to deeper parts. Although the curves are representative of mechanical compaction phenomenon, still a considerable deviation is visible at shallow depths where the sediments compact mechanically by increasing effective stress. The reason for the observable deviation can be explained by the uplift of the study area (Jaspen and Chalmers 2000; Cavanagh et al., 2006; Marcussen et al., 2008; Ohm et al., 2008; Henriksen et al., 2011). By moving down the data points in the velocity-depth plot, a good match is observed between the data points and the experimental curves (Fig. 5.13b).

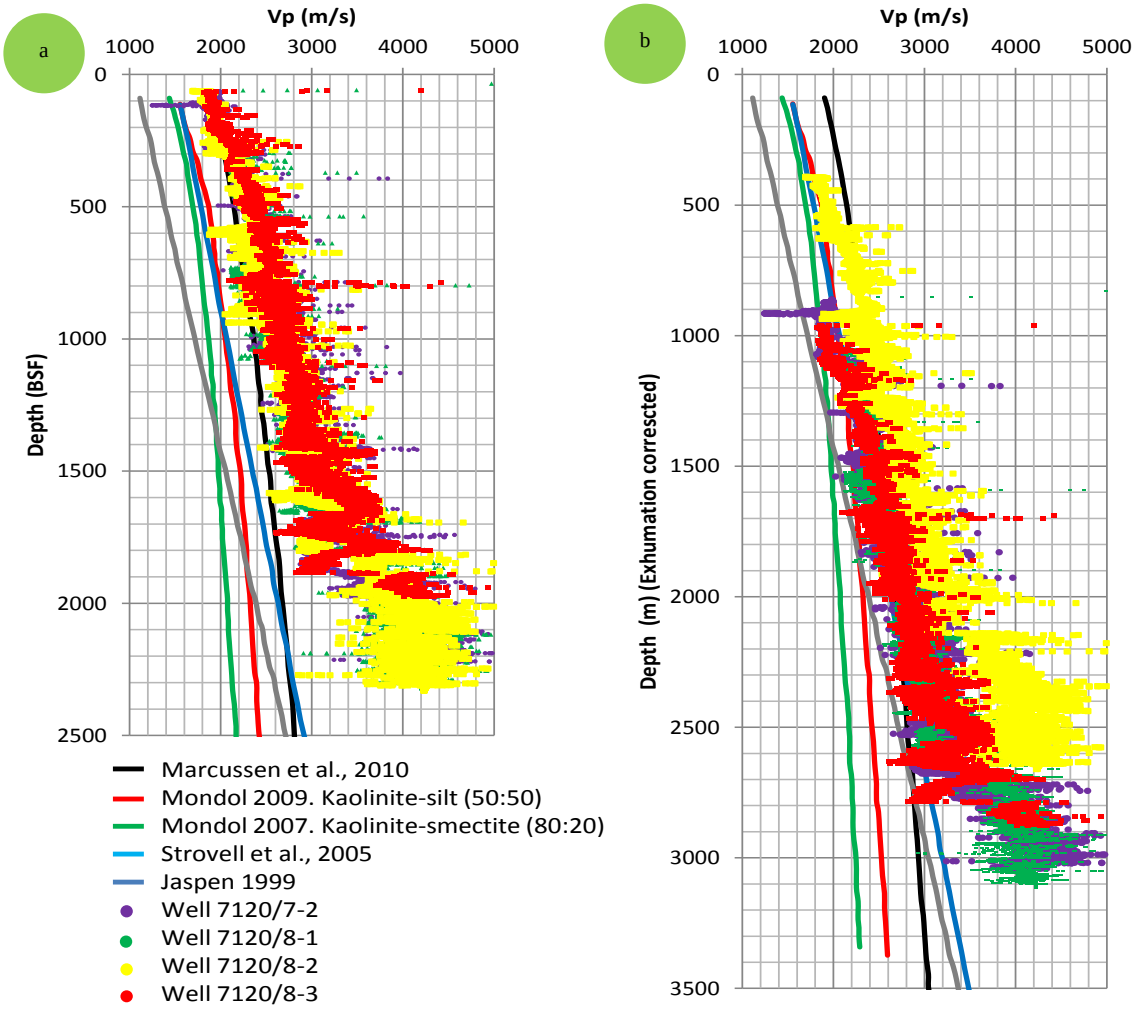

Fig. 5.13. Crossplot of velocity versus depth for wells in the Askeladd area to investigate the velocity trend before (a) and after (b) correction of exhumation. The published natural and experimental compaction curves have been included for comparison.

Among the published experimental compaction trend, the kaolinite-silt (50:50) introduced by Mondol (2009) is chosen due to two main reasons: it is considered that the effect of fluid and also mixed of clay and silt seems more realistic in composition for quantifying the amount of exhibition. Figure 5.14 demonstrates the approximate calculation of exhumation for each well. The black window shows the deviation from the experimental published line of Mondol 2009 while at the right side sediments move down after correction of exhumation corresponding to velocity-depth trend as a function of compaction. Volume of Shale is used as lithology control for each plot. After exhumation correction there is still a mismatch in deeper parts. This is indicative of rock stiffening due to chemical compaction and quartz cementation. It is implies the point, chemical compaction does not match with experimental trend may be due to temperature effect on minerals that we cannot handle it property.

Exhumation estimation for each well is also indicated in Table 5.1 (see section 5.1.2). Among these wells, well 7120/8-3 which is located in the northern part of Askeladd discovery shows highest amount of exhumation (900 m), while in Askeladd central, it is declines to approximately 300 m burial depth. This study mainly focuses on estimation of exhumation based on the sonic velocity log, whereas it seems vitrinite data provides more accurate and appropriate estimation (Ohm et al., 2008).

In addition, the uplift values calculated in each well has been interpolated for the whole study area and displayed in Figure 5.15. Regarding the study area discussed in this thesis which can be found in Figure 5.15 under the dashed line, an increasing trend in exhumation observed from west to east. Whilst regionally, a decreasing trend is observed from the east to the west after taking into account the information from the other wells drilled in adjacent area (the area located above the dashed line in Figure 5.15.

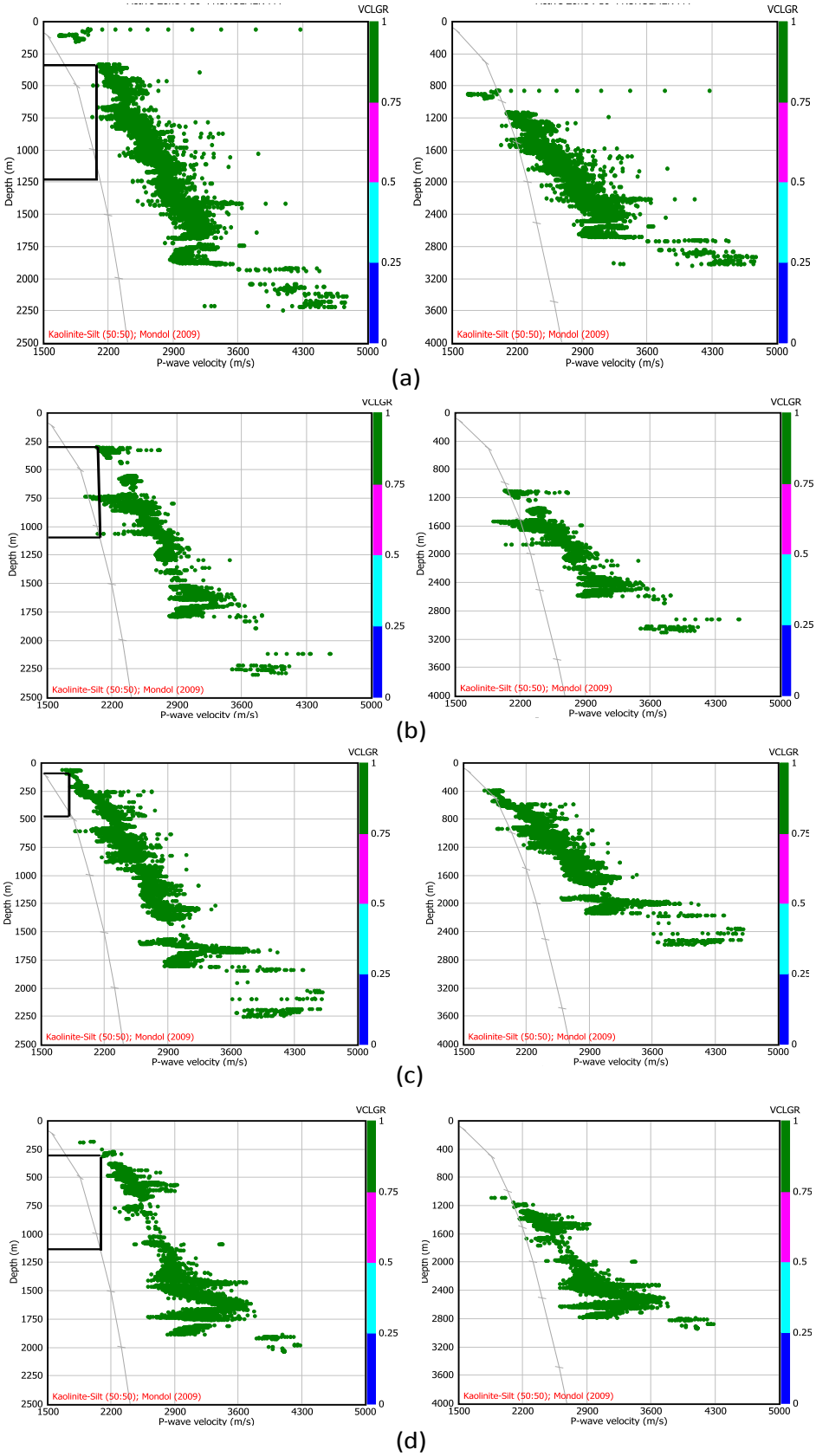

Fig. 5.14. Estimation of exhumation observed in wells (a) 7120/7-2, (b) 7120/8-1, (c) 7120/8-2, and (d) 7120/8-3, based on experimental published compaction trend of Mondol 2009. Kaolinite-silt (50:50).

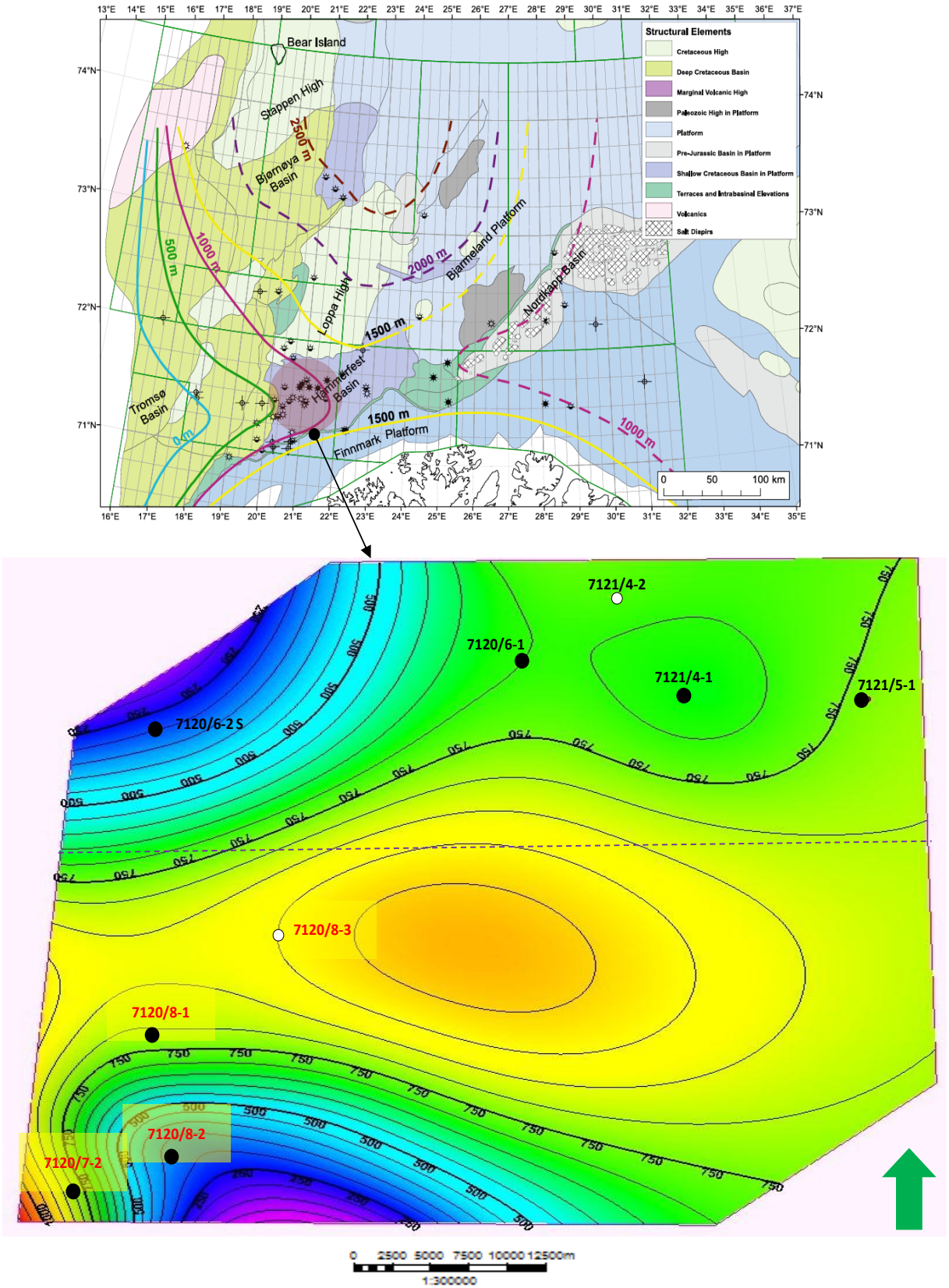

Fig. 5.15. Tentative uplift map based on vitrinite reflection and temperature data for Norwegian Barents Sea (a) and local contour map shows exhumation estimated in Askeladd discovery by interpolation of data for each well (b). Dash line represents an approximate boarder between Snøhvit field (up) and Askeladd discovery (down). These field are located in the Hammerfest Basin where the amount of uplift ranging between around 500 m to close 1500 m.

5.2. Discussion

Compaction trends derived from well logs give general overview of how rock properties change as a function of compaction in sedimentary basins. The velocity-depth trends for all wells except well 7120/8-4 represent pretty near linear trends for the sediments of Askeladd discovery in the Barents Sea. However, one can specify two distinct intervals (Figs. 5.2, 5.4, 5.5 and 5.6) in terms of factors controlling compaction processes. First interval (MC) starting from the surface and continuing down until around 1700 m (average values for different wells) burial depth show gradual increase in velocity, corresponding to mechanical compaction. Effective stress increase during burial is a determining factor in mechanical compaction and is controlled by overburden pressure and pore pressure (Bjørlykke et al., 2010). On the other hand, temperature is a key factor at the second interval (CC) and causes considerable increase in velocity during burial due to quartz cementation. These results are consistent with the previous studies of compaction in sedimentary basins which points out that velocity slightly increases downward before the onset of quartz cementation, but after precipitation of only 2% to 4% quartz cement, it increases sharply (Marcussen et al., 2010; Bjørlykke et al., 2010). Although cementation process is a continuous process and quartz cement percentage normally increases with increasing depth and temperature (Bjørlykke and Jahren, 2010), velocity increase does not show continuation in the same dramatic gradient. After a very sharp increase at the onset of chemical compaction domain, rate of velocity increase becomes slower (Fig. 5.1a). Since the quartz precipitation begins to occur at grain contacts, rocks get stiffness and their velocity rise sharply. The later quartz cement crystals, however, are precipitated in pore spaces and their contribution for stiffening the rock is not as much as the earlier cement minerals (Vernik and Nur, 1992; Storvoll et al., 2005, Marcussen et al., 2010)

The Hekkingen source rock does not obey the velocity-depth trend and demonstrates deviation from normal velocity-depth trend. Velocity shows decrease between top and bottom of formation (3500 m/s to 2900 m/s). It is the main source rock in Norwegian Barents Sea and consists of deep marine shale including high amount of organic matter (20%). Physical properties of kerogen seem to be a main reason for reduction in velocity values in Hekkingen source rocks (Storvoll et al., 2004). Unlike velocity, porosity increases throughout Hekkingen formation because of hydrocarbon generation that prevents further cementation and porosity losses (Bjørlykke et al., 2010). Bulk density does not show much difference within Hekkingen

Formation because rock density ranges are close to each other. Nevertheless, density has been decreased slightly in the lower parts of the formation which may be due to presence of kerogen or higher porosity.

The upper part of Torsk Formation encountered in well 7120/7-2 shows anomalously lower density and velocity as outlined by green ellipses (Fig. 5.2a and 5.2b). Lower velocity and density can be resulted from overpressure (Storvoll et al., 2005). In terms of lithology, Torsk Formation is dominated by generally non-calcareous claystones and tuffaceous horizons can also be seen within the formation (NPD Factpages). Tuffaceous horizons which consist of volcanic ash deposited during the volcanic activity in Late Paleocene and Early Eocene (Knox and Morton, 1988; Skogseid and Eldholm, 1988) are rich in smectite clay minerals. Smectite rich shales show a substantial reduction in velocity with depth (Thyberg, 2000). Moreover, overpressure can happen in smectite clays even in shallow depths since smectite have very low permeability (Storvoll et al., 2005).

Density ranges approximately between 1.9 g/cc and 2.7 g/cc for all wells (Fig. 5.1b). Density also increases with depth, but still relatively independent of quartz cementation. However, carbonate cementation possibly causes considerable increase in density (Bjørlykke and Jahren, 2010). Therefore, density-depth trend probably is not a good indicator to determine the starting point of chemical compaction and precipitation of quartz cement. Density-velocity trend is more appropriate for this case because velocity changes significantly in spite of relatively the same density distribution (Fig. 5.1d).

One can specify two different clusters from density versus velocity crossplot (Fig. 5.1d). The blue cluster represents the mechanically compacted successions where there is no noticeable increase in velocity. These changes sharply at the onset of quartz cementation (green cluster). Porosity decreases with depth in siliciclastic rocks as a function of compaction. However, the rate of porosity loss reduces by the start of quartz cementation and then rock becomes stiffer, resulting in significant rise in velocity. Previous studies have reported velocity as highly dependent on rock porosity (Rafavich et al., 1984) and as will be discussed later, the results also affirm that by increasing porosity, velocity decreases.

Transition between mechanical and chemical compaction probably occurred in the Knurr Formation according to analysis of well logs. Well 7120/8-2 (reference well) clearly shows this zone by a sharp increase in velocity throughout the Knurr Formation (Fig. 5.10). It also

reveals that within rather uniform lithology, chemical compaction is a process related to increase of velocity. Gamma ray log does not show too much variation within Knurr Formation (Fig. 5.10) indicating relatively uniform lithology distribution; thus onset of quartz cementation as a function of temperature is probably responsible for the increase in velocity.

The transition from mechanical to chemical compaction occurs at 1640 m burial depth (BSF) corresponding to temperature of around 61^0C when geothermal gradient has been considered at about 37^0C/km. However, after correction for exhumation it reaches to approximately 2000 m burial depth corresponding to temperature of about 74^0C (Table 5.1). It conforms to studies stating that at shallow depths (down to 2 - 2.5 km), mechanical compaction is the main compaction process and is controlled by increasing effective stress, whereas at the deeper part of basins where temperature is higher than 70-80^0C sediments are governed by chemical compaction (Bjørlykke et al., 2010).

Quartz cement in sandstones is sourced from quartz grain dissolution, whereas clay minerals act as the source of quartz cements in mudstones (Bjørlykke et al., 2010). As discussed, Knurr formation almost consists entirely of shale; hence the source of quartz cement in this zone is most likely connected to dissolution of smectite in presence of K-feldspar which releases illite and quartz (Bjørlykke et al., 2010). Consequently, transformation of kaolinite to illite supplies quartz cement for shales at the deeper parts of basins (see section 4.1.2).

Chemical compaction is a continuous process, but still grain coating prevents further chemical compaction and preserves porosity (Bjørlykke & Jahren, 2010). It has been considered to be a significant process that stops cementation in considerable number of reservoirs (Bjørlykke & Jahren, 2010). The results demonstrate this fact quite nicely where the average porosity calculated from bulk density (DPHI) and neutron log (NPHI) in Stø Formation as the main reservoir is about 20% which represents good to excellent reservoir quality. It can be classified as intermediate buried sandstones (2.0-2.5 km, 50-120^0C), but it seems to be situated shallower than the time of deposition due to extensive uplift. The bulk density variation in Stø reservoir is higher compared to other formations. This implies the presence of hydrocarbon particularly gas in this formation. The Nordmela Formation also demonstrates relatively good reservoir quality, however, based on completion report of wells in the Askeladd discovery, hydrocarbon accumulation has only been observed within Stø Formation (NPD Factpages).

Barents Sea is geologically different from the rest of the Norwegian continental shelf due to the extensive sediment uplift which occurred particularly during the Cenozoic time. Results of this study reveals that estimation of exhumation (uplift) roughly affirms the previous studies done by Cavanagh et al., (2006) and Ohm et al., (2008), suggesting 500-1500 m and 500-1000 m uplift for the Hammerfest basin and 0-2500 uplift for Norwegian Barents Sea respectively. It is essential to emphasize that the method they have used for estimating the exhumation was based on vitrinite reflectance and temperature data, whilst velocity with depth as a function of compaction processes was employed in this study. It is believed that the ice sheet erosion was the most significant factor controlling extensive Cenozoic uplift in the Southwestern Barents Sea (Cavanagh et al., 2006).

Table 5.1 displays the amount of exhumation occurred in the area of study with temperature corresponding to this burial depth where the amount of exhumation increases toward north considering the well location. Among the wells available in Askeladd field, well 7120/8-3 demonstrates the highest amount of exhumation (900 m), whereas Askeladd central shows reduction in uplift and reaches to 330 m in well 7120/8-2. It is also good to know that the amount of exhumation occurred in Snøhvit field located at northeast, is lower than Askeladd field (Fig. 5.15). Therefore, toward the east, the amount of exhumation increases throughout Hammerfest Basin; however, it is not necessarily fit locally due to geological complexities taken place in the Barents Sea.

We have not worked in detail about the influences of uplift on petroleum system in the area of study. Nevertheless, previous studies reveal relatively high leakage throughout the cap rocks due to uplift (Doré 1995; Gabrielsen and Kløvjan 1997). It is also consistent with exploration results which was mostly unsuccessful in spite of the fact that Hekkingen Formation has been located in oil window prior of uplift (Storvoll et al., 2005; Ohm et al., 2008).

Chapter 6
Rock Physics Diagnostics

Rock physics has been developed to become a significant tool for reservoir characterization (Avseth et al., 2010). For each specific area in consideration to the compaction and depositional environment, rock physics models are possibly determined and rock properties are able to extrapolate away from available wells (Avseth, 2005). Nonetheless, every model has its own advantages and pitfalls because they derived from distinct geological settings (Avseth et al., 2010). In this chapter, we mainly focus on rock physics diagnostic of Kapp Toscana Group particularly Stø Formation. We had shear velocity only for well 7120/8-4; therefore this well chosen as reference well for rock physics diagnostics.

6.1. Result

6.1.1. Net to gross ratio

Stø Formation is the main prominent reservoir in this area. Although this formation is mainly constituted of sand, some shaley zones are interbeded within the sand body. Net to gross (N/G) ratio, which is defined here as the ratio of overall clean sand thickness to whole reservoir section, is an important factor in reservoir characterization and production management? Assuming clay volume less than 30% as clean sand, N/G ratio of Stø Formation in the wells drilled in study area is show in Table 6.1. Besides, well correlation associated with gamma ray content for different groups and formations dominated in Askeladd filed demonstrates more and less similar lithology distribution in Stø reservoir (Fig 6.1). The thickness of Stø formation is ranging from 106 m in well 7120/7-2 (SW) to 96 m in well 7120/8-4 (NE) of Askeladd discovery. Overall thickness trend also shows decrease from SW to NE in the area of study. Other formations of Kapp Toscana Group however have shown good reservoir properties but exploration result within those formations was unsuccessful (NPD Factpages).

Table.6.1. Net to gross ratio values in different wells penetrated Stø Formation.

Wellbore name	Gross	Net	Net/Gross
7120/7-2	106	87	0.82
7120/8-1	98	84	0.86
7120/8-2	108	92	0.84
7120/8-3	85	67	0.79
7120/8-4	96	86	0.89

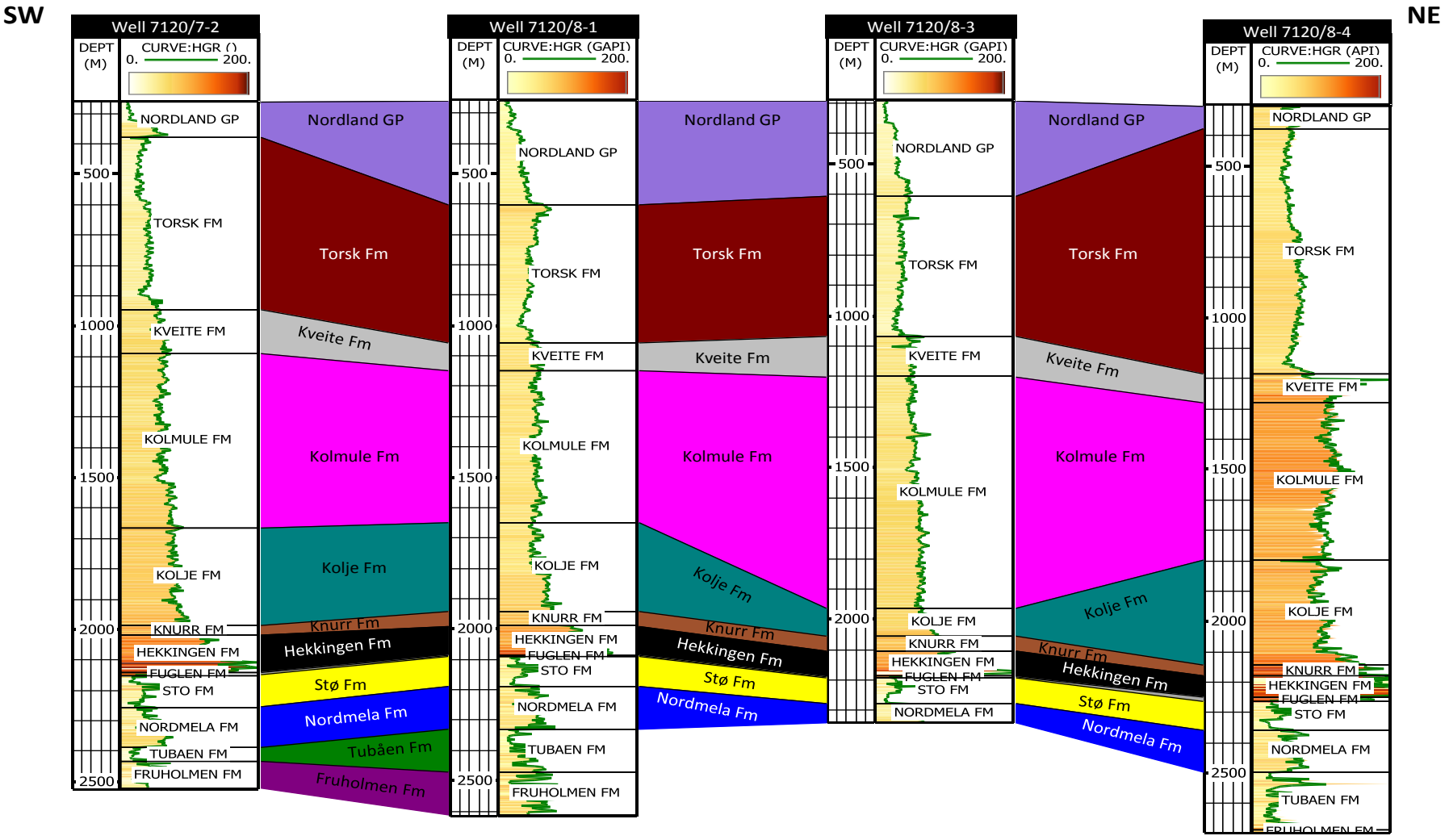

Fig. 6.1. Well correlation of different formation in the Askeladd discovery. A key reservoir unit of prograding coastal sandstones is Stø Formation with Early to Middle Jurassic age.

6.1.2. V_p-V_s relation

By combining the shear velocity data with P-wave velocity one can specify lithology distribution from seismic or sonic log data. It is also important in order to identifying the pore fluid type and as a result helpful for reservoir characterization. As we can see in figure 6.2, by plotting the P-wave velocity versus shear velocity, quite clear separation observed between Kapp Toscana Group as main reservoir in the area of study and Adventdalen Group that is mostly composed of shale and mudstones. Also, relatively linear trend in this plot probably states lithology variation that is become more shaliness downward. Among the rocks with higher amount of shale, Hekkingen Formation (black dot) again demonstrates unusual behavior may be implies the effect of organic matter content that can be reduce velocity (Storvoll et al., 2005).

In addition, we compare the real shear velocity data with different published empirical V_p-V_s relations (Fig. 6.a). Generally the empirical relations of Han (1986) and Castagna et al., (1993) indicating the best fit with our data while largely misfit observe from Krief (1950) empirical relation. Figure 6.2b represents the comparison of different published empirical relation of velocity with relation resulted from this study (see section 3.6). Shear velocity computed for well 7120/8-4 shows ranging between published empirical V_p-V_s relation of mudrock line (Castagna et al., 1985) and Castagna et al., (1993).

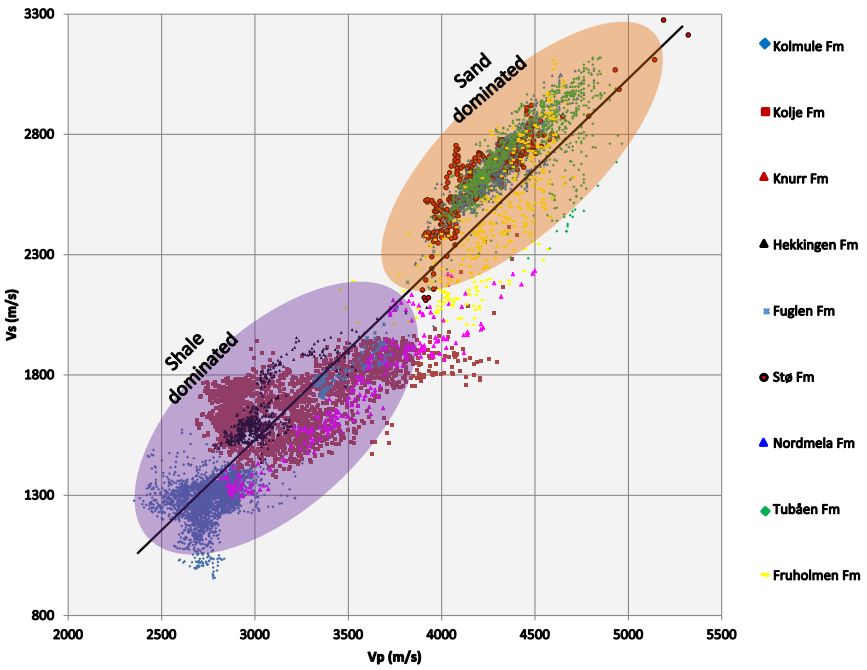

Fig. 6.2. Crossplots of Vp versus Vs for well 7120/8-4. The black trend line represents schematic linear trend among the data point that almost all data fall around this line.

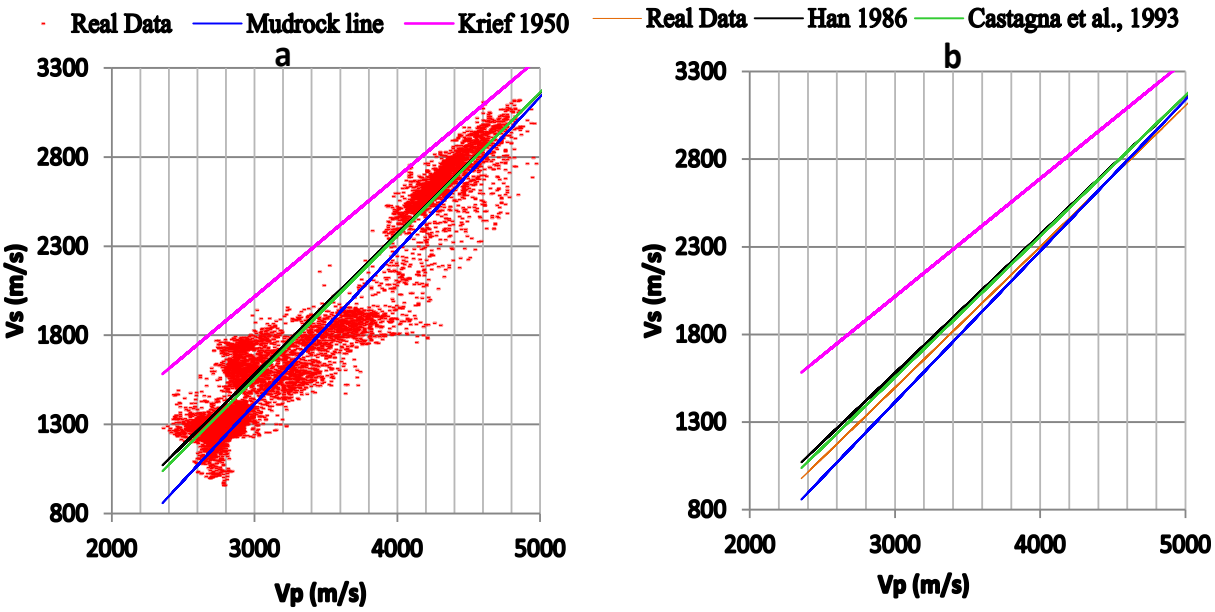

Fig. 6.3. Vp-Vs relation plotted from well 7120/8-4 showing the deviation of empirically shear velocity relation from real shear sonic data.

6.1.3. Rock physics template (RPTs) of AI versus V_p/V_s

The most common rock physics template is crossplots of acoustic impedance (AI) versus V_p/V_s ratio to discriminate lithology and also pore fluids saturation from well logs. Although the reliability of rock physics template is highly depends on the quality of input data as well as model assumption (Ødegaard and Avseth, 2004). Apart from well 7120/8-4, shear velocity is possibly obtained from the published empirical relation. Well 7120/7-2 chosen to investigate the reliability of rock physics template of AI versus V_p/V_s when the shear velocity calculated from published empirical relation of Castagna et al (1993).

The result shows nearly similar trend for whole lithology distribution without considerable separation in respect to fluid saturation in Kapp Toscana Group. No significant separation of fluid may be related to the effect of initial cement which will reduce the fluid sensitivity of sandstones (Avseth et al., 2010); hence it is not helpful in order to lithology and pore fluid separation which is the main target of rock physics analysis (Fig. 6.4).

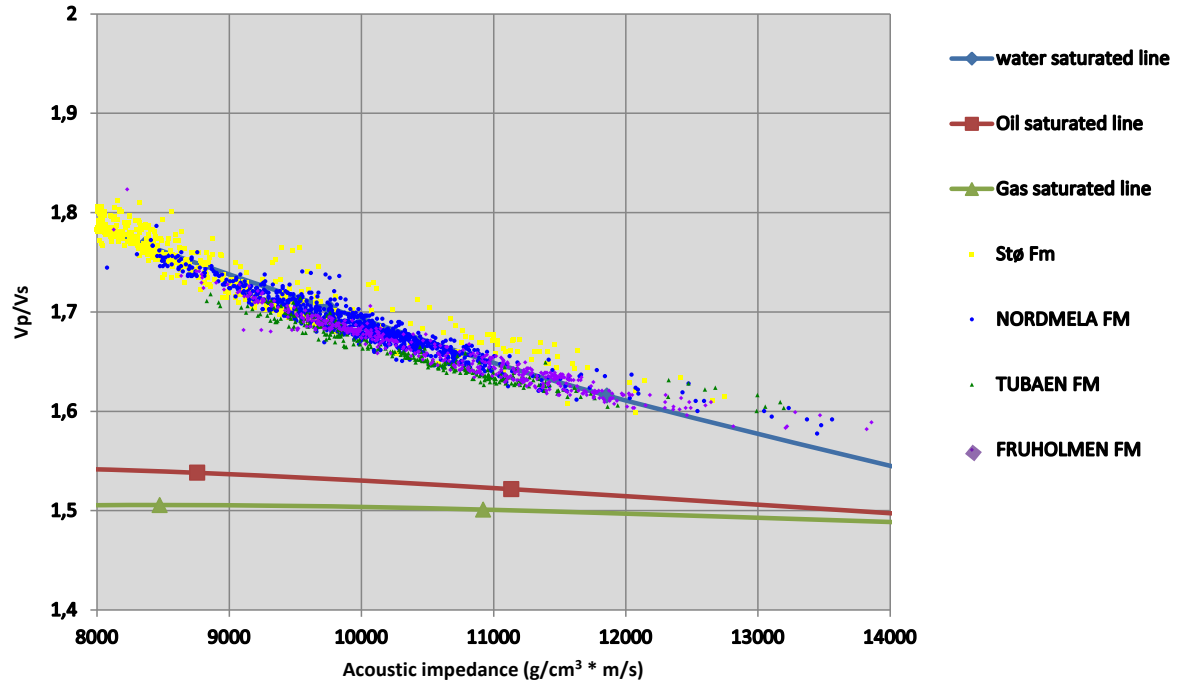

Fig. 6.4. Crossplot of AI versus Vp/Vs in well 7120/7-2. Shear velocity calculated from published empirical relation (Castagna et al., 1993) to show the importance of reliability of input data.

In well 7120/8-4 as we can see, almost all data points concentrating along a narrow zone between water saturated line and oil saturated line (Fig 6.5). However Stø Formation shows more variations along the fluid saturation lines whereas Fruholmen Formation demonstrates extremely large scattering outside the fluid saturation lines. This is occurs probably due to influence of clay content as this formation is dominated by shales. Nordmela Formation represents not much different distribution from Stø Formation while Tubåen and Fruholmen Formation represent more disperses within and outside the fluid saturation lines.

High V_p/V_s ratio associated with high acoustic impedance leads, the data points mostly concentrate in a narrow zone; hence lithology and pore fluid discrimination become more difficult. Variation of V_p/V_s ratio for Stø Formation shows ranging approximately 1.5 to around 1.7 associated with relatively high acoustic impedance from about 9500 g/cm^3*m/s to around 11500 g/cm^3*m/s. Nordmela Formation demonstrates higher acoustic impedance than Stø Formation (9500 to 12000 g/cm^3*m/s) but the V_p/V_s ratio shows more and less similar values. Tubåen and Fruholmen formations represents much diversity in both acoustic impedance (9500 to 12500 g/cm^3*m/s) and V_p/V_s ratio (1.5 to 1.75).

One important observation from this template is, not too much fluid saturation segregation can be identified from the input. It probably implies a brine saturated sand without significant

quantity of gas or oil. This observation is supported by exploration result that shows this well is dry (NPD Factpages).

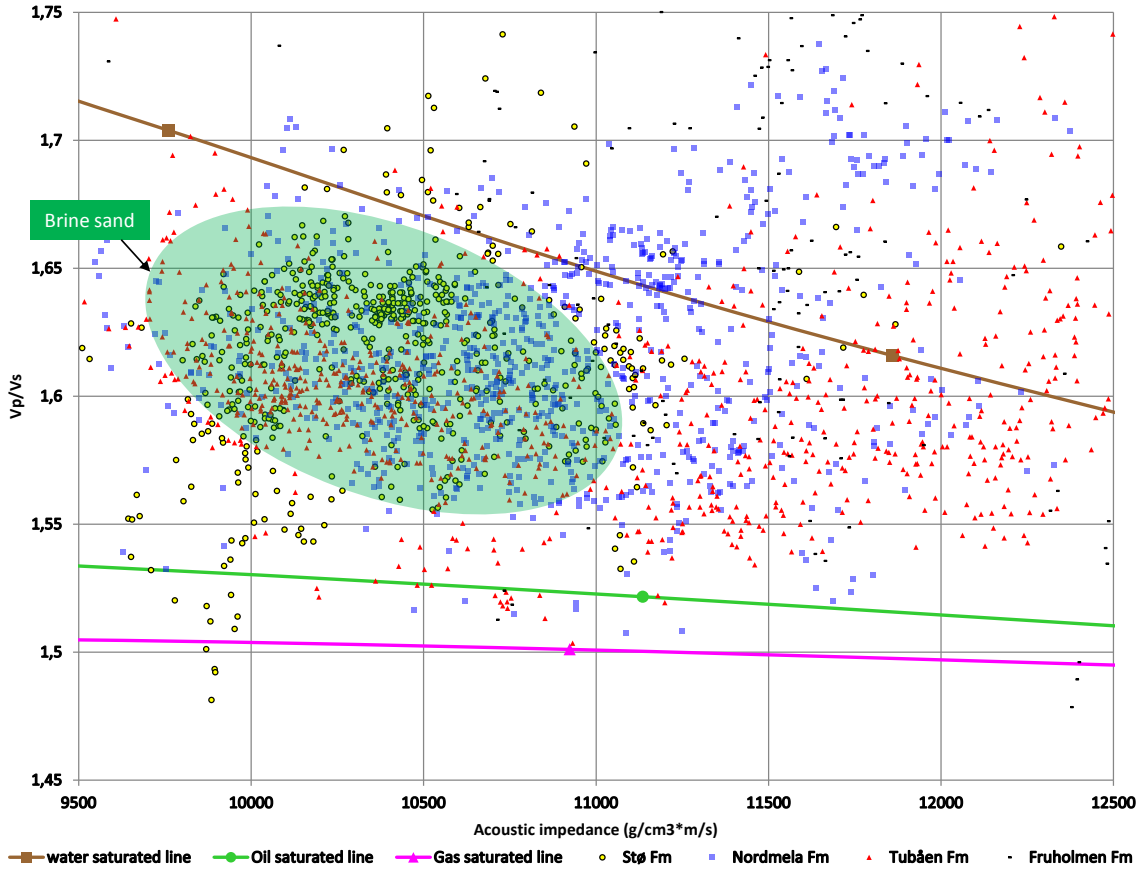

Fig. 6.5. Crossplot of AI versus Vp/Vs for well 7120/8-4. Data point mainly concentrate close to the water saturated line indicating brine sand. According to NPD Factpages this well is dry.

6.1.4. Rock physics diagnostic of Stø Formation

Well 7120/8-4 as reference well chosen for further analysis of Stø Formation because it was the only well with shear velocity data (Fig. 6.6). Arrows may be implying the different trends such as porosity, cementation, shaliness and gas saturation. Additionally, we make cross plots of AI versus V_p/V_s that is color coded by different parameters such as velocity, shale volume and porosity. It can help us in order more reliable interpretation. For example increasing in porosity can be observed from Fig 6.7d when the porosity increases while acoustic impedance decreases.

When velocity (P-wave or shear velocity) increases, acoustic impedance also increases. This is happen may be due to cementation and as discussed Stø Formation dominated by chemical compaction; hence cementation is a common process within this formation. When clay

content increases, the V_p/V_s ratio also show increase (Fig. 6.7c) and therefore shaliness trend defined as Figure 6.6 (arrow 4). Arrow (2) in Figure 6.6 shows the porosity trend which demonstrates slight increase in V_p/V_s ratio because the influence of porosity on V_p and V_s is different (Figs 6.7e and 6.7f). The P-wave velocity increases dramatically by decrease of porosity (Fig. 6.7e) whereas shear velocity represents slight increase when porosity decreases (Fig. 6.7f).

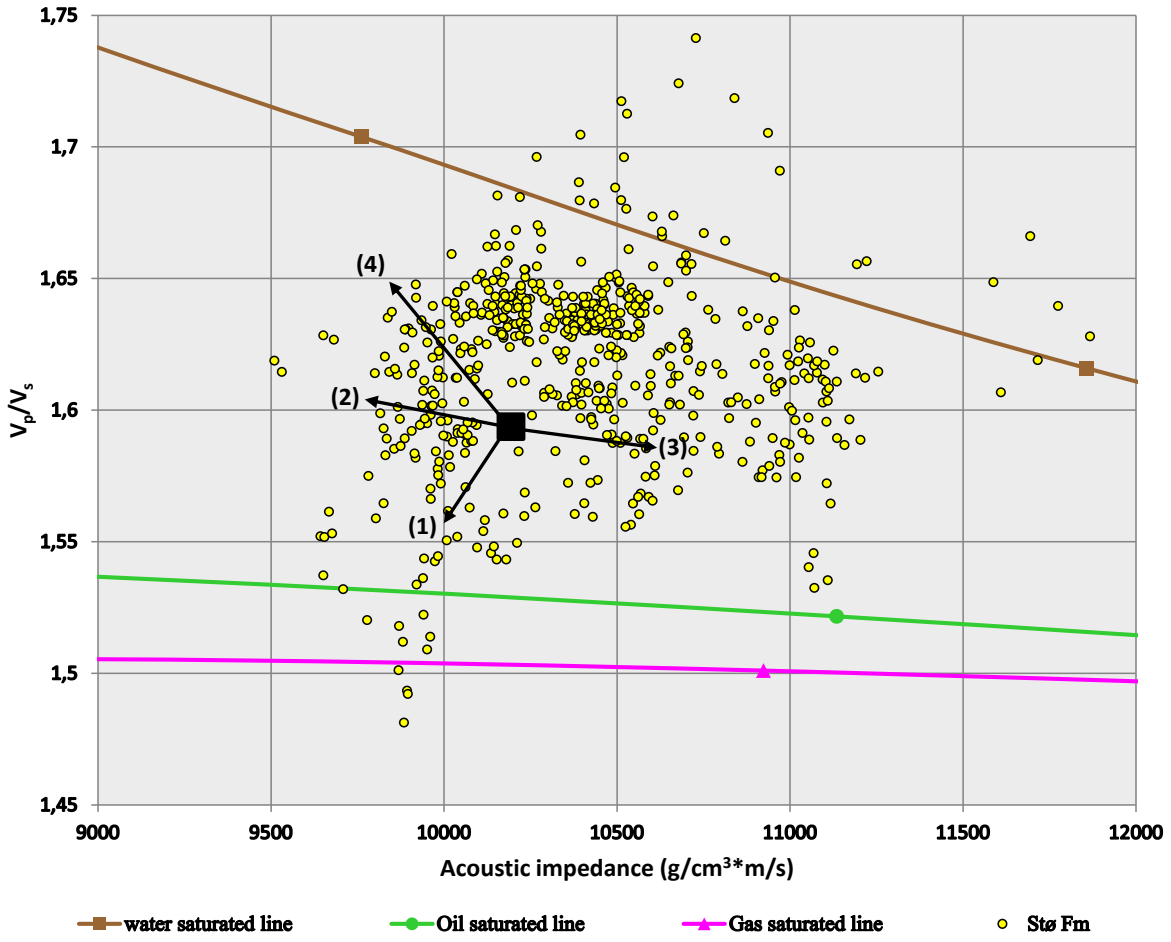

Fig. 6.6. Crossplots of AI versus Vp/Vs for Stø reservoir in well 7120/8-4. Arrows show geologic trends including: (1) increasing gas saturation (2) increasing porosity (3) increasing cementation (4) increasing shaliness.

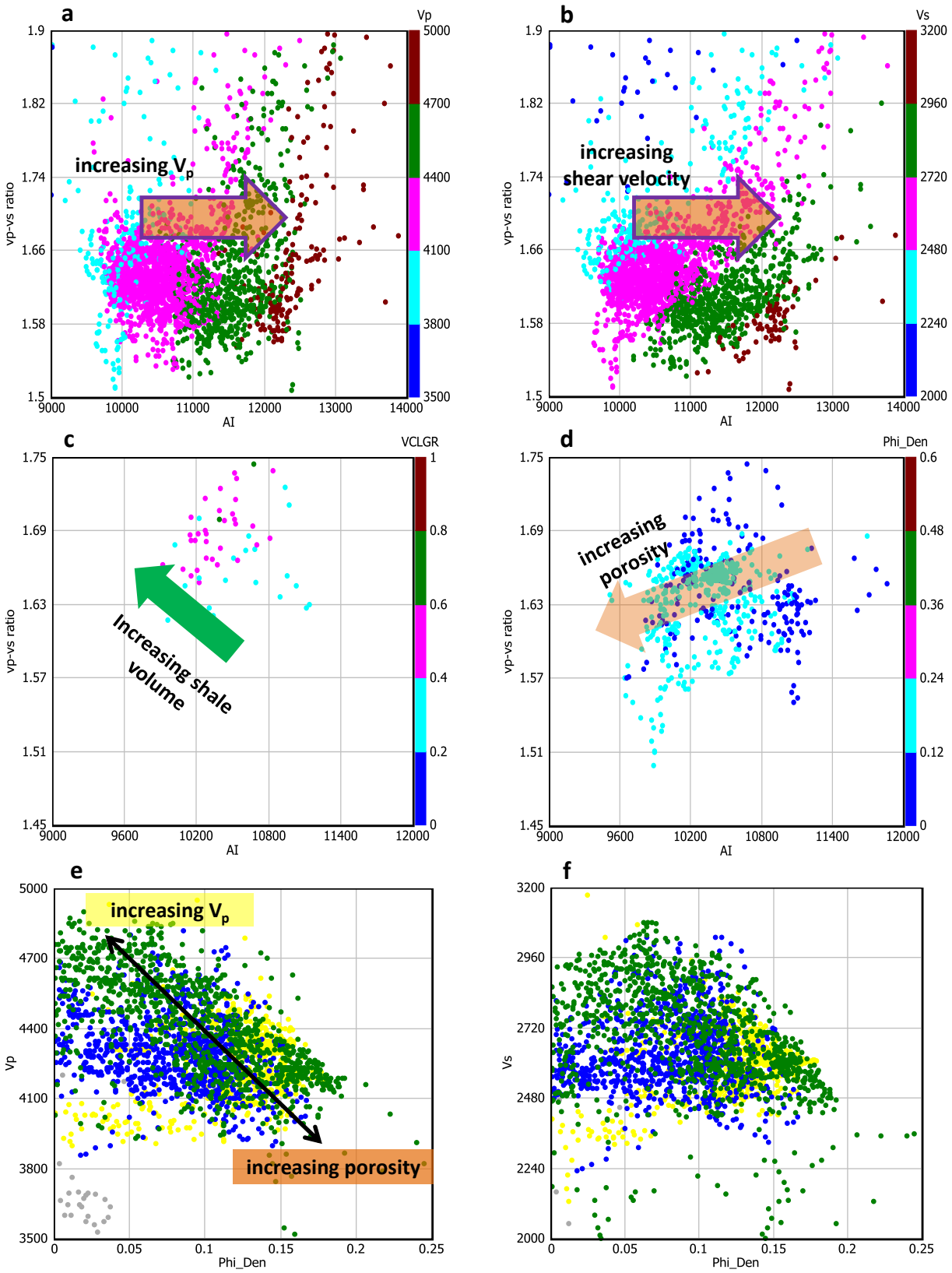

Fig. 6.7. Crossplots of AI versus Vp/Vs for Stø reservoir in well 7120/8-4. Color coded with (a) P-wave velocity, (b) shear velocity, (c) shale volume and, (d) porosity. Arrows also show increasing in different parameters; (a) P-wave velocity, (b) shear velocity, (c) shale volume and, (d) porosity. Arrows also show increasing in different parameters; (a) P-wave velocity, (b) shear velocity, (c) shale volume and, (d) porosity.

6.2. Discussion

Rock physics can help us to characterize a potential reservoir in terms of porosity, clay content, saturation and lithology by using the seismic properties of rocks like acoustic impedance, V_p/V_s ratio, bulk density and, elastic moduli (Avseth et al., 2010). In this study we concentrate on rock physics diagnostics of Kapp Toscana Group particularly Stø Formation as main reservoir rock in Askeladd gas filed. Net-to-gross ratio estimated in order to find the lateral distribution of Stø Formation and then explain its depositional environments (Table 6.1). Overall net-to-gross ratio derived from wells represents excellent reservoir properties for Stø Formation. It is also shows agreement with well completion report (NPD Factpages) which have shown good to excellent reservoir quality for Stø Formation. The average net/gross ratio is 0.84 but the best result comes from well 7120/8-4 with nearly 0.90 net-to-gross ration. However exploration result was disappointing for this well (NPD Factpages). Stø formation is located within Kapp Toscana Group that is mostly dominated by sandstones and shales; hence shallow marine to deltaic (fluviodeltaic) deposits may be represented the depositional environment for this group (Mørk et al., 1982). Well correlation for Stø formation demonstrates rather similar lateral distribution of coastal to shallow marine sandstones interbeded with silt and shale (see gamma ray log in Fig. 6.1) entire the area (Fig. 6.1).

Earlier studies of V_p-V_s relation have shown, influence of nonfluid parameters such as porosity, shaliness, and pore pressure is almost similar in both V_p and V_s (narrow zone in Fig. 6.2) whereas fluid saturation changes this linear and narrow trend to different zone (Avseth 2005). This observation particularly very important for reservoir monitoring where, pore pressure changes and saturation changes, discriminate two trend positioning perpendiculars each other's (Avseth, 2005). Comparison of published empirical V_p-V_s relation and real data in well 7120/8-4 implies relatively good match among them (Fig. 6.3). One can specify two distinct lithology distributions falling along a narrow zone which implies different initial composition as well as compaction history. The upper zone shows higher V_p and V_s probably due to initial mineralogical composition and also undergone by chemical compaction. The lower zone indicates higher amount of clay, higher porosity and pore pressure (regarding to burial depth) which is essentially corresponds to mechanical compaction; and as a result it shows lower velocity.

Lithology discrimination as well as pore fluids type is the most important objectives of plotting acoustic impedance versus V_p/V_s ratio (Fig. 6.5). However the input data significantly affect the result so that for instance in well 7120/8-4, high V_p/V_s ratio and acoustic impedance positioning the concentration of our data in a narrow zone. Therefore, distinguish different type of lithology become more difficult. On the other hand previous studies have shown this well is dry (NPD Factpages) may be due to leakage taken place along the fault boundaries (Bernal 2009). Apart from technical problem, the results still help us to get some ideas about lithology as well as fluid saturation in different formations of Kapp Toscana Group. Nearly whole data concentrate close to the water saturated line although high acoustic impedance also observed outside this line (Fig. 6.5).

Among the formations, Stø was selected for further study due to good reservoir properties like high net-to-gross ratio likewise resistivity values (NPD Factpages). By plotting (AI) versus V_p/V_s we can determine different geologic trend including shaliness, cementation, porosity and fluid saturation. These trends are important because they reduce the uncertainties in seismic reservoir prediction (Avseth et al., 2010). As we can see in Figure 6.6, each arrow corresponds to the specific geologic trend. For example, increasing in gas saturation shows by trend (1) where data points demonstrate a downward trend toward the gas saturation line because gas saturation tends to decrease velocity which resulted lower acoustic impedance and also V_p/V_s ratio. This observation also is supported by plotting AI versus V_p/V_s ratio color coded by V_p values (Fig. 6.7a).

Porosity is one of the most important factors control velocity (Rafavich et al., 1984; Bjørlykke et al., 2010); therefore an increase in porosity produces a decrease in velocity (Eberli et al., 2003). However shear velocity shows relatively slight increase with decreasing porosity and P-wave velocity shows dramatic increase as porosity decreases (Fig. 6.7d). Relatively constant change in shear velocity as a function of porosity may be reveals the fact that shear velocity is insensitive to pore fluid while the P-wave velocity affected by fluid saturation. Based on these observation one can define a porosity trend throughout the Stø Formation (Fig 6.7f).

Increasing in stiffness as a function of cementation causes considerable increase in acoustic impedance because it is controlled by velocity and bulk density; hence increasing in velocity or density as a function of compaction corresponds to higher acoustic impedance. We can clearly observe the influence of velocity increase on acoustic impedance when we color coded

the AI versus V_p/V_s base on V_p and V_s variation (Fig 6.7a and 6.7b). In other words, cementation (quartz cementation) reduces the pore spaces as well as increasing the strength of rock bodies that both lead us to higher velocity likewise acoustic impedance. However the amount of shale in Stø Formation is low and it is mainly consists of sandstones, but still is enough to distinguishing the shaliness trend within this formation. When we crossplot AI versus V_p/V_s which is color coded by volume of shale for Stø Formation, it tends to increasing upward (Fig 6.7c). This upward increasing trend possibly makes a shaliness trend within the Stø reservoir (Fig 6.7c).

The net-to-gross ratio as well as initial cementation shifted the data points up and down along the fluid saturated lines respectively. In fact if homogeneous, unconsolidated sand filled for example by oil, the fluid discrimination is good (Avseth et al., 2010). On the other hand, it is difficult to distinguish the fluid in heterogeneous sands. In well 7120/7-2 the data point concentrate along a narrow zone fits with brine saturated line in considering this well contain gas. This probably happens due to initial cementation that is reducing the fluid sensitivity. Another reason related to lower net-to-gross ratio that is causes the data points move up and as a result higher V_p/V_s ratio (Avseth et al., 2010).

In well 7120/8-4, cementation seems the main factor controlled the movement of data points. The data points move down throughout the rock physics templates (RTPs) as an impact of cementation and therefore the fluid separation become difficult (Avseth et al., 2010). By comparison of these wells (well 7120/7-2 and 7120/8-4), one can observes the influence of cementation and net-to-gross ration in lithology and fluid discrimination in the study area. However well 7120/7-2 is containing gas, fluid sensitivity is lower compare to well 7120/8-4 (dry) may be because of lower net-to-gross ratio (heterogeneity) as well as high cementation rate. Stø Formation therefore probably categorizes as heterogeneous cemented reservoir in study area. This is supports by compaction studies mentioned in this study where Stø Formation undergone by chemical compaction.

Chapter 7
Summary and Conclusion

The Barents Sea is a large epicontinental sea bounded by different basins and it is covered by a thick sedimentary deposits. Therefore the area is highly concerned in terms of petroleum exploration. Previously it was believed that Barents Sea was only containing gas, but findings of Goliath and Nucula discoveries as well as recent finding of Skrugard and Havis rejected this belief. Although, the main reservoir explored in the Russian sector contains giant reserves of gas/condensate occurring in Shtokmanovskoye field, the Norwegian Barents Sea has achieved a little exploration success. Barents Sea is known to be an overfilled petroleum system, but several stages of uplift during the evolution of this basin have led to leakage and depletion of large amounts of hydrocarbons. The Hammerfest Basin is considered as the main prospect for hydrocarbon accumulation in the Norwegian Barents Sea and has several discoveries including Snøhvit, Askeladd, Alka and Albatross. Among these discoveries, Snøhvit gas field has shown the best exploration result.

This study focuses on Askeladd discovery which is located in the south-western part of the Hammerfest Basin. The Hammerfest Basin has developed in Mesozoic (Late Jurassic to Early Cretaceous) as blocks bounded by faults. Lithology varies from shallow marine sandstones to deep marine shales all over the basin. The main reservoir rock is Stø Formation of Early to Middle Jurassic age deposited by shallow marine sandstones with good to excellent reservoir properties. The Late Jurassic Hekkingen Formation is detected as a mature source rock that constitutes deep marine dark grey shales containing high amounts of organic matter. Two main potential cap rock units in this area are Fuglen and Hekkingen shales though Cenozoic uplift has affected on their seal integrity. A rifting episode in Late Jurassic to Early Cretaceous has made tilted fault blocks which are suitable traps for accommodating hydrocarbon. While, leakage along the fault boundaries may be the most probable reason for lack of a complete petroleum system. In this study, a reservoir characterization workflow for Stø Formation is carried out in terms of compaction, rock property evolution and rock physics diagnostics.

Investigating compaction behavior in Askeladd discovery based on petrophysical log data such as velocity, density and porosity demonstrates a good agreement with several studies carried out previously (Storvoll et al., 2005; Ohm et al., 2008). As expected velocity and density increase with depth, and porosity decrease. Transition from mechanical to chemical compaction is identified by using sonic velocity log data as well as density-velocity cross-plot. Abrupt velocity increases in a single lithology (Knurr Formation) implies on the onset of quartz cementation. The Knurr Formation which is mainly dominated by shale is detected as

the most probable transition zone from mechanical to chemical compaction. Moreover, exhumation correction is estimated for each well after investigating the mismatch between the real data points plotted in V_p-depth plot and the experimental relationships achieved under mechanical compaction circumstances. The values estimated as exhumation ranges from 330 m (well 7120/8-3) to 900 m (well 7120/8-2).

Rock physics templates (RPTs) can be used as tool for lithology and pore fluid discrimination. Acoustic impedance versus V_p/V_s ratio is plotted to investigate several geologic trends such as cementation, porosity, shaliness and, fluid saturation within the Stø reservoir. While, according to data points of well 7120/8-4 as the only available well owning V_s data, it is difficult to distinguish these trends in the area of study. Overconsolidation of reservoir rock which causes the data points fall in a too narrow region among the pre-defined templates can give an explanation for this difficulty.

In spite of limitations and uncertainties associated with this study, these conclusions can be highlighted:

- Regardless of several parameters such as overpressure (Kolje Formation), presence of organic matter (Hekkingen Formation) and smectite clay (Torsk Formation) which make the depth trend to behave anomalously, the general compaction trend behave as it is expected in different wells in the Askeladd discovery.
- The transition zone is distinguished throughout the Knurr Formation by using the sonic logs and also density-velocity cross-plots. This transition is observed at depth of 1640 m (BSF) corresponding to 74^0C in well 7120/8-2. Since it shows misfit with general compaction trends, correction of exhumation needs to be performed to probe the rock properties properly.
- The exhumation estimations in the study area ranging from 350 m to 900 m and it is higher in comparison with Snøhvit field.
- The average net-to-gross ratio is calculated to be about 0.84, indicating excellent reservoir quality of Stø Formation.
- The shear velocity is only available for one well. On the other hand, this well is dry. Therefore, it is difficult to characterize the Stø reservoir based on rock physics models as the V_s is an important parameter for many rock physics studies.

References

References:

Asquith, G., and Krygowski, D., 2004. Basic well log analysis. AAPG methods in Exploration Series 16, 224 pp.

Avseth, P., Mukerji, T., Mavko, G., 2005. Quantitative seismic interpretation: Applying rock physics tools to reduce interpretation risk. Cambridge University Press, New York.

Avseth, P., Dvorkin, J., Mavko, G., Rykkje, J., 2000. Rock physics diagnostic of north sea sands: Link between microstructure and seismic properties. Geophysics Research Letter 27**,** 2761-2764.

Avseth, P., Mukerji, T., Mavko, G., Dvorkin, J., 2010. Rock-physics diagnostics of depositional texture, diagenetic alterations, and reservoir heterogeneity in high-porosity siliciclastic sediments and rocks. A review of selected models and suggested work flows. Geophysics 75**,** 75A31-75A47.

Barrère, C., Ebbing, J., Gernigon, L., 2009. Offshore prolongation of Caledonian structures and basement characterisation in the western Barents Sea from geophysical modelling. Tectonophysics 470**,** 71-88.

Berglund, L. T., Augustson, J., Færseth, R., Gjelberg, J., Ramberg-Moe, H., 1986. The evolution of the Hammerfest Basin. Norwegian Petroleum Society, 319-338.

Bernal, A., 2009. Controls on economical hydrocarbon accumulations in the Askeladd Field, Barents Sea: a post-mortem fault seal analysis: extended abstract for the European Association of Geoscientists & Engineers. 2nd International Conference on Fault and Top Seals- from Pore to Basin Scale, 21–24 September. Montpellier France, 3.

Bjørlykke, K., Mo, A., Palm, E., 1988. Modeling of thermal convection in sedimentary basins and its relevance to diagenetic reactions. Marine and Petroleum Geology 5, 338-351.

Bjørlykke, K., 1998. Clay mineral diagenesis in sedimentary basins - a key to the prediction of rock properties. Examples from the North Sea Basin. Clay Minerals 33, 15-34.

Bjørlykke, K., Chuhan, F., Kjeldstad, A., Gundersen, E., Lauvrak, O., Høeg, K., 2004. Modelling of sediment compaction during burial in sedimentary basins in Stephansson O.,

Hudson, J., King, L., (eds.). Coupled Thermo-Hydro- Mechanical-Chemical Processes in Geo-Systems. Elsevier, Amsterdam, 699-708.

Bjørlykke, K., Høeg, K., Mondol, N. H., 2010. Introduction to Geomechanics: Stress and Strain in Sedimentary Basins in: Petroleum Geoscience. Springer Berlin Heidelberg.

Bjorlykke, K., and Jahren, J., 2010. Sandstones and Sandstone reservoirs in Bjorlykke, K., 2010. Petroleum Geoscience: from Sedimentary Environments to Rock Physics, Berlin, Heidelberg, Springer-Verlag Berlin Heidelberg, 113-140.

Castagna, J. P., Batzle, M. L., Eastwood, R. L., 1985. Relationships between Compressional-Wave and Shear-Wave Velocities in Clastic Silicate Rocks. Geophysics 50, 571-581.

Castagna, J. P., Batzle, M. L., Kan, T. K., 1993. Rock physics - The link between rock properties and AVO response, in offset-dependent reflectivity - Theory and practice of AVO analysis, ed. J. P. Castagna and M. Backus. Investigation in Geophysics 8, SEG, Tulsa, Oklahoma, 135-171.

Cavanagh, A. J., Di Primio, R., Scheck-Wenderoth, M., Horsfield, B., 2006. Severity and timing of Cenozoic exhumation in the southwestern Barents Sea. Journal of the Geological Society 163, 761-774.

Chuhan, F. A., Bjørlykke, K., Lowrey, C. J., 2001. Closed-System Burial Diagenesis in Reservoir Sandstones: Examples from the Garn Formation at Haltenbanken Area, Offshore Mid-Norway. Journal of Sedimentary Research 71**,** 15-26.

Chuhan, F. A., Kjeldstad, A., Bjørlykke, K., Høeg, K. 2002. Porosity loss in sand by grain crushing-experimental evidence and relevance to reservoir quality. Marine and Petroleum Geology 19**,** 39-53.

Cornford, C., 2009. Source Rocks and Hydrocarbons of the North Sea. Petroleum Geology of the North Sea. Blackwell Science Ltd.

Dalland A., Worsley D., Ofstad, K., 1988. A lithostratigraphic scheme for the Mesozoic and Cenozoic succession offshore mid and northern Norway. Norwegian Petroleum Directorate Bulletin 4, 65.

Dvorkin, J., and Nur, A., 1996. Elasticity of high-porosity sandstones: Theory for two North Sea data sets. Geophysics 61(5), 1363-1370.

Doré, A. G., 1995. Barents Sea Geology, Petroleum Resources and Commercial Potential. Arctic 48 (3), 207-221.

Doré, A. G., and Jensen, L. N., 1996. The impact of late Cenozoic uplift and erosion on hydrocarbon exploration: offshore Norway and some other uplifted basins. Global and Planetary Change 12, 415-436.

Eberli, G. P., Baechle, G. T., Anselmetti, F. S., Incze, M. L., 2003. Factors controlling elastic properties in carbonate sediments and rocks. The Leading Edge 22**,** 654-660.

Eidsvik, J., Avseth, P., Omre, H., Mukerji, T., Mavko, G., 2004. Stochastic reservoir characterization using prestack seismic data. Geophysics 69**,** 978-993.

Eldholm, O., Faleide, J. I., Myhre, A. M., 1987. Continent-ocean transition at the western Barents Sea/Svalbard continental margin. Geology 15**,** 1118-1122.

Faleide, J. I., Gudlaugsson, S. T., Jacquart, G., 1984. Evolution of the western Barents Sea. Marine and Petroleum Geology 1**,** 123-150.

Faleide, J. I., Vågnes, E., Gudlaugsson, S. T., 1993. Late Mesozoic-Cenozoic evolution of the south-western Barents Sea in a regional rift-shear tectonic setting. Marine and Petroleum Geology 10**,** 186-214.

Gabrielsen, R. H., 1984. Long-lived fault zones and their influence on the tectonic development of the southwestern Barents Sea. Journal of the Geological Society 141**,** 651-662.

Gabrielsen, R.H., and Færseth, R.B., 1988. Cretaceous and Tertiary reactivation of master fault zones of the Barents Sea (extended abstract). Norsk Polarinstitute Report Series 46, 93-97.

Gabrielsen, R.H., Færseth, R.B., Jensen, L.N., Kalheim, J.E., Riis, F., 1990. Structural elements of the Norwegian continental shelf, Part I. The Barents Sea Region. Norwegian Petroleum Director Bulletin 6, 33.

Gabrielsen, R. H., and Kløvjan, O. S., 1997. Late Jurassic-early Cretaceous caprocks of the southwestern Barents Sea: fracture systems and rock mechanical properties in Møller-Pedersen, P., and Koestler, A. G., (eds.). Norwegian Petroleum Society, Special Publications. Elsevier.

Gassman, F., 1951. Elastic waves through a packing of spheres. Geophysics 16, 673-685.

Gelius, L. J., and Johansen, T. A., 2010. Petroleum Geophysics, Unigeo, Bergen.

Han, D., Nur, A., Morgan, D., 1986. Effect of porosity and clay content on the wave velocities in sandstones. Geophysics 51(11), 2093-2107.

Haq, B. U., Hardenbol, J., Vail, P. R., 1987. Chronology of Fluctuating Sea Levels Since the Triassic. Science 235**,** 1156-1167.

Hashin, Z., and Shtrikman, S., 1963. A variation approach to the elastic behavior of multiphase materials. Journal of Mechanical physics. Solids 11, 127-140.

Henriksen, E., Ryseth, A. E., Larssen, G. B., Heide, T., Rønning, K., Sollid, K., Stoupakova, A. V., 2011. Chapter 10 Tectonostratigraphy of the greater Barents Sea: implications for petroleum systems. Geological Society, London, Memoirs 35**,** 163-195.

Hermanrud, C., Gunn, M., Teige, G., Vik, E., Paasch, B., Vensaas, L., Nordgrd, H.M., 1998. Overpressures in shales-do we know what they are and why they are there? Overpressures in Petroleum Exploration, Pau, Conference Extended Abstracts.

Japsen, P., and Chalmers, J. A., 2000. Neogene uplift and tectonics around the North Atlantic: overview. Global and Planetary Change 24, 165-173.

Johansen, S.E., Ostisty, B.K., Birkeland, Ø., Fedorovsky, Y.F., Martirosjan, V.N., Bruun Christensen, O., Cheredeev, S.I., Ignatenko, A.A., Margulis, M., 1993. Hydrocarbon potential in the Barents Sea region: Play distribution and potential in Vorren T.O. et al., (Eds.), Arctic Geology and Petroleum Potential, NPF Special Publication 2. Elsevier, New York, NY, 273-320.

Karlsen, D. A., and Skeie, J. E., 2006. Petroleum migration, faults and overpressure, part i: calibrating basin modelling using petroleum in traps - a review. Journal of Petroleum Geology 29**,** 227-256.

Knox, R. W, O'B., Morton, A. C., 1988. The record of early Tertiary N Atlantic volcanism in sediments of the North Sea Basin. Geological Society of London, Special Publication 39, 407-419.

Laberg, J. S., Andreassen, K., Vorren, T. O., 2012. Late Cenozoic erosion of the high-latitude southwestern Barents Sea shelf revisited. Geological Society of America Bulletin 124**,** 77-88.

Magoon L.B., and Dow, W.G., 1994. The petroleum system in Magoon L.B., and Dow, W.G., (Eds.). The Petroleum System-From Source to Trap. American Association of Petrolem Geologists Memoir 60, 3-24

Makurat, A., Bjorn, T., Monsen, K., Rawlings, C., 1992. Cenozoic uplift and caprock seal in the Barents sea: fracture modeling and seal risk evaluation. Socity of Petroleum Engineers, SPE Annual Technical Conference and Exhibition, 4-7 October 1992, Washington, D.C.

Marcussen Ø., Thyberg B. I., Peltonen C., Jahren J., Bjørlykke K., Faleide, J. I., 2009. Physical properties of Cenozoic mudstones from the northern North Sea: Impact of clay mineralogy on compaction trends. AAPG Bulletin 93, 127-150.

Marcussen, Ø., Maast, T. E., Mondol, N. H., Jahren, J., Bjørlykke, K., 2010. Changes in physical properties of a reservoir sandstone as a function of burial depth-The Etive Formation, northern North Sea. Marine and Petroleum Geology 27**,** 1725-1735.

Mavko G., Mukerj,i T., Dvorkin, J., 2009. The rock physics handbook: Tools for seismic analysis of porous media. Cambridge University Press, New York.

Mondol, N. H., Bjørlykke, K., Jahren, J., Høeg, K., 2007. Experimental mechanical compaction of clay mineral aggregates-Changes in physical properties of mudstones during burial. Marine and Petroleum Geology 24**,** 289-311.

Mondol N. H., 2009. Porosity and permeability development in mechanically compacted silt-kaolinite mixtures. SEG Houston International Exposition and Annual Meeting.

Mørk A., Karud R., Worsley, D., 1982. Depositional and diagenetic environments of the Triassic and lower Jurassic succession of Svalbard. Canadian Society of Geologist, Calgary, Alberta, Canada, 371-398.

Norwegian Petroleum Directorate (NPD) Factpages and Factmaps (www.npd.no). Latest visited 30th of May.

Nyland, B., Jensen L. N., Skagen, J., Skarpnes, O., Vorren, T., 1992. Tertiary uplift and erosion in the Barents Sea: magnitude, timing and consequences, in Larsen, R. M., Brekke, H., Larsen, B. T., Talleraas, E., (eds). Structural and Tectonic modeling and its application to petroleum geology. Amsterdam, Elsevier, 153-162.

Ohm, S. E., Karlsen, D. A., Austin, T. J. F., 2008. Geochemically driven exploration models in uplifted areas: Examples from the Norwegian Barents Sea. AAPG Bulletin 92, 1191-1223.

Ostanin, I., Anka, Z., di Primio, R., Bernal, A., 2012. Identification of a large Upper Cretaceous polygonal fault network in the Hammerfest basin: Implications on the reactivation of regional faulting and gas leakage dynamics, SW Barents Sea. Marine Geology, Available online 30 March 2012.

Palmer, A. R., 1983. The Decade of North American Geology 1983 Geologic Time Scale. Geology 11**,** 503-504.

Peltonen, C., Marcussen, Ø., Bjørlykke, K., Jahren, J., 2008. Mineralogical control on mudstone compaction: a study of Late Cretaceous to Early Tertiary mudstones of the Vøring and Møre basins, Norwegian Sea. Petroleum Geoscience 14**,** 127-138.

Rafavich, F., Kendall, C. H. St. C., Todd T. P., 1984. The relationship between acoustic properties and the petrographic character of carbonate rocks. Geophysics 49, 1622-1636.

Raymer, L.L., Hunt, E.R., Gardner, J.S., 1980. An improved sonic transit time to porosity transform. 21st SPWLA Annual Meeting, 1–13.

Skogseid, J., and Eldholm, O., 1988. Early Cenozoic evolution of the Norwegian volcanic passive margin and the formation of marginal high. Geological Society of London, Special Publication 39, 407-419.

Spencer, A. M., 1984. Petroleum Geology of the North European Margin. Norwegian Petroleum Soceity, 436.

Storvoll, V., Bjørlykke K., Mondol, N. H., 2005. Velocity-depth trends in mesozoic and cenozoic sediments from the Norwegian shelf. AAPG Bulletin 89, 359-381.

Storvoll, V., and Brevik, I., 2008. Identifying time, temperature, and mineralogical effects on chemical compaction in shales by rock physics relations. The Leading Edge 27**,** 750-756.

Terzaghi, K., 1943. Theoretical soil mechanics. John Wiley, New York, 510.

Thyberg, B. I., Jordt, H., Bjørlykke, K., Faleide, J. I., 2000. Relationship between sequence startigraphy, mineralogy and geochemistry in Cenozoic sediments of northern North Sea. Geological Society of London, Special Publication 167, 245-272.

Thyberg, B., Jahren, J., Winje, T., Bjørlykke, K., Faleide, J.I., 2009. From mud to shale: rock stiffening by microquartz cementation. First Break 27, 27-33.

Thyberg, B., Jahren, J., Winje, T., Bjørlykke, K., Faleide, J. I., Marcussen, Ø., 2010. Quartz cementation in Late Cretaceous mudstones, northern North Sea: Changes in rock properties due to dissolution of smectite and precipitation of micro-quartz crystals. Marine and Petroleum Geology 27**,** 1752-1764.

Vernik, L., and Nur, A., 1992. Petrophysical classification of siliciclastics for lithology and porosity prediction from seismic velocities. AAPG Bulletin 76, 1295–1309.

Waples, D. W., and Couples, G. D., 1998. Some thoughts on porosity reduction -- rock mechanics, overpressure and fluid flow. Geological Society of London, Special Publications 141, 73-81.

Westre, S., 1984. The Askeladden gas find-Troms I in Spencer, A. M., (Eds.). Petroleum Geology of the North European Margin. Graham and Trotman, London, 33-39.

Worsley, D., 2008. The post-Caledonian development of Svalbard and the western Barents Sea. Polar Research 27**,** 298-317.

Wyllie, M. J. R., Gregory, A. R., Gardner, L. W., 1956. Elastic wave velocities in heterogeneous and porous media. Geophysics 21, 41-70.

Ødegaard, E., and Avseth, P., 2004. Well log and seismic data analysis using rock physics templates. First break 23, 37-43.